

# Engineering a Robotic Exoskeleton for Space Suit Simulation

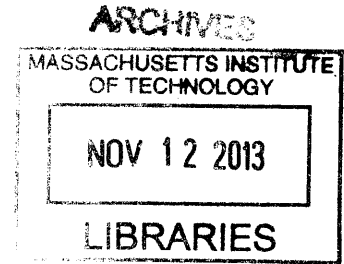
by

Forrest Edward Meyen

B.S. in Mechanical Engineering

B.S. in Biological Engineering

University of Missouri, 2011



Submitted to the Department of Aeronautics and Astronautics

In Partial Fulfillment of the Requirements for the Degree of

Master of Science in Aeronautics and Astronautics

at the

MASSACHUSETTS INSTITUTE OF TECHNOLOGY

September 2013

© 2013 Massachusetts Institute of Technology. All rights reserved.

Signature of Author .....  
Department of Aeronautics and Astronautics  
August 20, 2013

Certified by .....  
Dava J. Newman, Ph.D.  
Professor, MacVicar Faculty Fellow  
Department of Aeronautics and Astronautics  
Thesis Supervisor

Accepted by .....  
Eytan H. Modiano  
Professor of Aeronautics and Astronautics  
Chair, Graduate Program Committee





# **Engineering a Robotic Exoskeleton for Space Suit Simulation**

by

Forrest Edward Meyen

Submitted to the Department of Aeronautics and Astronautics

In Partial Fulfillment of the Requirements for the Degree of

Master of Science in Aeronautics and Astronautics

September 2013

## **Abstract**

Novel methods for assessing space suit designs and human performance capabilities are needed as NASA prepares for manned missions beyond low Earth orbit. Current human performance tests and training are conducted in space suits that are heavy and expensive, characteristics that constrain possible testing environments and reduce suit availability to researchers. Space suit mock-ups used in planetary exploration simulations are light and relatively inexpensive but do not accurately simulate the joint stiffness inherent to space suits, a key factor impacting extravehicular activity performance. The MIT Man-Vehicle Laboratory and Aurora Flight Sciences designed and built an actively controlled exoskeleton for space suit simulation called the Extravehicular Activity Space Suit Simulator (EVA S3), which can be programmed to simulate the joint torques recorded from various space suits. The goal of this research is to create a simulator that is lighter and cheaper than a traditional space suit so that it can be used in a variety of testing and training environments. The EVA S3 employs pneumatic actuators to vary joint stiffness and a pre-programmed controller to allow the experimenter to apply torque profiles to mimic various space suit designs in the field. The focus of this thesis is the design, construction, integration, and testing of the hip joint and backpack for the EVA S3. The final designs of the other joints are also described. Results from robotic testing to validate the mechanical design and control system are discussed along with the planned improvements for the next iteration of the EVA S3. The final EVA S3 consists of a metal and composite exoskeleton frame with pneumatic actuators that control the resistance of motion in the ankle, knee, and hip joints, and an upper body brace that resists shoulder and elbow motions with passive spring elements. The EVA S3 is lighter (26 kg excluding the tethered components) and less expensive (under \$600,000 including research, design, and personnel) than a modern space suit. Design adjustments and control system improvements are still needed to achieve a desired space suit torque simulation fidelity within 10% root-mean-square error.

Thesis Supervisor: Dava J. Newman

Title: Professor of Aeronautics and Astronautics



## Acknowledgements

This master's thesis project has been a dream for me. I have worked with an amazing group of engineers on a fantastic and challenging engineering project. Spending these past two years at MIT has been an extraordinary experience.

To my advisor, Professor Dava Newman, thank you for your support throughout my time at MIT. You care about me as a person and as a researcher. You have given me so many once in a lifetime experiences, from a research retreat in Honduras to dinner with Buzz Aldrin. I have you to thank for some of my most memorable stories of graduate school.

I am grateful to Professor Jeffrey Hoffman for your advice and guidance regarding your experiences in the EMU and for being the first person to try on the completed EVA S3.

Thank you Dr. Jessica Duda, for assembling this awesome team with the folks at Aurora Flight Sciences and MIT. You allowed me to have a great amount of freedom while designing the hip and backpack of the EVA S3. Your confidence in my abilities helped my creativity flourish during the design process. I will miss our productive yet always entertaining team meetings. I would also like to thank my other EVA S3 team members, Jeff Chambers, Namir Jawdat, Roedolph Opperman, Charlie De Vivero, and Andie Gilkey (who shares my frustrations with robot repairs). I could not have asked for a better group of people to work with.

I owe much of my sanity to my friends and colleagues in the Man Vehicle Laboratory. Thank you for all of the lab lunches, Friday trips to the Muddy, Warfish, game nights, and extracurricular adventures. I enjoy being around a group of people so passionate about space exploration.

Thanks to all my MSRP buddies, as well as Monica Orta and Dean Jones for introducing me to this awesome place. I credit MSRP for helping me get my foot in the door at MIT.

Thank you to all the machinists and staff members who helped me, Todd Billings, Dave Robertson, from Aero/Astro, Mark from the Edgerton Machine Shop, and everyone at Central Machine Shop. Thanks to the administrative assistants, Liz Zotos, Quentin Alexander, and Sally Chapman.

To my UROPs Lyndsy and Joe, Thanks for all of the help on the project. I hope that you learned something about how much fun engineering can be.

Thank you to the NSF Graduate Research Fellowship Program and NASA. Your funding made it possible for me to study at this world-class institution.

To Rachel, I can't wait for our big day. Thank you for being my best friend and supporter.

Thanks to my parents, Brad and Kathleen. You guys keep getting cooler as you get older. I cannot wait to come home and do some hiking and skiing with you both.

And finally, thanks to the Lord, for giving me my talents and making this beautiful universe for us to explore.



# Table of Contents

Abstract .....	3
Acknowledgements .....	5
Table of Contents .....	7
List of Figures .....	10
List of Tables .....	16
List of Abbreviations .....	17
1. Introduction.....	18
1.1 Motivation .....	18
1.2 Contribution .....	24
1.3 Problem Statement and Hypothesis.....	24
1.4 Thesis Outline .....	25
2. Background.....	26
2.1 Introduction to Exoskeletons.....	26
2.2 Early Exoskeleton History .....	27
2.3 Modern Exoskeleton Designs .....	30
2.4 Pneumatically actuated exoskeletons .....	33
2.5 Summary .....	35
3. Methods.....	36
3.1 Requirements.....	36
3.2 Conceptual Development .....	40
3.2.1 Actuator Selection.....	40
3.2.2 Structural Concepts .....	46

3.3	Torque transmission .....	49
3.3.1	Actuator size specifications .....	55
3.3.2	Spool Design Variants .....	59
3.4	Actuator assembly .....	65
3.5	Fitting the Human Operator .....	67
3.5.1	Exoskeleton/body interface.....	67
3.5.2	Sizing and adjustments .....	69
3.6	Material Selection .....	75
3.7	Finite Element Analysis for Structural Design .....	77
3.8	Construction and Design Revisions .....	80
3.9	Integration and Testing.....	84
3.9.1	Qualitative Testing.....	84
3.9.2	Robotic Space Suit Testing.....	86
3.10	Summary of Methods .....	94
4.	Results and Discussion .....	95
4.1	EVA S3 Architecture .....	95
4.1.1	Hip and Backpack Design.....	95
4.1.2	Knee Design.....	101
4.1.3	Ankle Design .....	105
4.1.4	Upper Body Design.....	107
4.1.5	Pneumatic and Control System Design.....	108
4.1.6	Integrated Design .....	113
4.2	Fit and Human Use.....	115

4.3	Simulator Results .....	120
4.3.1	Prototype Test Results .....	120
4.3.2	Final Test Results.....	125
5.	Conclusion .....	136
5.1	Thesis Summary and Contributions .....	136
5.2	Hypothesis Evaluation.....	137
5.3	Limitations .....	139
5.4	Future Work .....	139
5.4.1	Device Modifications.....	139
5.4.2	Research Applications .....	141
5.5	Broader Impacts .....	142
5.6	Final Summary .....	143
Appendices.....		145
Appendix A. Development of Other EVA S3 Components.....		145
6.1.1	Knee .....	145
6.1.2	Ankle.....	153
6.1.3	Upper Body.....	155
6.1.4	Pneumatics and Control .....	161
Appendix B. Early Optimization Code.....		170
Appendix C. RSST Repairs .....		173
References.....		177

## List of Figures

Figure 1.1 - The eZLS (Perusek, DeWitt et al. 2007).....	20
Figure 1.2 - The ARGOS (NASA 2013) .....	21
Figure 1.3 - Passive Knee Space Suit Simulator (Ferreira 2007) .....	22
Figure 1.4 - A lower body exoskeleton to simulate space suit locomotion(Carr and Newman 2008).....	23
Figure 1.5 - Knee joint prototype (Duda, Newman et al. 2011) .....	23
Figure 2.1- From the early 19 <sup>th</sup> century painting “Locomotion” by Robert Seymour. Perhaps the earliest depiction of an exoskeleton (Hoggett 2010).....	26
Figure 2.2- Artist’s conception of Man Amplifier (Clark, DeLeys et al. 1962) .....	28
Figure 2.3 - Hardiman 1 Prototype Assembly (Makinson 1971).....	30
Figure 2.4 - The Berkley Lower Extremity Exoskeleton (Zoss and Kazerooni 2005) .....	31
Figure 2.5 - Robot Suit HAL (CYBERDYNE 2013) .....	32
Figure 2.6 - Ratheon SARCOS XOS 2 (Guizzo 2011).....	33
Figure 2.7 – Some possible antagonistic actuator configurations (Beyl, Van Damme et al. 2008) .....	34
Figure 2.8 – A pneumatic rehabilitative exoskeleton on a treadmill (Beyl, Van Damme et al. 2008).....	34
Figure 2.9 – A ankle foot orthosis powered by pneumatic muscles (Ferris, Czerniecki et al. 2005).....	35
Figure 3.1 – Differences in joint angle sign convention. (A) Neutral point aligns with trunk (NASA 1995) (B) Neutral point perpendicular to trunk (Morgan and Center 1996) .....	37
Figure 3.2 – Space Suit Simulator (EVA S3) Joint Convention (Gilkey 2012).....	38
Figure 3.3 – Various pneumatic exoskeleton designs. (A) A dual pneumatic cylinder hip exoskeleton (Lewis and Ferris 2011). (B) Quadruple McKibben actuator ankle exoskeleton (Jamwal, Shengquan et al. 2010). (C) Dual antagonistic McKibben actuator ankle exoskeleton (Ferris, Czerniecki et al. 2005). (D) Serially linked quad McKibben knee exoskeleton (Beyl, Van Damme et al. 2008). .....	43
Figure 3.4 – The three sizes of Fluidic Muscles available from FESTO. (FESTO 2011) .....	45
Figure 3.5 – Force/displacement diagram for a Festo Fluidic Muscle with a 20 mm diameter 200 mm length (FESTO 2011).....	45
Figure 3.6 – Jester’s pants concept (Duda and Hart 2010) .....	46
Figure 3.7 – BLEEX hip structure design (Zoss, Kazerooni et al. 2006) .....	47



Figure 3.8 – Initial hip concept rendering with thigh brace on left side. ....	48
Figure 3.9 – The phase 1 space suit simulator knee joint (Duda, Newman et al. 2011) .....	51
Figure 3.10 – A free body diagram of the knee joint of the exoskeleton modeled as a two link system (Gilkey 2012). .....	52
Figure 3.11 – Improper and unsafe use of a Fluidic Muscle (FESTO 2011) .....	53
Figure 3.12 - Some possible antagonistic actuator configurations (Beyl, Van Damme et al. 2008).....	54
Figure 3.13 – Diagram of torque spool concept .....	55
Figure 3.14 – Early concept where antagonistic actuator pairs pull on a single spool (orange cylinder) .....	59
Figure 3.15 – An early concept of the dual spool design with appropriately sized actuators .....	60
Figure 3.16 – Prototype cam concept with weight saving holes.....	62
Figure 3.17 – Front and back view of spool concept.....	63
Figure 3.18 – Exploded view of retractable spool (A). Side view of Spool (B). .....	63
Figure 3.19 – Retractable spool prototype front (A), side (B) .....	64
Figure 3.20 - Final spool with extended cable guides.....	65
Figure 3.21 – Detail of prototype spool assembly .....	66
Figure 3.22 – Detail of final spool assembly .....	66
Figure 3.23 – Renderings of prototype I hip flexion extension actuator assembly (A) and final hip flexion/extension assembly (B).....	67
Figure 3.24 – Potential COTS options to secure the EVA S3 hip to the operator. (A) Osprey Bioform Hipbelt (REI 2012). (B) Alpinestars Touring Kidney Belt (Alpinestars 2012). (C) Black Diamond Climbing Harness (REI 2012). (D) Donjoy ROM hip brace (DonJoy 2012). .....	68
Figure 3.25 – Kelty Trekker 65 external frame backpack (Kelty 2013). .....	69
Figure 3.26 – Early concept with interlocking plate adjustments. Bolts could be moved to adjust the width in half inch increments.....	70
Figure 3.27 – Telescopic pole concept for hip joint alignment.....	71
Figure 3.28 – Telescopic cylinder and sliding rail combination for hip joint alignment in final design .....	71
Figure 3.29 – Simplified model showing horizontal adjustment of hip abduction/adduction axis center .....	72
Figure 3.30 – Concept where abduction/adduction spools are adjustable but the actuators are fixed to the backpack frame. ....	73

Figure 3.31 - Simplified model showing a vertical adjustment of hip abduction/adduction axis center. This adjustment also changes the vertical alignment of the hip flexion/extension center .....	74
Figure 3.32 – The final design also included mounting bolt holes to increase range of vertical alignment .....	74
Figure 3.33 – Composite structures. The carbon fiber greave and aluminum mold (A). Carbon fiber telescopic tubes in the hip prototype (B). .....	76
Figure 3.34 – FEA of the hip rear spool shows the von Mises stress does not exceed 101 MPa. ....	77
Figure 3.35 – Loading condition on the prototype hip flexion/extension actuator assembly structure .....	78
Figure 3.36 – Factor of safety FEA profile of a hip flexion/extension actuator assembly structure deisgn iteration ..	79
Figure 3.37 – von Mises stress in the final hip flexion/extension actuator assembly structure deisgn. ....	80
Figure 3.38 – Prototype hip and backpack design .....	81
Figure 3.39 – (A) Some prototype components ready to be assembled.(B) The assembly of the protoype spool.....	82
Figure 3.40 – Manufacturing EVA S3 components using a water jet cutter (A) and a CNC mill (B).....	82
Figure 3.41 – The prototype secured to a subject .....	83
Figure 3.42 – A qualitative fit check (A) and a general mobility test (B) .....	84
Figure 3.43 – A rear view of an early EVA S3 prototype .....	85
Figure 3.44 – The Robotic Space Suit Tester (RSST) .....	86
Figure 3.45 - Manual control of the Robotic Space Suit Tester.....	87
Figure 3.46 – Knee flexion/extension calibration data .....	88
Figure 3.47 – Method for determining joint angle using a protractor and a plumb line .....	88
Figure 3.48 - Right lower body of EVA S3 mounted to the RSST.....	90
Figure 3.49 – Torque vs. angle, net measured value for RSST knee for three cycles .....	91
Figure 3.50 – Torque vs. angle plot of the unsuted RSST knee for three cycles .....	92
Figure 3.51 – EVA S3 Knee torque vs. angle for four cycles.....	93
Figure 4.1 – Renderings of the EVA S3 hip and backpack components .....	95
Figure 4.2 – Rendering of the EVA S3 hip abduction/adduction actuator assemblies .....	96
Figure 4.3 - Rendering of hip flexion/extension position adjustment system excluding padding .....	97
Figure 4.4 – The completed backpack with hip abduction/adduction actuator assemblies.....	98

Figure 4.5 – Rendering of hip F/E joint assembly detailing ankle, knee, and hip distance adjustments .....	99
Figure 4.6 – Rendering of hip flexion/extension joint assembly .....	99
Figure 4.7 – Completed hip flexion/extension assembly .....	100
Figure 4.8 – Detail of hip flexion/extension actuators with a subject wearing the EVA S3. Seen from the side (A) and back (B) .....	100
Figure 4.9 – Rear view of EVA S3 hip assembly on a subject.....	101
Figure 4.10 – The EVA S3 knee component front and back. ....	102
Figure 4.11 – Detail of the binding clasp (A) and slider rail (B) .....	103
Figure 4.12 – Side and front view of the EVA S3 knee.....	104
Figure 4.13 – The EVA S3 ankle without the rear pneumatic cylinder .....	106
Figure 4.14 – Both EVA S3 ankles worn by a human subject. The pneumatic cylinder can be seen behind the ankle on the right.....	106
Figure 4.15 – The upper body passive exoskeleton.....	107
Figure 4.16 – Detail of passive shoulder (red circle) and elbow joints (dashed green circle). ....	108
Figure 4.17 - Intel STK600 processor and AT32UC3C0512C 32-bit microcontroller.....	108
Figure 4.18 – Simple control system diagram. ....	109
Figure 4.19 – Pneumatic control system diagram.....	110
Figure 4.20 Pneumatic pathway design. ....	111
Figure 4.21 – The solenoid stack (A), and the manifold air pressure inlet (B) .....	112
Figure 4.22 – (A) Signal conditioning circuitboards. (B) Pneumatics and control system assembly layout. ....	113
Figure 4.23 – Side and back views of the integrated EVA S3.....	114
Figure 4.24 – Donning the upper body of the EVA S3.....	115
Figure 4.25 – Donning the EVA S3. (A) Adding the backpack. (B) Adjusting the knee and ankle assembly. ....	116
Figure 4.26 –Attaching the hip flexion/extension component (A). Donning the EVA S3 from a seated position (B). ....	117
Figure 4.27 – Pneumatic control system and hardware. ....	120
Figure 4.28 – Prototype hip and knee joints mounted to the Robotic Space Suit Tester. ....	121

Figure 4.29 – Hip flexion/extension at 20 psi.....	121
Figure 4.30 – RSST and control hardware (A), Prototype knee mounted to the RSST (B), Detail of potentiometer (blue) mounted to prototype knee joint (C). .....	123
Figure 4.31– Knee torque vs position for statically pressurized actuators at 0, 138, 276, and 414 kPa (0, 20, 40, 60 psi) .....	124
Figure 4.32 - (A) EMU requirements graph (in blue) that we are attempting to replicate (Schmidt, Newman et al. 2001) (B) Test using controlled actuation. Data, in blue, plotted with torque-vs-angle of the robot alone (green). .....	125
Figure 4.33 – EVA S3 hip flexion/extension torque vs. angle .....	126
Figure 4.34 – EVA S3 hip flexion/ extension torque vs. angle (blue) overlaid on EMU torque data (black) (Frazer 2003). .....	127
Figure 4.35 – EVA S3 hip abduction/adduction torque vs. angle .....	129
Figure 4.36 – EVA S3 abduction/adduction torque vs. angle (blue) overlaid onto the EMU data (grey) from (Stirling 2008) and (Schmidt, Newman et al. 2001) .....	129
Figure 4.37 – EVA S3 Knee torque vs. angle for three cycles .....	131
Figure 4.38 – EVA S3 knee torque vs. angle (blue) overlaid onto the EMU data (grey) (Schmidt, Newman et al. 2001) .....	131
Figure 4.39 - View of ankle test setup. An L-bracket was used to manually move the ankle, since the RSST actuation was not working .....	133
Figure 4.40 – EVA S3 ankle flexion torque vs. angle over ten cycles .....	134
Figure 4.41 – EVA S3 flexion/extension torque vs. angle (blue) overlaid onto the EMU Data (grey) from (Frazer 2003) .....	134
Figure 6.1: (A) Side and (B) Isometric view of detailed EVA S3 knee joint design .....	146
Figure 6.2: EVA S3 knee prototype design with component descriptions and flexion-inhibiting actuator shown ...	146
Figure 6.3: Festo Fluidic Muscles and Actuator Slider Bearing Assembly .....	148
Figure 6.4: Greave design (all dimensions in inches).....	148
Figure 6.5: (A) Silicone plug with mold sections (B) Silicon plug for use during carbon fiber layups.....	149
Figure 6.6: The carbon fiber greave layup process.....	150
Figure 6.7 – The greave after being removed from the mold .....	150
Figure 6.8: S3 prototype donned by subject .....	151
Figure 6.9. DonJoy TROM knee brace.....	151

Figure 6.10 – Prototype ankle joint .....	153
Figure 6.11 – Black Diamond contact crampon (BlackDiamond 2013).....	154
Figure 6.12 – DonJoy MaxTrax ROM Walker .....	155
Figure 6.13 - Three families of shoulder braces. Left: McDavid Universal Shoulder Support. Center: Cadlow Shoulder Stabilizer. Right: DonJoy Quadrant Shoulder Brace .....	157
Figure 6.14 - Left: DonJoy Hinged Elbow Guard. Right: DonJoy IROM Hinged Elbow Brace .....	158
Figure 6.15 - Options for resistive elements on an exoskeleton-type brace. Left: torsion spring. Right: concept drawing using linear extension springs.....	159
Figure 6.16 – Spiral torsion springs.....	159
Figure 6.17 - Complete right side of the upper body. All gray padded portions are part of the COTS DonJoy shoulder brace .....	161
Figure 6.18 - (Left) elbow joint; (center) shoulder flexion joint; and (right) shoulder abduction joint, with shoulder flexion joint visible in the background. ....	161
Figure 6.19 – Block diagram on pneumatic controller .....	162
Figure 6.20 – Early Prototype Controller .....	163
Figure 6.21 – Pneumatic control system.....	164
Figure 6.22 – Controller schematic.....	165
Figure 6.23 – Pneumatic system using a solenoid (system shown for one actuator).....	167
Figure 6.24 – Pneumatic system using a pressure regulator (system shown for on actuator) .....	167
Figure 6.25 – The hydraulic fluid leak originates from the RSST elbow joint.....	174
Figure 6.26 - The leak at the elbow is bypassed by connecting the hydraulic input and output lines at the shoulder. ....	174
Figure 6.27 - Left: knee angle calibration (note protractor and plumb line). Right: hip flexion/extension torque calibration (note weight hanging from ankle).....	175

## List of Tables

Table 3.1 – EVA S3 range of motion and torque requirements (Gilkey 2012) .....	39
Table 3.2 – Hip torque and range of motion requirements used.....	40
Table 3.3 – Actuator comparison (Pratt, Krupp et al. 2002, Pons 2008, Chen and Liao 2010).....	44
Table 3.4 – Hip Flexion/Extension Actuator Placement Concepts (Side view). .....	50
Table 3.5 – Actuator selection table for hip actuators .....	58
Table 3.6 – Tests, results, and actions taken during the prototype testing.....	83
Table 4.1 – Labels corresponding to Figure 4.20. ....	111
Table 4.2 – Risks and mitigation strategies for human testing of the EVA S3.....	119
Table 6.1 – Example COTS braces that might be considered for passive joint resistance (Mosher, Mitchell et al. 2006) .....	156
Table 6.2 – Pressure Regulators Tested.....	169

## List of Abbreviations

ABS	Acrylonitrile Butadiene Styrene
ARGOS	Active Response Gravity Offload System
BLEEX	Berkeley Lower Extremity Exoskeleton
EMU	Extravehicular Mobility Unit
EVA S3	Extravehicular Activity Space Suit Simulator
eZLS	enhanced Zero-gravity Locomotion Simulator
FEA	Finite Element Analysis
HAL	Hybrid Assistive Limb
ISB	International Society of Biomechanics
MIT	Massachusetts Institute of Technology
NASA	National Aeronautics and Space Administration
PID	Proportional Integral Derivative
PMA	Pneumatic Muscle Actuator
RSST	Robotic Space Suit Tester

# 1. Introduction

There is a fundamental yearning that touches the heart of mankind: the need to explore and, in the words of Gene Roddenberry, “to boldly go where no man has gone before.” It is this drive that has inspired some of the greatest historic events and why our species still values achievements of “firsts” above all else. These “firsts” can be explorations of the mind, such as Einstein’s proposed theory of special relativity, or feats of human ingenuity, like Oliver and Wilber Wright’s first flight of a powered aircraft. Perhaps the most astounding “first” of the 20<sup>th</sup> century was when Neil Armstrong first set foot on the moon. Space exploration continues to present challenges that stretch the capabilities of mankind. The greatest historic event of the 21<sup>st</sup> century may be when the first human sets foot on another planet, Mars. While the path to accomplishing this feat is uncertain, it is unanimous that substantial technology improvements are needed to enable such a feat. One such technology is the space suit. The garment worn in extreme environments is so intimate to the explorer. Space suits provide needed oxygen, pressure, thermal management, and communication equipment. However, the isolation from the natural world that affords the explorer the ability to survive also comes at a cost. Mobility in a space suit is severely limited. The joints of a gas-pressurized space suit resist bending motions and increase the metabolic costs of a mission. It is important to understand these suit induced limitations in order to balance tradeoffs in the design of better space suits, and to comprehend the impact of these limitations during exploration missions.

## 1.1 Motivation

The space suits currently in service use gas pressurization to provide a breathable atmosphere and to protect astronauts from exposure to the vacuum of space. One of the major limitations of gas pressurized space suits, such as the United States’ Extravehicular Mobility Unit (EMU) or the Russian ORLAN space suit, is that the joints significantly resist motion (Skoog, Abramov et al. 2002, Thomas and McMann 2006). This resistance, also known as imposed joint torque, is the result of structural resistance, volume changes, and pressure effects (Holschuh, Waldie et al. 2009). Multiple methods are used to quantify space suit joint torques. Methods include robotic testing (Schmidt, Newman et al. 2001, Meyen, Holschuh et al. 2011), manually pulling a limb of a suited subject with a fish scale attached at a fixed distance from the joint to calculate torque (Bowen



1968, Matty and Aitchison 2009) and making suited motions while fixed to a dynamometer (Morgan and Center 1996). The joint torques of space suits have a significant effect upon human strength and metabolic costs when suited (Carr and Newman 2007 A and B). NASA quantified differences in suited and unsuited strength of the EMU to aid the decisions of mission planners and human factors engineers (Morgan and Center 1996). Space suit stiffness adds further complexity to the biomechanics of human locomotion than simply reducing strength. Carr and McGee proposed the Apollo number to describe the role of space suit self-support for when the run-walk transition will occur in reduced gravity (Carr and McGee 2009). In 2010 NASA published a technical report on simulated partial gravity comparisons for suited and unsuited locomotion (Norcross, Clowers et al. 2010) following previous research on suited locomotion (Newman and Alexander 1993, Newman, Alexander et al. 1994, Carr and Newman 2005, Carr and Newman 2007 A and B).

The significant reductions to mobility and metabolic efficiency caused by the use of a space suit underlie the necessity of training astronauts and simulating missions under similar physiological constraints. In NASA's underwater Neutral Buoyancy Laboratory, astronauts train wearing an EMU weighted to be neutrally buoyant in the large pool. This controlled environment is one of the few places where a full space suit can be used for training. Weight, cost, and availability make the EMU prohibitive to use in many other environments. An EMU weighs approximately 125 kg (275 lb) (Thomas and McMann 2006). The cost of a space suit is hard to determine because of the high cost of research and development. ILC Dover estimated that a spare EMU cost 2 million dollars (ILC Dover 1994), while more recent estimates put the cost at 12 million dollars (Freudenrich 2011). Development cost for a next generation suit are estimated to be between 300 and 700 million dollars (Harris 2001). Because of the high costs, a limited number of spacesuits are made and even fewer are available for training and experimental purposes.

The Neutral Buoyancy Laboratory is not the only space simulation environment NASA uses, but it is the only environment that consistently operates with astronauts in pressurized space suits. Some examples of other space environment simulators include the enhanced Zero-g Locomotion Simulator (eZLS), and the Active Response Gravity Offload System (ARGOS). Research in these environments would benefit greatly from the creation of a device that can accurately simulate the

joint torques felt by wearing a space suit, but is also cheaper, lighter, and less operationally complicated than using a pressurized space suit.

The eZLS is a vertical treadmill that supports a subject from their back with bungees. A harness pulls the body towards the treadmill to simulate exercise in different gravity levels (Perusek, DeWitt et al. 2007). The eZLS is based on previous successful work of Cavanagh, Polliner (1989) and the original supine suspension system at NASA Langley Research Center. The eZLS is being used to assess intravehicular exercise countermeasures in space, but with a device that could mimic the constraints of a space suit. The eZLS could be used to simulate planetary EVA performance.



Figure 1.1 - The eZLS (Perusek, DeWitt et al. 2007)

The ARGOS at NASA's Johnson Space Center is a large weight offload system similar to an overhead bridge crane. ARGOS is used to simulate surface operation studies, crew training, and technology development. (NASA 2013). A space suit simulator could add realistic physiological constraints to the simulation when a space suit is not available.



Figure 1.2 - The ARGOS (NASA 2013)

The utility of both of these space environment simulators could be improved with the addition of a space suit simulator. A few space suit simulators have been built to emulate the stiffness of space suit joints, but these designs have primarily focused on the knee joint. A space suit simulator for the EMU knee joint (Figure 1.3) was built by researchers at ATA Engineering (San Diego, CA) and tested on the Robotic Space Suit Tester (RSST) in the MIT Man Vehicle Laboratory (Schaffner 2007).

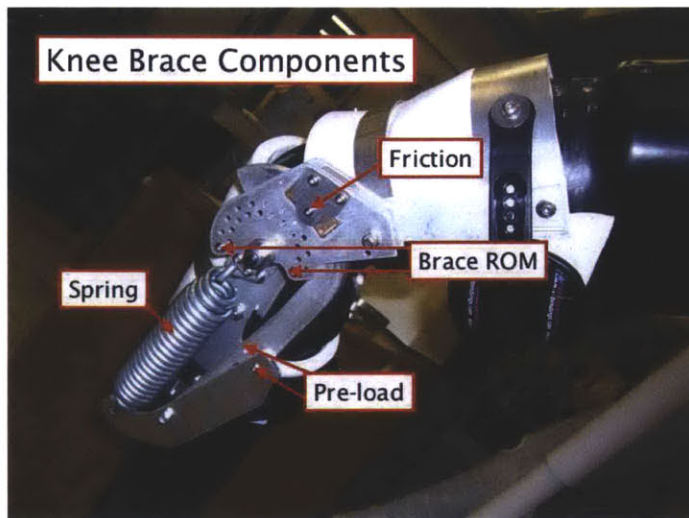


Figure 1.3 - Passive Knee Space Suit Simulator (Ferreira 2007)

The ATA-MIT simulator was comprised of a knee brace attached to a spring with an adjustable pre-load. The simulator was able to simulate the hysteresis trend observed in space suit joints but was limited in its ability to fine tune the system. The MIT Man Vehicle Laboratory developed a knee space suit simulator that used fiberglass springs connected between a hip harness and a pair of modified bicycling shoes. The exoskeleton simulated nonlinear springs in parallel with the legs (Carr and Newman 2008).

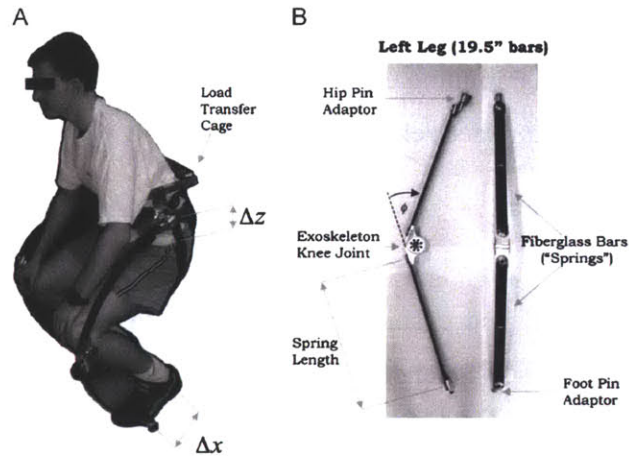


Figure 1.4 - A lower body exoskeleton to simulate space suit locomotion(Carr and Newman 2008)

To improve space suit simulator fidelity and adjustability, engineers from Aurora Flight Sciences (Cambridge, MA) and the MIT Man Vehicle Laboratory created an actively controlled space suit simulator for the knee joint (Duda, Newman et al. 2011) (Figure 1.5).

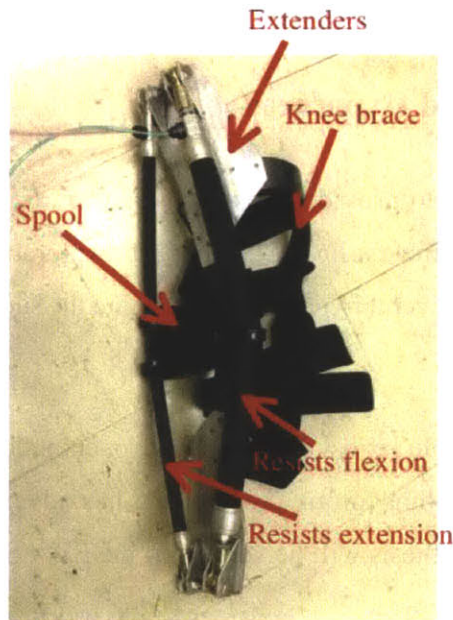


Figure 1.5 - Knee joint prototype (Duda, Newman et al. 2011)

This knee simulator uses pneumatic McKibben actuators, often referred to as pneumatic muscles, to vary the torque resisting motion. The knee simulator was tested on MIT's Robotic Space Suit

Tester. The simulator produces a similar torque pattern to EMU data except for an error in the vertical offset attributed to a programming error. This research demonstrated the viability of using McKibben actuators in future actively controlled space suit simulators.

## **1.2 Contribution**

To improve the accessibility of space suit like constraints to the space biomedical research community, MIT and Aurora Flight Sciences developed the Extra Vehicular Activity Space Suit Simulator, also known as the EVA S3. This device is an exoskeleton with actively controlled resistance to joint movements. The goal of this device is to accurately simulate the joint torques of space suits, while being significantly cheaper, lighter, easier to put on, and more accessible than a modern space suit. The EVA S3 can reasonably simulate the torque and range of motion of modern space suits, with the hope that future space suits will have improved mobility and will also be able to be accurately represented by the EVA S3. The focus of and contribution of this thesis to the EVA S3 is the creation of the hip joint and backpack components of the exoskeleton, including the actuation method, torque transmission, hip joint component design, testing, and modifications.

## **1.3 Problem Statement and Hypothesis**

The EVA S3 is a tool designed to provide a research platform for space biomedical researchers and physiologists studying the metabolic costs of space exploration, improving space suits, or developing mission scenarios. Several hypotheses determine the success of the EVA S3 to varying degrees.

Hypothesis 1: A programmable exoskeleton using pneumatically powered actuators can effectively simulate space suit joint torque profiles and has advantages in fidelity over passive space suit simulators. This hypothesis will be verified if the EVA S3 can

- Match each joint to Extravehicular Mobility Unit (EMU) joint torque data within a root mean square (RMS) error of 10% for the hip, knee, and ankle joints.
- Achieve the range of motion (ROM) requirements outlined in the survey of studies of space suit joint mobility.
- Simulate patterns of hysteresis often observed in space suit joint torques.

Hypothesis 2: A programmable exoskeleton can be designed to weigh significantly less than the EMU to allow testing research environments that are not submerged (such as NASA's Neutral Buoyancy Laboratory) or require attachment to a crane or other support.

- This weight will be defined by what is considered acceptable for backpacking: approximately 27.2 kg (60 lb).

Hypothesis 3: The cost of a fully programmable exoskeleton will be significantly cheaper than a space suit, which could allow for greater researcher access to space suit like constraints. This can be tested by

- Determining if the whole cost of materials and development for an effective space suit simulator is 10% of the cost of a production space suit.

## **1.4 Thesis Outline**

This thesis is comprised of 5 chapters. Chapter 1 covers the motivation for creating the EVA S3, including background on joint torque testing and space suit simulators. The hypotheses are also covered in Chapter 1. Chapter 2 elaborates on previous exoskeleton work, with a special focus on resistive exoskeletons and pneumatically driven exoskeletons. Chapter 3, the Methods section, details the development of the hip portion of the exoskeleton. It describes the process of developing actuation and torque transmission methods as well as the conceptual design process. The focus then shifts to the first iteration design and results, followed by the final design and construction process. The final part of the methods section details the data collection procedures using MIT's Robotic Space Suit Tester (RSST), affectionately known as M. Tallchief. Chapter 4 is the Results and Discussion. In this chapter, the data from the robotic space suit testing is presented, as well as the final design of the exoskeleton, including the ankle, knee, and shoulder designs in addition to the hip design. The control system and control system hardware will also be described in this section. Conclusion and Recommendations, Chapter 5, reviews the major results of the work, evaluation of the hypotheses, limitations, future work, and the broader impacts of the study.



## 2. Background

### 2.1 Introduction to Exoskeletons

Some define exoskeletons as a wearable robot, and others define them as simply an orthotic that actively strengthens the body. The term exoskeleton is borrowed from biology and is used to describe a shell or carapace of an animal that provides protection or support, a characteristic trait of invertebrate arthropods. Perhaps one of the earliest depictions of an exoskeleton device to augment a human was in an early 19<sup>th</sup> century painting by Robert Seymour that parodied the idea that steam engines were unlocking the potential to power all sorts of new contraptions.

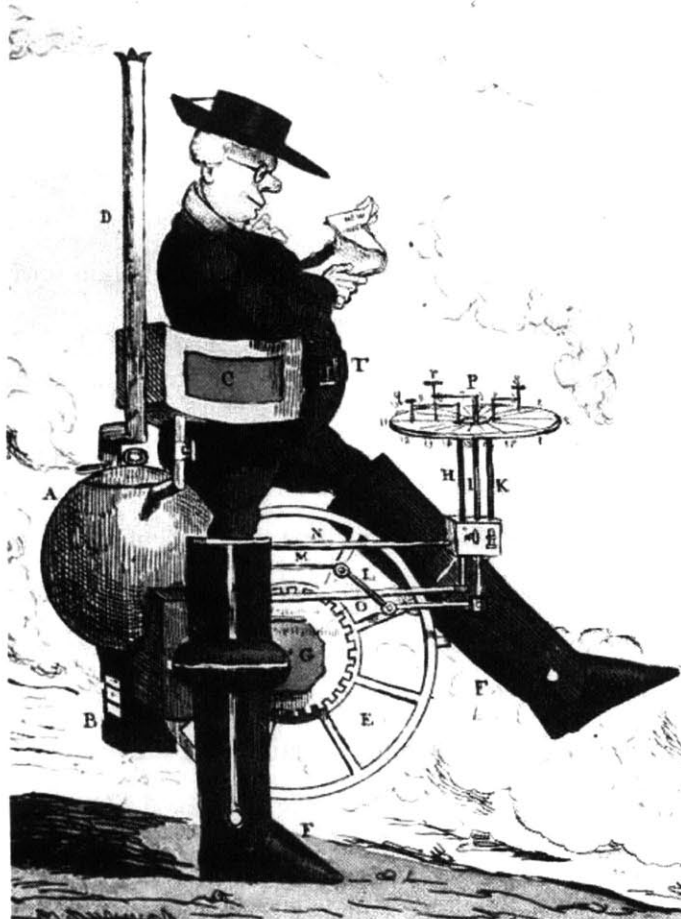


Figure 2.1- From the early 19<sup>th</sup> century painting “Locomotion” by Robert Seymour. Perhaps the earliest depiction of an exoskeleton (Hoggett 2010)



Exoskeletons range in purpose, but generally they are used to enhance human function by making human limbs stronger, faster, or more accurate. Sometimes this enhancement is for rehabilitative purposes and other times for pure enhancement of human performance. Pratt, Krupp et al. (2004) distinguish an exoskeleton from other extensions of the human body such as a car by clarifying that an exoskeleton has mechanisms that correspond to natural locomotion. An ideal exoskeleton is completely transparent to the user. The exoskeleton seamlessly integrates with the user and is relatively unnoticed. Pratt further elaborates on what makes an ideal exoskeleton transparent. It must successfully

- Determine the user's intent
- Apply forces where appropriate
- Present low impedance, i.e. "get out of the way" (Pratt, Krupp et al. 2004)

These three principles guided the design of the EVA S3. Position sensors and signal filters determined the user's intent, actuators and torque transmission methods were selected to apply the appropriate forces, and the joints were designed to minimize the impedance while the joints were unpowered.

## **2.2 Early Exoskeleton History**

The early studies on exoskeleton systems to augment human performance began in the early 1960's. The Cornell Aeronautical Laboratory developed the concept of a Man Amplifier (Clark, DeLeys et al. 1962). Citing that human strength paled in comparison to his advanced intellect, the laboratory developed concepts for a Man Amplifier that could theoretically lift 6670 N (1,500 lb). Loading heavy munitions in remote environments was presented as a possible use for the system. Figure 2.3 is a drawing that features an early concept of the Man Amplifier.

## MAN AMPLIFIER

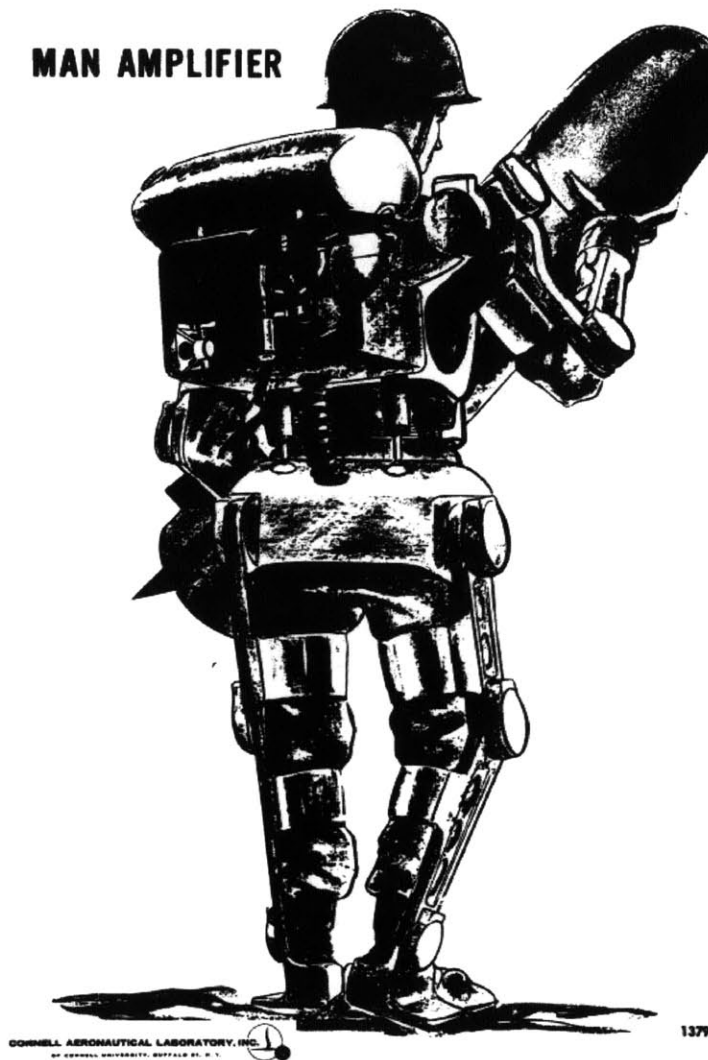


Figure 2.2- Artist's conception of Man Amplifier (Clark, DeLeys et al. 1962)

The Man Amplifier concept had a self-contained power supply and a support structure constructed of aluminum alloy. The whole system, excluding the operator, was estimated to be 181 – 226 kg (400–500 lb). The weight was considered advantageous as it improved the system's static stability during lifting operations. Hydraulic servomechanisms were selected because they provide high torque-speed characteristics and maximum torque at stall, allowing the exoskeleton to move heavy objects with reasonable speed as well as to hold them in place for long periods of time. Engineering challenges included size adjustability, range of motion, safety, ease of donning and doffing, and high (25 to 30 horsepower) power requirements (Clark, DeLeys et al. 1962). Following the

conceptual development of the Man Amplifier, the Cornell Aeronautical Laboratory developed the Myotron (Miller 1968) a servo-controlled, 2-axis arm exoskeleton with integral force and position transducers. This exoskeleton was designed to take dynamic measurements of skeletal muscle forces and behavior, while mounted to a table. Motors to drive the servos were stored underneath the table, and power was transmitted to the joint gear box by a flexible shaft. A force-sensing ring around the wrist determined the forces that the arm was producing. The control system was implemented with analogue circuits and had two control modes: position following and force following. The researchers cautioned that a full body 33-axis version was technically possible at the time; however, the operational complexity and data processing challenges would reduce its utility (Miller 1968).

The first known powered, full body exoskeleton was the Hardiman I Prototype, initiated by a joint Army-Navy program from 1965-71 and developed by General Electric (Makinson 1971). The Hardiman I consisted of two connected exoskeletons: a master exoskeleton that attached directly to the operator, and a slave exoskeleton that followed the intent of the master and augmented strength. The exoskeleton force was generated with 30 hydraulic actuators. One arm was tested to lift weights of 340 kg (750 lb) (Makinson 1971). However, the exoskeleton was not without problems. The Hardiman I was fully assembled but never walked unsupported. According to the final report, “Activation in both legs simultaneously resulted in violent and uncontrollable motion by the machine”(General Electric Company 1971).



Figure 2.3 - Hardiman 1 Prototype Assembly (Makinson 1971)

### **2.3 Modern Exoskeleton Designs**

In the past fifteen years there has been a resurgence of research on exoskeletons, including studies in the areas of rehabilitation, augmentation, and simulation. Advances in control systems, materials, energy storage, and actuation methods have helped make some of these new designs technically feasible. Some exoskeleton designs have matured and are current commercial products. A notable research exoskeleton is the Berkeley Lower Extremity Exoskeleton (BLEEX). The purpose of BLEEX is to offload the weight of a loaded backpack to the frame of the exoskeleton. Potential applications include any job in which heavy loads need to be transported by foot. The joints are actuated by hydraulic cylinders. Feedback is provided by pressure sensors in the foot, an

accelerometer and inclinometer mounted on the frame, and force sensors, encoders, and linear accelerometers at each joint. A unique feature of BLEEX is that it carries its own power supply and can carry a load (Zoss, Kazerooni et al. 2006).



Figure 2.4 - The Berkley Lower Extremity Exoskeleton (Zoss and Kazerooni 2005)

The Hybrid Assistive Limb (HAL) exoskeleton is being developed by the University of Tsukuba and the company CYBERDYNE in Japan. The purpose of HAL is to directly assist limb movements. The applications include assisting those with mobility impairments to a training tool for rehabilitation. HAL uses direct current motors to drive the joints based on bioelectrical signals read from sensors on the operator's body. HAL is unique in that it supports motions with multiple joints simultaneously and has an onboard power system (Suzuki, Mito et al. 2007).

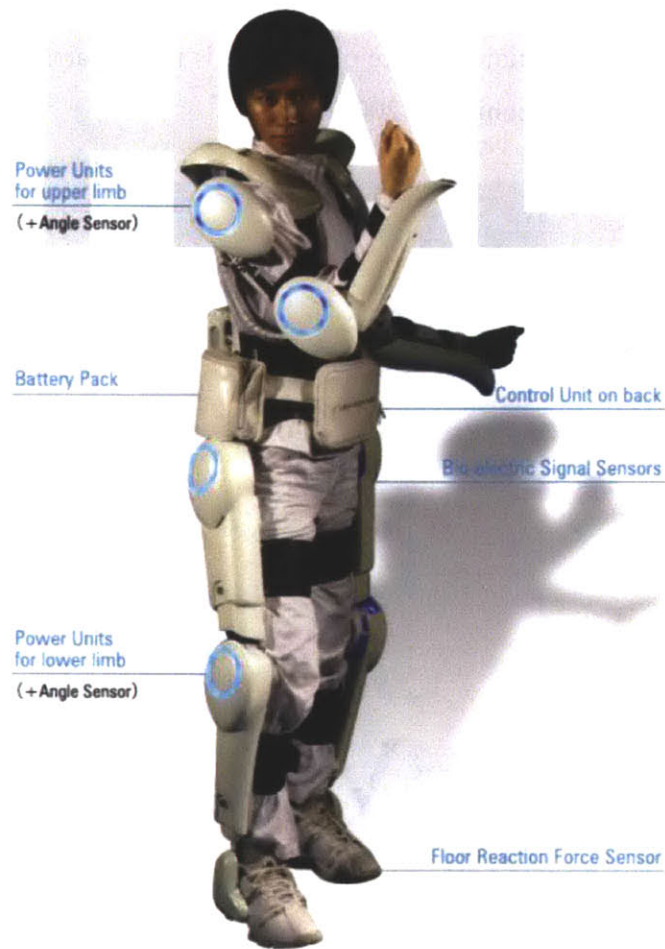


Figure 2.5 - Robot Suit HAL (CYBERDYNE 2013)

Sarcos, a company owned by Raytheon, is creating an exoskeleton called XOS 2. This modern exoskeleton is similar in purpose to the original Hardiman I Prototype by General Electric, though smaller and with a lower predicted carrying capacity. The XOS 2 is a hydraulically actuated, full body exoskeleton, designed to substantially increase the strength of the operator. The current version is tethered to a hydraulic power station. According to Raytheon, the XOS 2 enables the wearer to easily lift 91 kg (200 lb) several hundred times without tiring (Shields 2010).

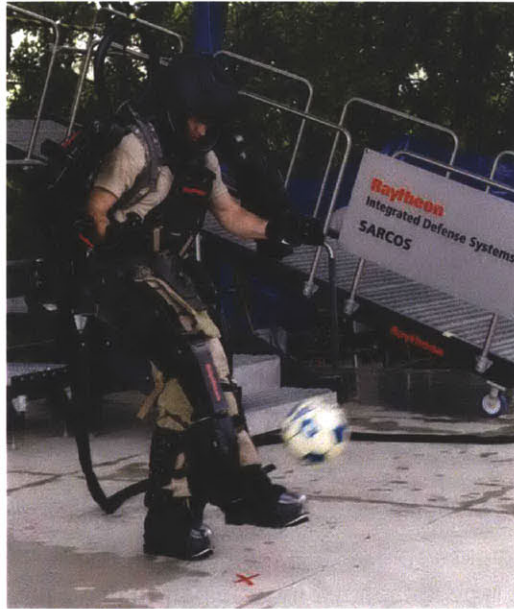


Figure 2.6 - Raytheon SARCOS XOS 2 (Guizzo 2011)

## 2.4 Pneumatically actuated exoskeletons

Pneumatic McKibben actuators, also known as pneumatic muscle actuators (PMA), were developed by J. L. McKibben in the 1950's to power orthoses of polio patients. McKibben Actuators are made out of a rubber tube reinforced with a woven fiber mesh that is crimped on both ends. When the tube is pressurized, the mesh expands radially and contracts axially. McKibben actuators demonstrate similar force-length properties to that of Hill muscle model (Klute, Czerniecki et al. 1999). McKibben actuators have been used in various orthotic devices. The advantage of these actuators for use in exoskeletons is their compliant behavior, extremely low weight, and medium bulk. The actuators, like muscles, can only produce force during contraction; therefore, to achieve bi-directional torques the actuators need to be arranged in an antagonistic configuration.



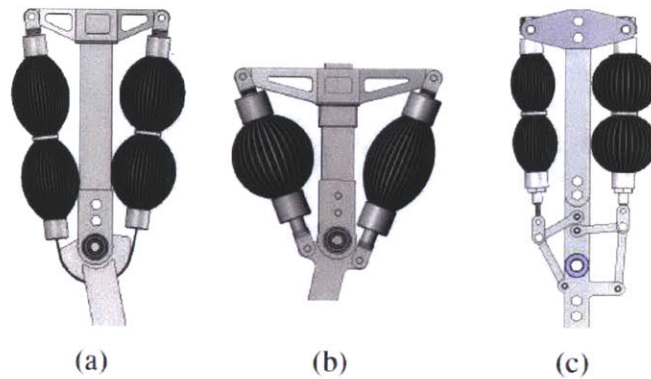


Figure 2.7 – Some possible antagonistic actuator configurations (Beyl, Van Damme et al. 2008)

Beyl et al. selected a four bar type antagonist muscle pair to drive the linkages on a knee joint of a robotic gait rehabilitation exoskeleton. This exoskeleton used a tethered air source to minimize weight. This type of actuator was specifically to “provide the necessary soft touch for better human-robot interaction.” The exoskeleton was used to validate a proxy-based sliding mode control strategy as opposed to a proportional-integral-derivative (PID) controller (Beyl, Van Damme et al. 2008).

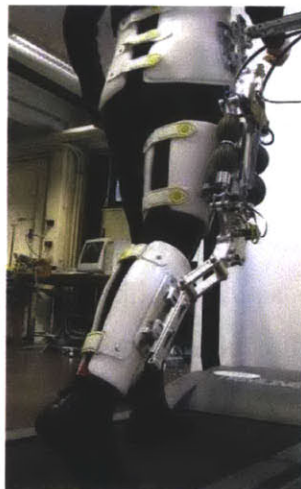


Figure 2.8 – A pneumatic rehabilitative exoskeleton on a treadmill (Beyl, Van Damme et al. 2008)

On some joints of the human body it is possible to place antagonist actuators on opposite sides of the joint to further reduce complexity and weight. The University of Michigan created a powered



orthosis for the human ankle joint with one actuator that induces dorsiflexion and another for planter flexion. The actuators were mounted to a carbon fiber frame that was molded to the subject's foot and lower leg. The researchers tethered the system to an air source to further reduce weight. The purpose was to test proportional myoelectric control of the system using electromyography (EMG) sensors to detect muscle activation. The orthosis provided 50% of the peak plantarflexion net muscle moment and 400% of the peak dorsiflexion net muscle movement during unassisted walking (Ferris, Czerniecki et al. 2005).

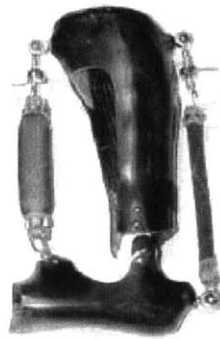


Figure 2.9 – A ankle foot orthosis powered by pneumatic muscles (Ferris, Czerniecki et al. 2005)

## 2.5 Summary

Exoskeleton designs have been steadily evolving since their formal conception in the 1960's. Initially conceived to strengthen soldiers for moving heavy munitions, the technology is now widely applied for rehabilitation, simulation, and research. Modern exoskeletons take advantage of digital control algorithms, onboard microcontrollers, novel materials, and a vast array of actuations and energy storage devices. These advancements have established the groundwork for the development of the EVA S3, which utilizes microcontrollers, carbon fiber composites, and pneumatic actuators.

### **3. Methods**

The EVA S3 provides an affordable and easily modified alternative to using a real space suit for research and training. This section describes the design process of the EVA S3, with a particular focus in the design of the hip joint. The joint torque and position requirements are described, followed by early conceptual development. Once the concepts were developed, power transmission methods were selected and design requirements, goals, and constraints were used to create a more developed concept. The first prototype was constructed, and lessons learned were used to alter the design of the final product. Calculations verified the design parameters for torque transmission and range of motion. Finite element analysis was used to validate and improve the structural design of the exoskeleton. The exoskeleton prototypes were evaluated through qualitative fit checks and quantitative testing while mounted to the Robotic Space Suit Tester.

#### **3.1 Requirements**

The first step in any design process is to define design requirements and project goals. The purpose of this project is to create a robotic space suit simulator that can actively control the joint torques felt by the user. Active control is viewed as a necessary tool to accurately simulate the hysteresis observed in space suit joint torques as well as to facilitate adjustments to simulate different space suits (Duda, Newman et al. 2011). The joint torques should be able to be adjusted to simulate any current space suit design, as well as future designs. It is assumed that future suit designs will be an improved version of current suits; therefore, the requirements were developed by looking at the maximum range of torques of current operational space suits such as the Extravehicular Mobility Unit (EMU) and concept suits such as NASA's Mark III.

The accepted International Society of Biomechanics (ISB) standard sign convention was adopted to establish torque and position conventions. For example, NASA Standard 3000 indicates that the neutral point (0 degrees) for shoulder flexion is when the arm is aligned to the trunk (NASA 1995), but a NASA report on EMU mobility assigned the neutral point to be perpendicular to the trunk (Morgan and Center 1996).

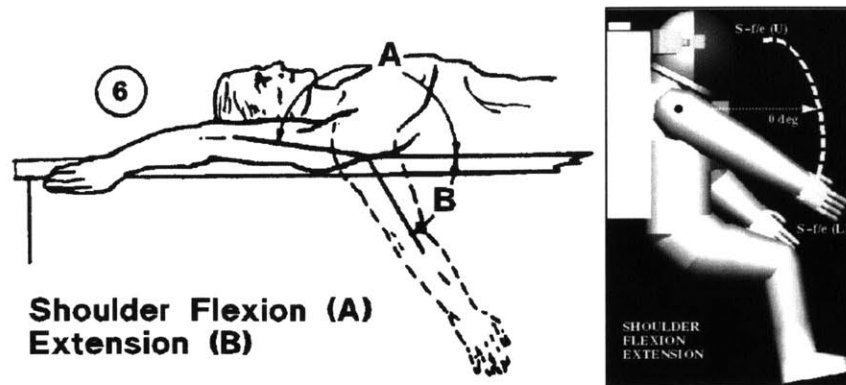


Figure 3.1 – Differences in joint angle sign convention. (A) Neutral point aligns with trunk (NASA 1995)  
 (B) Neutral point perpendicular to trunk (Morgan and Center 1996)

Figure 3.2 is the convention selected for the design of the EVA S3. For a particular joint, the blue limb represents the fixed reference, and the red limb is the moving reference. The angle is measured as the angle between the axis oriented axially through the blue reference and the axis through the red reference. Positive angles are measured in the direction of the black arrow in the diagram.

The lower body joints were selected for active control and upper body joints were designed for passive control due to the scope of the study. Lower body movements simulated include hip abduction, hip flexion, knee flexion, and ankle flexion. Upper body joints simulated include elbow flexion, shoulder abduction, and shoulder flexion. Torso rotation, torso anterior flexion, wrist rotation, hip rotation, ankle inversion, and ankle rotation were neglected because of poor reference data, added complexity, and the minimal perceived gain in simulator fidelity from adding calibrated restrictions to those motions.

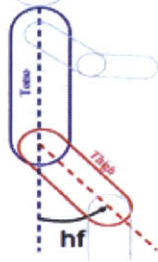
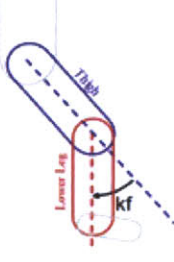
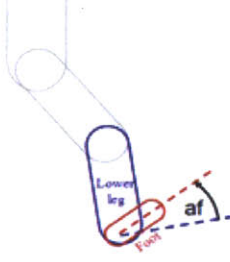
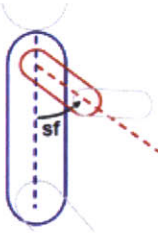
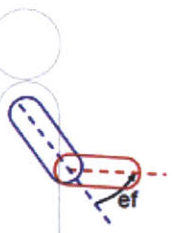
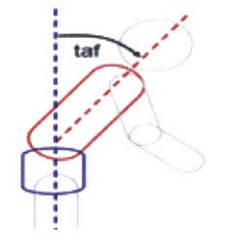

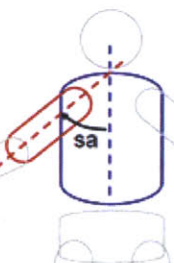
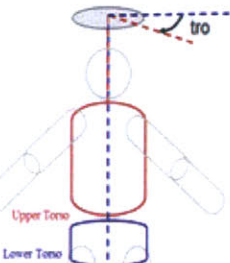
 <p><b>Hip Flexion (hf)</b> Positive angle: flexion (leg moves up)</p>	 <p><b>Knee Flexion (kf)</b> Positive angle: flexion (lower leg moves up)</p>	 <p><b>Ankle Flexion (af)</b> Positive angle: flexion (foot moves up)</p>
 <p><b>Shoulder Flexion (sf)</b> Positive angle: flexion (arm moves up)</p>	 <p><b>Elbow Flexion (ef)</b> Positive angle: flexion (forearm moves up)</p>	 <p><b>Torso Anterior Flexion (taf)</b> Positive angle: flexion (torso moves forward and down)</p>
 <p><b>Hip Abduction (ha)</b> Positive angle: abduction (leg moves out and up)</p>	 <p><b>Shoulder Abduction (sa)</b> Positive angle: abduction (arm moves out and up)</p>	 <p><b>Torso Rotation (tro)</b> Positive angle: torso rotates to the right</p>

Figure 3.2 – Space Suit Simulator (EVA S3) Joint Convention (Gilkey 2012)

Space suit torque and angle requirements are critical to determining what actuators, torque transmission methods, and structural designs can be used. Table 3.1 is a table of torque and angle requirements compiled by Gilkey 2012 from various space suit joint testing literature.

Table 3.1 – EVA S3 range of motion and torque requirements (Gilkey 2012)

Joint	Minimum Angle (deg)	Maximum Angle (deg)	Minimum Torque (N-m)	Maximum Torque (N-m)
<b>Knee Flexion/Extension (KF)</b>	0	146	-40	32
<b>Elbow Flexion/Extension (EF)</b>	0	166	-18	15
<b>Shoulder Flexion/Extension (SF)</b>	-88	217	-25	32
<b>Shoulder Abduction/Adduction (SA)</b>	-25	110	-32	36
<b>Humerus Rotation (HR)</b>	-131	97	-15	24
<b>Shoulder Interior/Exterior Transverse Rotation (SI)</b>	-151	57	-23	32
<b>Hip Flexion/Extension (HF)</b>	-20	148	-41	72
<b>Hip Abduction/Adduction (HA)</b>	-30	45	-52	165
<b>Thigh Rotation (TR)</b>	-49	45	-4	3
<b>Torso Anterior Flexion/Extension (TAF)</b>	-30	55	-34	72
<b>Torso Lateral Flexion (TLF)</b>	-30	30	N/A	N/A
<b>Torso Rotation (TRO)</b>	-46	46	-7	11
<b>Ankle Flexion/Extension (AF)</b>	-91	42	-15	9
<b>Ankle Inversion (AI)</b>	-33	30	N/A	N/A
<b>Ankle Rotation (AR)</b>	-47	55	-1	1

During the design process, an incomplete version of the space suit torque and range of motion performance database was mistaken as the final database. Joint torque requirements for the hip were developed from this incomplete database, resulting in a design optimized for reduced torque values. The values used for hip flexion/extension and hip abduction/adduction were from a NASA suit performance comparison study that used a fish scale type method for measuring joint torque in a variety of empty, pressurized space suits. The requirements did not include data collected from robotic space suit testing. Robotic space suit testing records much higher and more repeatable torque values. The torque and range of motion requirements used to develop the EVA S3 hip joint are listed in Table 3.2.

Table 3.2 – Hip torque and range of motion requirements used

Joint	Minimum Angle	Maximum Angle	Minimum Torque	Maximum Torque
Hip Flexion/Extension	-20°	90°	-28 N m	31 N m
Hip Abduction/Adduction	-30°	45°	-32 N m	43 N m

## 3.2 Conceptual Development

The primary focus of this thesis is the design of the exoskeleton hip joints. This includes two main components: the structural design and the method of torque transmission. The focus of the structural design is to create a frame that interfaces well with the human body in order to safely hold the exoskeleton components in place. Secondary goals are to minimize the weight and bulk of this structure so that the exoskeleton is efficient and usable. Considerations were made for methods to interface the hip portion of the exoskeleton with the other components and to ensure that the entire exoskeleton is easily donned and doffed.

### 3.2.1 Actuator Selection

Actuator selection was one of the first decisions made for the EVA S3 architecture. It is essential to select this early on, since the actuation type affects the design of every component of the exoskeleton structure. Almost every actuator type has been used in exoskeletons, including electric motors, hydraulic actuators, pneumatic actuators, magneto rheological fluids, and passive spring components.

#### 3.2.1.1 Hydraulic Actuators

Hydraulic actuators convert hydraulic pressure into force in linear hydraulic actuators, and directly into torque in rotary hydraulic actuators. Hydraulic actuators are often selected because they have high force output and are relatively compact. A downside to using hydraulic actuators is the use of hydraulic fluid can increase maintenance costs. They also have poor low force performance due to stiction. In exoskeletons, linear hydraulic actuators are typically mounted parallel to the limbs and apply torque to joints by acting on cantilevers and linkages. Rotary hydraulic actuators can be fixed in locations that align with the axis of the joint. Some examples of hydraulically actuated exoskeletons include the Berkeley Lower Extremity Exoskeleton (Zoss, Kazerooni et al. 2006),

the Lockheed Martin HULC (Lockheed Martin 2008), the Sarcos XOS 2 (Guizzo 2011), and the original Hardiman I by General Electric Company (1971).

### **3.2.1.2 Electric Actuators**

Electric actuators are popular in the exoskeleton community and have been implemented in various configurations. The robot suit HAL by CYBERDYNE uses direct current motors to apply assistive torque to limbs at their axis of rotation (CYBERDYNE 2013). Yobotics Inc. (Cambridge, MA) developed the RoboKnee, an exoskeleton to assist walking. The RoboKnee uses a series elastic actuator for force control (Pratt, Krupp et al. 2004). Series elastics actuators are linear electric actuators coupled with an inline spring to reduce the stiffness of the actuator. A position sensor measures deflection and uses Hooke's law to calculate the force exerted by the actuator (Pratt, Krupp et al. 2002). This concept has been applied to the Active Ankle Foot Orthoses by researchers at MIT (Blaya, Newman et al. 2002). The Florida Institute for Human and Machine Cognition (IHMC) coupled an elastic element with electric motors in the rotary series elastic actuators used in the IHMC Mobility Assist Exoskeleton (Hian Kai, Noorden et al. 2009). Series electric elements add compliance to an exoskeleton for added operator safety. Electric actuation methods generally produce high to medium torques but are often heavy and bulky.

### **3.2.1.3 Magnetorheological fluids**

Magnetorheological (MR) fluids are fluids with magnetic particles suspended in a carrier fluid. When a magnetic field is applied through the fluid, the magnetic particles align with the direction of the field. A shear stress is required to disrupt the particle chain. These fluids have been incorporated into dampers in exoskeleton joints in order to vary resistance of motion or to completely prevent joint motion. Researchers at MIT developed a knee prosthesis that used a MR break to control the damping of a knee prosthesis to adapt to a user's gait cycle. The device was able to successfully control early stance dampening. An advantage of the MR break design is that it had low power consumption and could be used for an entire day without needing a battery recharge (Herr and Wilkenfeld 2003). Researchers at the Chinese University of Hong Kong developed a knee exoskeleton that uses an electric motor attached to an MR actuator as an

adjustable break and clutch for the motor. They found that the MR actuator worked well at transferring torque with low power consumption (Chen and Liao 2010).

#### **3.2.1.4 Pneumatic Actuators**

Pneumatic actuators use pressurized air to apply forces to a system. Pneumatic cylinders, McKibben actuators, and pneumatic billows actuators are some examples of pneumatic actuators. Pneumatic actuators are popular in exoskeleton designs because of their inherent compliance (air is a compressible fluid), clean working fluid (compared to hydraulic fluids), and light actuator weight. Pneumatic cylinders convert air pressure into force at the cylinder head that drives a piston. McKibben actuators are comprised of a rubberized weave that expands radially and contracts axially when pressurized. An example of pneumatic cylinders used in an exoskeleton is Boston University's bilateral pneumatically powered hip exoskeleton (Lewis and Ferris 2011). McKibben actuators have been used exoskeleton designs such a quadruple actuator ankle (Jamwal, Shengquan et al. 2010), a dual antagonistic actuator ankle (Ferris, Czerniecki et al. 2005), and in a serially linked quad actuator knee (Beyl, Van Damme et al. 2008). An in-depth discussion of pneumatic actuators and exoskeletons is in Section 2.4.



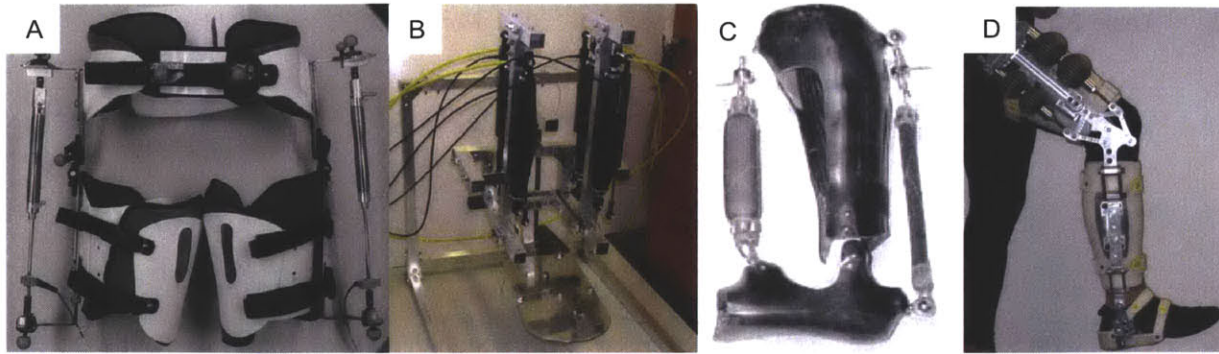


Figure 3.3 – Various pneumatic exoskeleton designs. (A) A dual pneumatic cylinder hip exoskeleton (Lewis and Ferris 2011). (B) Quadruple McKibben actuator ankle exoskeleton (Jamwal, Shengquan et al. 2010). (C) Dual antagonistic McKibben actuator ankle exoskeleton (Ferris, Czerniecki et al. 2005). (D) Serially linked quad McKibben knee exoskeleton (Beyl, Van Damme et al. 2008).

### 3.2.1.5 Final Actuator Selection

The actuator choice was made on the basis of what actuator type can be used to create a system with both low bulk and low weight. Bulk should be minimized so that movement is not encumbered by extraneous spatial restrictions that are not observed in a real space suit. More bulk can also offset the center of mass and moment of inertia to a position that is more unlike that of a space suit. A suit that is too bulky may also interfere with the ability to interface the suit with systems such as the eZLS and the ARGOS; therefore, the EVA S3 structure was designed with these constraints in mind. Weight should be minimized for multiple reasons. The first is that lower weight improves the ability of subjects to don and doff the exoskeleton with minimal assistance from other people. When donned, the exoskeleton is able to support some of its own weight reducing overall weight which also helps reduce the remaining load on the operator. Low weight reduces unwanted torques caused by weight as the user walks or kneels. Table 3.3 was compiled to compare the actuator types in terms of force production characteristics, speed, weight, and bulk to inform the EVA S3 design.

Table 3.3 – Actuator comparison (Pratt, Krupp et al. 2002, Pons 2008, Chen and Liao 2010)

<b>Actuation Type</b>	<b>Maximum Force</b>	<b>Maximum Speed</b>	<b>Low Force Ability</b>	<b>Weight</b>	<b>Bulk</b>
Pneumatic	Medium	Medium	Fair, Stiction	Low	Medium
Hydraulic	High	Medium	Poor, Stiction	Medium	Low
Electric Gear Motor	Medium/High	High	Poor, Stiction	High*	High
Electric Series Elastic Actuator	Medium/High	High	Excellent	High*	High
Magnetorheological (MR) Fluids	High	High	Poor	High*	High

After careful analysis of available actuators and previous exoskeleton designs, it was determined that comparatively, pneumatic actuators have the lowest weight and hydraulic actuators have the lowest bulk for our actuation. Pneumatic actuators were selected because air is safer and easier to handle than hydraulic fluid, and pneumatic McKibben type actuators are flexible and allow for more creative packaging. Pneumatic actuators also exhibit spring like characteristics that are similar to some space suit joint characteristics.

A pneumatic control system can drive a variety of actuators, including McKibben pneumatic muscles, double acting pneumatic cylinders, and single acting pneumatic cylinders. The EVA S3 uses McKibben pneumatic muscles for the majority of the actuation and takes advantage of this actuator interchangeability with the double acting pneumatic cylinders that drive the ankle joint. The McKibben actuators selected are from the company Festo (Brussels, Belgium) and are called “fluidic muscles” by the manufacturer (see Figure 3.4).

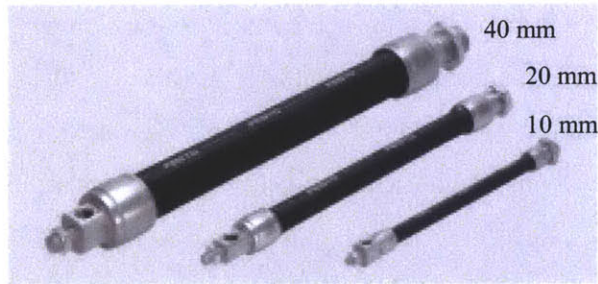


Figure 3.4 – The three sizes of Fluidic Muscles available from FESTO. (FESTO 2011)

The actuators come in diameters of 10 mm, 20 mm, and 40 mm and have a maximum lifting force of 630N, 1500N, and 6000N respectively. The maximum operating pressure is 80 kPa for the 10 mm actuator and 60 kPa for the 20 mm and 40 mm actuators. The contraction length of each actuator is 25% of the nominal length. Actuators can be purchased at a length customized by the millimeter from 40 mm to 9000 mm. Various custom end fittings are also available (FESTO 2011). The diameter dependent force generation capabilities and length dependent contraction lengths are used to determine what actuator specification will produce the required torques and range of motion for a particular design. Figure 3.5 below is a force/displacement function table for a 20 mm diameter, 200 mm long fluidic muscle actuator provided by Festo.

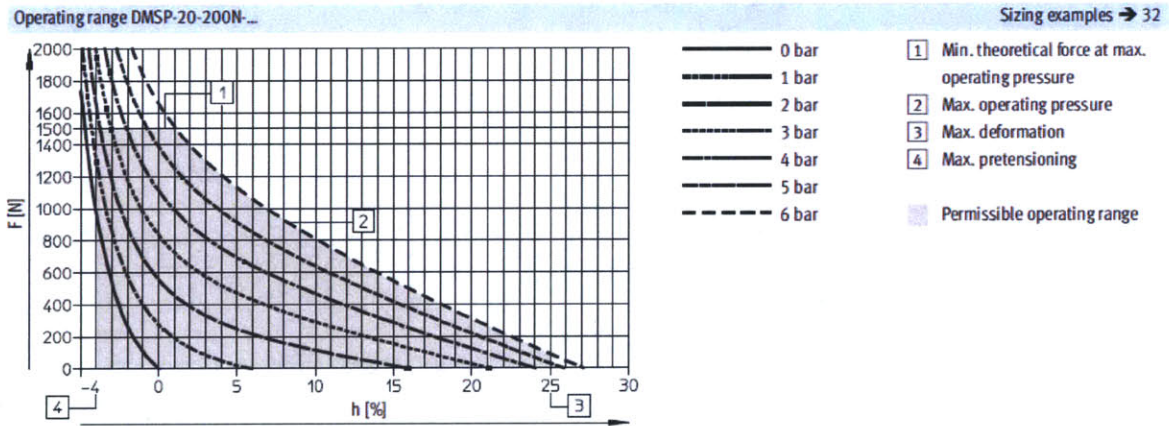


Figure 3.5 – Force/displacement diagram for a Festo Fluidic Muscle with a 20 mm diameter 200 mm length (FESTO 2011).

This diagram provides information on forces that can be achieved at various levels of contraction. Note the nonlinear nature of the force/displacement relationship. The less the actuator is

contracted, the higher forces it can generate. The number four on the graph indicates the point of maximum pre-tensioning. At this point the actuator is actually stretched 4%. Point three on the graph indicates the maximum deformation of 25%, where the actuator is producing virtually no force. This is important to consider during exoskeleton design. Any exoskeleton design must require the maximum force when the actuator is extended to its full length. Because these actuators can only produce force in one direction, the design must also incorporate actuators into antagonistic pairs.

### 3.2.2 Structural Concepts

An early concept of the EVA S3 was to minimize the structural needs by strapping actuators over the user's legs, in a manner that made them look like a pair of jester's pants (Figure 3.6).

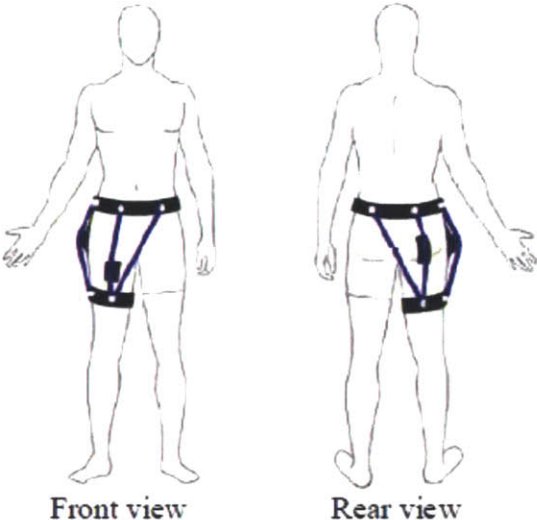


Figure 3.6 – Jester's pants concept (Duda and Hart 2010)

This concept takes advantage of the flexible nature of McKibben actuators to bend them over a spacer held against the skin. The spacer creates an offset for the point where force can be applied. The actuators would be attached between a waist belt and an upper thigh cuff. The actuator endpoints would be arranged to resist motion in hip flexion/extension and hip abduction/adduction. The advantage of this type of system is its low profile and extremely light weight, as all forces are transferred through the waistband or taken up by the subject's bone structure. A disadvantage of



this type of design is that the actuators could come in contact with the subject's skin, creating a possible safety hazard due to abrasion or uncomfortable pressure on the subject's skin. The variability in human anthropometrics would make this concept difficult to adjust as the moment arms for the torque applied would change with each subject. The compliance of skin and underlying tissues increase uncertainty in quantifying the torques transmitted to a human subject, especially when comparing data to validation tests on the noncompliant exterior of the Robotic Space Suit Tester (RSST).

An alternative concept was inspired from the hip frame of the Berkeley Lower Extremity Exoskeleton (BLEEX). This hip frame has joints that are aligned with two of the three degrees of freedom of the hip. In the BLEEX design, the abduction/adduction component, located near the human posterior, aligns with the abduction/adduction axis of the human hip perpendicular to the frontal plane. The flexion/extension joint axis of the exoskeleton is perpendicular to the sagittal plane and aligns with the flexion/extension joint of the human hip. The exoskeleton hip rotation axis is not collinear to the natural axis of rotation of the hip. A hip rotation point is located between the two abduction/adduction joints and an alternative hip rotation joint placed just above the flexion/extension joint (Zoss, Kazerooni et al. 2006).

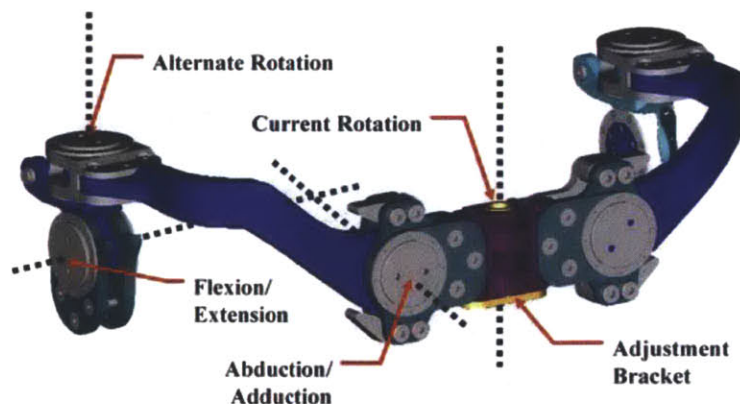


Figure 3.7 – BLEEX hip structure design (Zoss, Kazerooni et al. 2006)

To actuate this type of hip frame with McKibben actuators, a large disk would be mounted to the abduction/adduction rotation plates and the flexion/extension joints. The actuators would be mounted to the structure in antagonistic pairs with the disk in the center. When the actuators would contract, they would put pressure on the disk and impart torque to the joint. This concept would

leave the hip rotation components free to rotate. This design is advantageous when compared to the “jester’s pants” concept because the rigid structure would allow the torques to be easily quantified, and adjustments in size could be made without any changes to the actuators. The structure would also protect the subject from uncomfortable pressure points. Abrasion may still be an issue during movements between the structure and the subject but could be addressed with padding. The disadvantage of this system is the weight of the structure reduces some of the weight savings gained by using McKibben actuators. Given the advantages in safety and predictability, it was decided to develop a structural hip exoskeleton.

The first concept of the hip structure of the exoskeleton can be seen Figure 3.8. This rendering, viewed from the left posterior, shows a simple waist frame and an upper thigh structure (gold) on the left side. The green and blue plates join at the hip abduction/adduction axis of rotation. The width of this concept is adjustable, changing the bolt locations on the violet component that interlocks with the two green components.

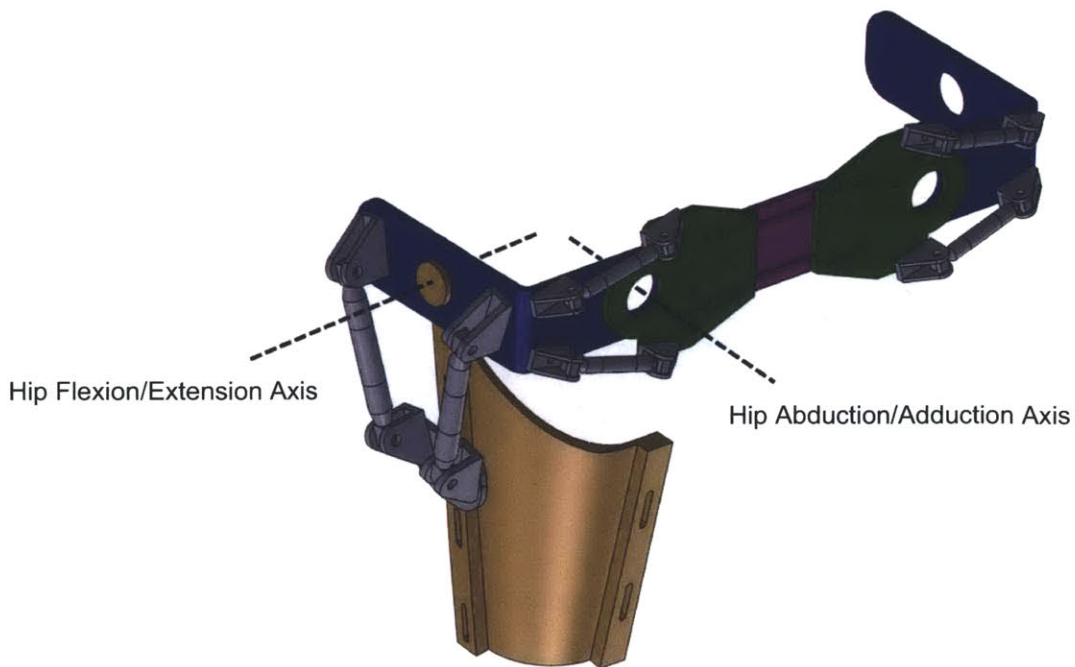


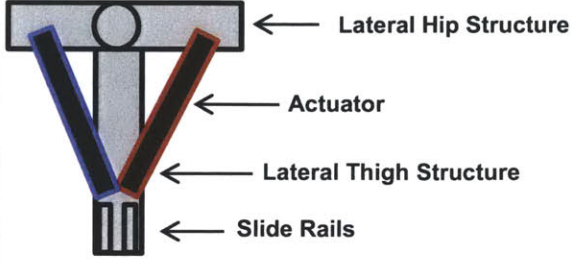
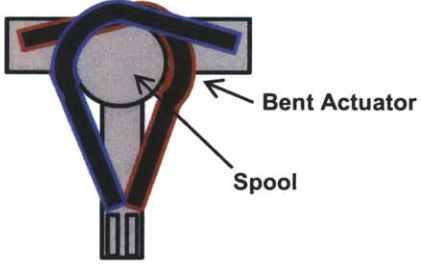
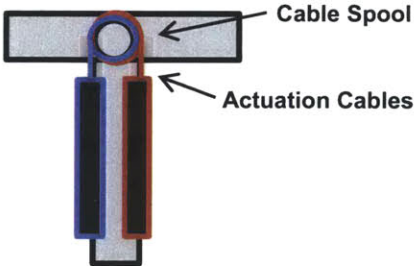
Figure 3.8 – Initial hip concept rendering with thigh brace on left side.

Two grey actuators are fixed between the upper thigh structure and the blue hip bracket. The top of the actuators are offset from the axis of rotation of the hip flexion. That offset creates a moment arm that allows the actuators to produce torque about the flexion/extension axis of the hip. Likewise, there are two actuators mounted around each abduction/adduction joint (green) with the ends anchored at an offset from the abduction/adduction axis. This “simple offset” method of generating torque was ultimately not chosen in the final design. This method and alternative methods considered are discussed in the torque transmission section on page 49.

### **3.3 Torque transmission**

Three methods of torque transmission were considered for the actuation of the hip flexion/extension and hip abduction/adduction actuators. These methods included connecting actuators from the thigh support to the waist structure (direct), bending actuators around a large spool at the point of rotation of the hip (bent), and using the actuators to apply force to cables attached to a waist structure mounted spool (cable). Table 3.4 illustrates each actuation option and predicted benefits and negatives to each method.

Table 3.4 – Hip Flexion/Extension Actuator Placement Concepts (Side view).

<p><b>Straight torque to moment arm (Direct)</b></p> <ul style="list-style-type: none"> <li>+Simple design</li> <li>-Large actuator contraction needed for ROM</li> <li>-Torque limited</li> <li>-Guiderails needed</li> </ul>	
<p><b>Actuator bent around a spool (Bent)</b></p> <ul style="list-style-type: none"> <li>+Large actuator contraction</li> <li>+Generates large forces</li> <li>-Heaviest option</li> <li>-Bulky</li> <li>-Requires bending actuator around a radius</li> <li>-Guiderails needed</li> </ul>	
<p><b>Actuating spool mounted cables (Cable)</b></p> <ul style="list-style-type: none"> <li>+Very adjustable</li> <li>+Can use spools or cams</li> <li>+Streamline</li> <li>+Slide rails not needed</li> <li>-May require more parts (spools)</li> </ul>	

The “direct” torque method appears to be ideal at first because of its simplicity. No spools or cables are required; the actuator connects directly to the frame some offset away from the point of rotation. This offset multiplied by the force of the actuator is the torque generated. This seemingly simple concept is why it was depicted in the original concept (Figure 3.8). In general, this can only be assumed for small angles using the small angle approximation. For hip flexion/extension



movements outside a few degrees, the moment arm is decreased and the torque generation is reduced. For example, if the leg is at 30 degrees, the moment arm is now the length of the original multiplied by cosine (30), effectively decreasing the maximum torque generation to 87% of what could be achieved at 0 degrees flexion. In this design, at the highest range of motion our actuators would produce the least amount of torque. In a space suit, the highest magnitude torques are observed at the maximum range of motion. At 90 degrees the actuator would be producing zero torque, limiting the maximum range of motion to much farther below 90 degrees in each direction from the neutral point. Furthermore, this design would require more space than just the actuators because a sliding rail at the base of the actuators would be added to prevent kinking of the actuator when the hip is bending in the opposite direction.

The second option for torque transmission is to bend the actuator about the radius of a spool. The “bent” actuator method is the same method used for the knee joint space suit simulator from phase 1 of the EVA S3 project (Figure 3.9).

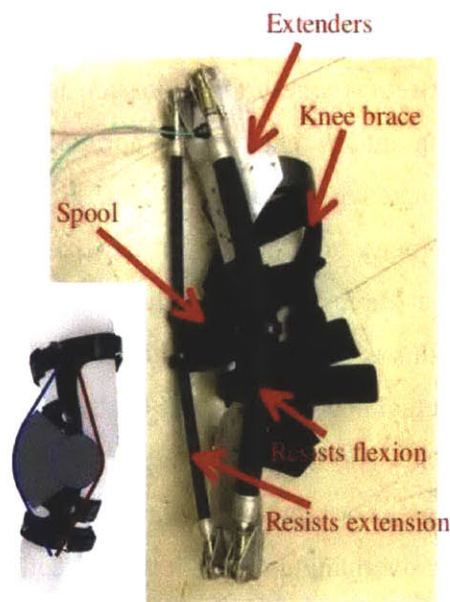


Figure 3.9 – The phase 1 space suit simulator knee joint (Duda, Newman et al. 2011)

The bent actuator method creates a torque about the knee by applying a normal force through the spool at the joint rotation point.

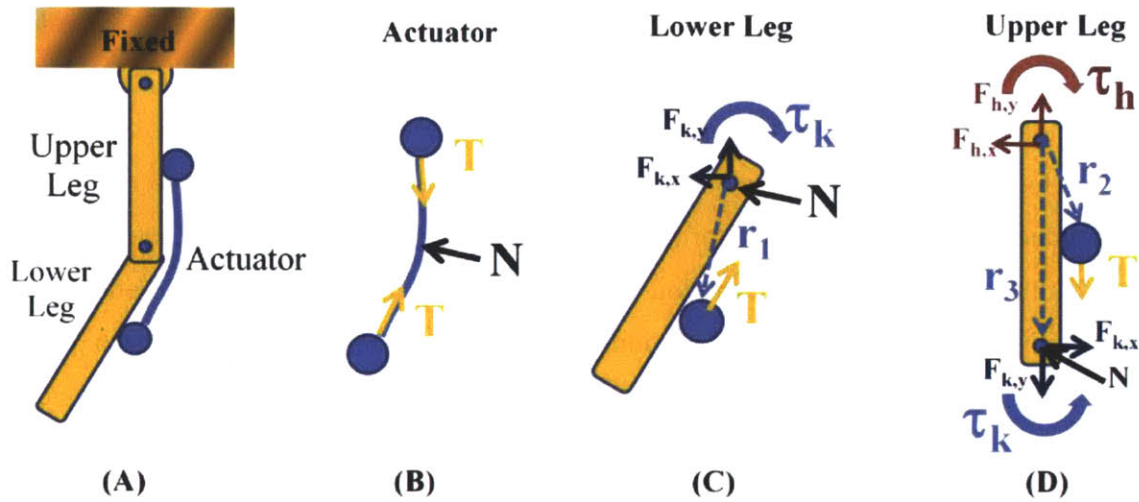


Figure 3.10 – A free body diagram of the knee joint of the exoskeleton modeled as a two link system (Gilkey 2012).

Unlike the “direct” method of actuator torque transmission, the “bent” method initially increases the torque generation capabilities as the joint progresses through the first part of the range of motion. In this simplified model, the magnitude of the normal force vector also increases as the angle of the bend increases. At extreme ranges of motion such as 180 degree bend the normal force is equal to  $2 \cdot T$ ; however, the moment arm between the normal force vector and the torque vector is minimized and can result in a reduction of maximum torque. Where this reduction occurs depends greatly on the joint geometry and location of the fixed points of the actuator. Another advantage of this method over the “direct” method is that it can take advantage of body geometry to reduce bulk. One example of this is the implementation of the knee concept in Figure 3.9. The actuator placement follows the actual bend of the knee. On the other hand, the geometry of the hip is much different, and there is not a good point to wrap an actuator around the hip. The actuator would need to be wrapped 90 degrees or more around an actuator spool as seen in Table 3.4. This may reduce some of the actuator overhang as seen in the “direct” option of Table 3.4 but would require a larger actuator to span the distance, and may increase weight with the inclusion of a spool to bend the actuator. The “bent” actuator method is preferable to the “direct” actuator because it has preferable torque and range of motion characteristics.

There are several improper loading conditions for these actuators that may cause damage and failure. These are shown in

Figure 3.11 to be (A) torsional forces (B) actuator crumpling (C) excessive radial offset of connectors, and (D) excessive overhang (FESTO 2011).

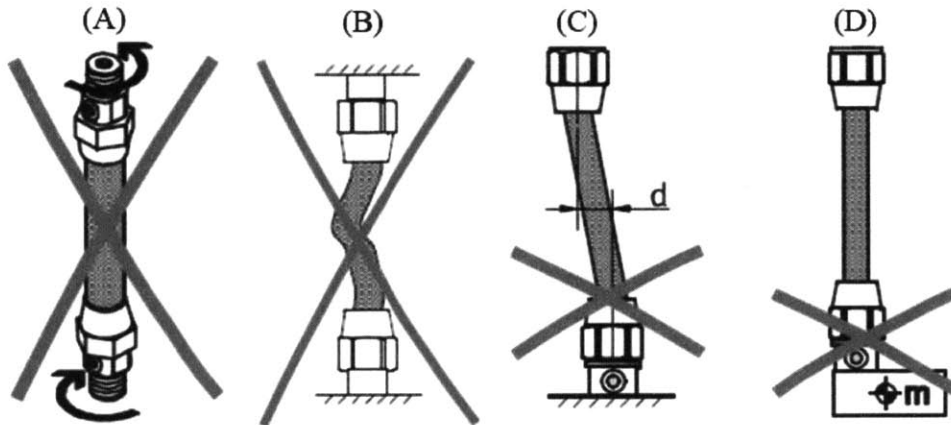


Figure 3.11 – Improper and unsafe use of a Fluidic Muscle (FESTO 2011)

Both the “direct” and “bent” options have a problem with the actuator crumpling when the joint is bent too far in one direction. In order to fix this, one end of the actuator must be fixed to a slider rail that allows it to move freely and avoid being crushed when the joint is moved past the active location for that actuator. Implementing sliders in this manner increases the total length of the actuator assembly. This is a disadvantage because space is limited in order to create room to fit this exoskeleton on smaller subjects. Section 4.1.2 describes the final knee design that includes these sliders in a “bent” design.

The “cable” method (Table 3.4) is a third option that further improves the torque and range of motion characteristics of the previous options, reduces exoskeleton bulk significantly, and does not require sliders that extend the length of the actuator assembly. In this method, the actuators are mounted parallel to the EVA S3 operator’s leg. The lower end of the actuators are fixed to the exoskeleton, and the upper end is connected to a cable that is anchored around a spool. The spool is attached to the waist portion of the exoskeleton and freely rotates about the vertical thigh structure. When the actuator is activated it creates a torque between the waist structure and the thigh structure. When the operator moves the hip exoskeleton into a position that the actuator is no longer active, the cable goes slack instead of crumpling the actuator. Methods for guiding slack cables are in Section 0. The diameter of the spool is the torque moment arm throughout the entire

range of motion, unlike the “direct” and “bent” torque transmission methods where the moment arm changes based on the leg position. The spool concept also has increased flexibility as the spools can be customized for each of the antagonistic actuators and can even be designed with a variable radius like a cam, in order to increase the moment arm at extreme ranges of motion to maximize torque generation. Considerations for both of these spool modifications are in Section 0.

Analysis indicated that it would be best to use the “cable” method for the hip flexion/extension and abduction/adduction joints of the EVA S3. This torque transmission is the most compact and adjustable of the proposed options.

A fourth option (Figure 3.12 C) is transmitting torque through use of a four bar linkage. This method was used in the rehabilitative exoskeleton designed by Robotics and Multibody Mechanics Research Group at Vrije Universiteit Brussel. They claim that their design combines the advantages of a pulley-and-belt type connection and a connection through fixed levers (“direct”) by its compactness and good torque matching (Beyl, Van Damme et al. 2008).

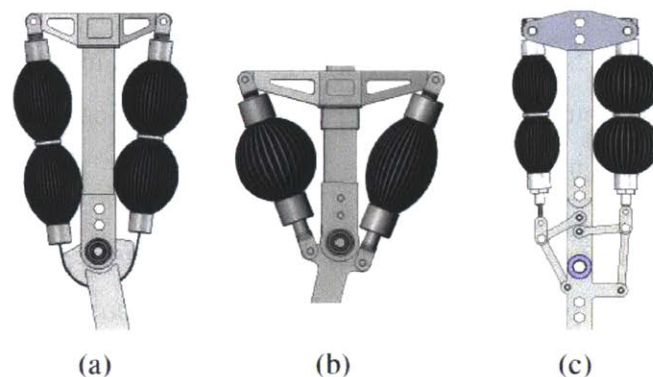


Figure 3.12 - Some possible antagonistic actuator configurations (Beyl, Van Damme et al. 2008)

The cable and pulley method examined by Beyl et al. did not have some of the distinct advantages of the “cable” method proposed for EVA S3. Using independent spools with the cables gives researchers the ability to tune the torque characteristics and range of motion for each



actuator with a compact form factor, while also providing a mechanism to avoid crumpling of the actuator by coiling the cable or letting it go slack.

### 3.3.1 Actuator size specifications

The ideal actuator assembly is as small and light as possible but still satisfies the minimum torque and range of motion requirements. The torque that can be generated is determined by two factors: the radius of the spool and the diameter of the actuator. An increase in the diameter of the spool increases the length of the moment arm,  $r$ , and likewise increases the torque that is applied for a particular force (Equation 3.1, Figure 3.13).

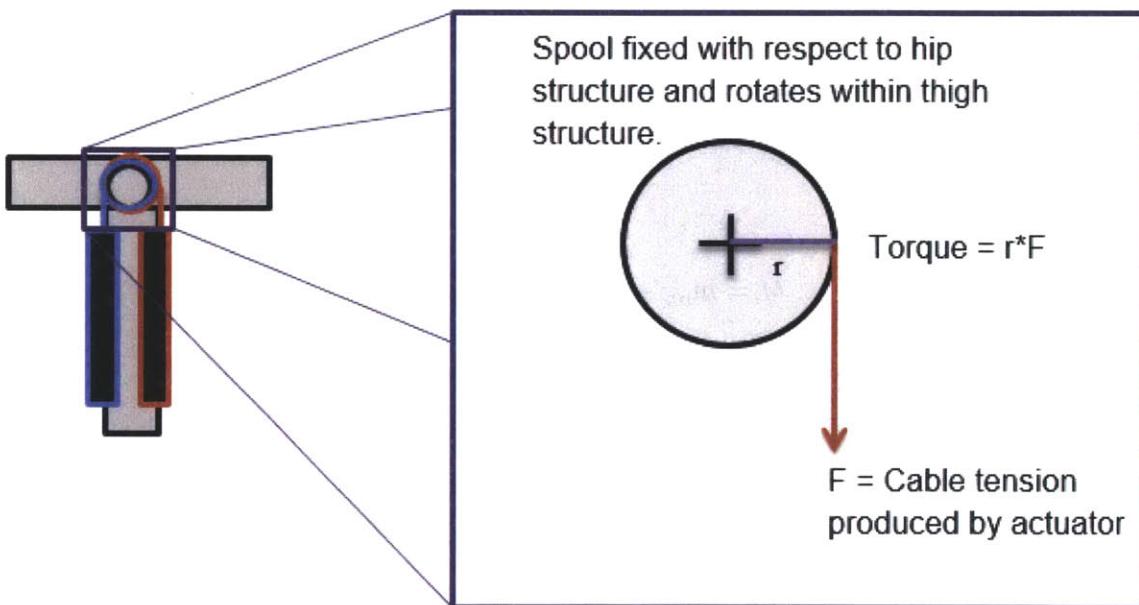


Figure 3.13 – Diagram of torque spool concept

Torque

$$T_{min} \leq T = r * F_d$$

3.1

The maximum force generated by each actuator varies by actuator diameter and is 630N, 1500N, and 6000N for the 10 mm, 20 mm, and 40 mm diameter actuators respectively. Therefore, a larger diameter actuator requires a smaller spool and vice versa.

Considering these factors alone would be relatively simple, the minimum weights for the three actuator and minimum spool size combinations could be simply compared. When factoring in the minimum range of motion requirements, the problem becomes more complex. The range of motion (ROM) for one actuator must be greater than the minimum range of motion (ROM<sub>min</sub>) required for the movement. This is determined by the linear contraction of the actuator and the perimeter of the spool. Each actuator, length  $l$ , can contract a fraction of its length ( $c$ ). The amount of rotation in degrees is the actuator contraction ( $c \cdot l$ ) divided by the perimeter of the circle ( $2 \cdot \pi \cdot r$ ) multiplied by 360 degrees (see equation 3.2). Festo pneumatic muscles contract 25% of the length of their active area ( $c = 0.25$ ). The smaller the spool, the shorter the actuator can be.

$$\text{Range of Motion} \quad ROM_{min} \leq ROM = \frac{c * L * 360}{2 * \pi * r} \quad 3.2$$

With every optimization problem, the solution depends on how you define your constraints and cost function. In early actuation selection, the cost function was simply the weight of the system (Equation 3.3).

$$\text{Mass} \quad M = m_{ao} + m_{al} * L + m_{sp} * r \quad 3.3$$

where the Mass is defined by  $m_{ao}$ , the base weight of the actuator end fittings, plus the mass of the active part of the actuator per unit length ( $m_{al}$ ), multiplied by the actuator length ( $l$ ), plus the estimated mass of the spool per unit radius ( $m_{sp}$ ) times the radius ( $r$ ). A constraint on the shear stress (Equation 3.4) of the spool was added as a quick check for feasibility during the design process, where  $T$  is torque,  $r$  is spool radius,  $\sigma_{max}$  is the maximum stress allowed based on the yield stress,  $\sigma_{yield}$ , divided by the factor of safety,  $FOS$ .

$$\text{Shear Stress} \quad \frac{2 * T}{\pi * r^3} = \sigma_{max} \leq \sigma_{yield} / FOS \quad 3.4$$

The optimization problem was coded into a MATLAB script (see Appendix A) and used the nonlinear optimization function `fmincon` to minimize the cost function (mass), subject to the constraints of torque and range of motion.

As the design progressed, it became evident that the length of the actuators was a critical factor in allowing the design to fit along the thigh of a 5 percentile female. The sitting buttox-knee length of a 5 percentile female is 49.8 cm (19.2 in) (NASA 1995). The actuator and the spool needs to fit in this space for proper sizing and to avoid conflicts with other components. Therefore, an additional constraint of a maximum actuator length of 30.5 cm (12 in) and spool diameter of 10.16 cm (4 in) was included. These constraints were ultimately added to the GRG nonlinear solver in Microsoft Excel to visualize different factors during the design process. The simple constraint on shear stress was dropped since failure would be addressed later in the design, and the constraint did not apply to designs of other materials or geometries.

Table 3.5 displays the best actuator option for each actuator diameter. Parallel pairs of actuators were also considered to double the force output of an actuator diameter. The advantage of a parallel pair is that they double force generation which reduces the required spool diameter and actuator length. Unfortunately, the added mass of additional cable anchors increases the total to a value that is higher than a single, longer actuator. The selected actuator specification is highlighted in blue. There is no data for the 10 mm hip flexion or the 10 mm hip adduction actuators because there is no solution that satisfies the maximum length requirement for those cases. In the final design, both hip abduction and adduction actuators selected were the same 20 mm actuator optimized for hip adduction. This decision was made to increase the simulator flexibility and simplicity. Based on the EVA S3 design, the size of the hip abduction/adduction assembly is determined by the largest actuator of the antagonistic pair. This choice resulted in a minimal weight penalty of 234 g for the EVA S3.

Table 3.5 – Actuator selection table for hip actuators

Actuator Diameter	Maximum Force (N)	Spool Radius (m)	Actuator Length (m)	Torque (Nm)	ROM (deg.)	Actuator Mass (g)	Total Mass (g)
<b>Hip Extension</b>							
10 mm	630	0.044	0.062	28.0	20.0	63.8	426.8
20 mm	1500	0.019	0.026	28.0	20.0	173.6	536.6
40 mm	6000	0.005	0.007	28.0	20.0	677.2	1040.2
<b>Hip Flexion</b>							
10 mm	--	--	--	--	--	--	--
2 x 10 mm	1260	0.025	0.155	31.0	90.0	145.1	871.1
20 mm	1500	0.021	0.130	31.0	90.0	192.1	555.1
2 x 20 mm	3000	0.010	0.065	31.0	90.0	361.1	1087.1
40 mm	6000	0.005	0.032	31.0	90.0	686.0	1049.0
<b>Hip Abduction</b>							
10 mm	630	0.051	0.106	32.0	30.0	68.0	431.0
2 x 10 mm	1260	0.025	0.053	32.0	30.0	126.0	852.0
20 mm	1500	0.021	0.045	32.0	30.0	177.0	540.0
2 x 20 mm	3000	0.011	0.022	32.0	30.0	346.0	1072.0
40 mm	6000	0.005	0.011	32.0	30.0	678.8	1041.8
<b>Hip Adduction</b>							
10 mm	--	--	--	--	--	--	--
2 x 10 mm	1260	0.034	0.107	43.0	45.0	136.2	862.2
20 mm	1500	0.029	0.090	43.0	45.0	185.0	548.0
2 x 20 mm	3000	0.014	0.045	43.0	45.0	354.0	1080.0
40 mm	6000	0.007	0.023	43.0	45.0	682.7	1045.7



### 3.3.2 Spool Design Variants

Early concepts consisted of two actuators that would pull on cables attached to a single spool as seen in Figure 3.14 below. In order to reduce the length of the actuators and design a more compact actuator assembly, dual spool and cam designs were explored.

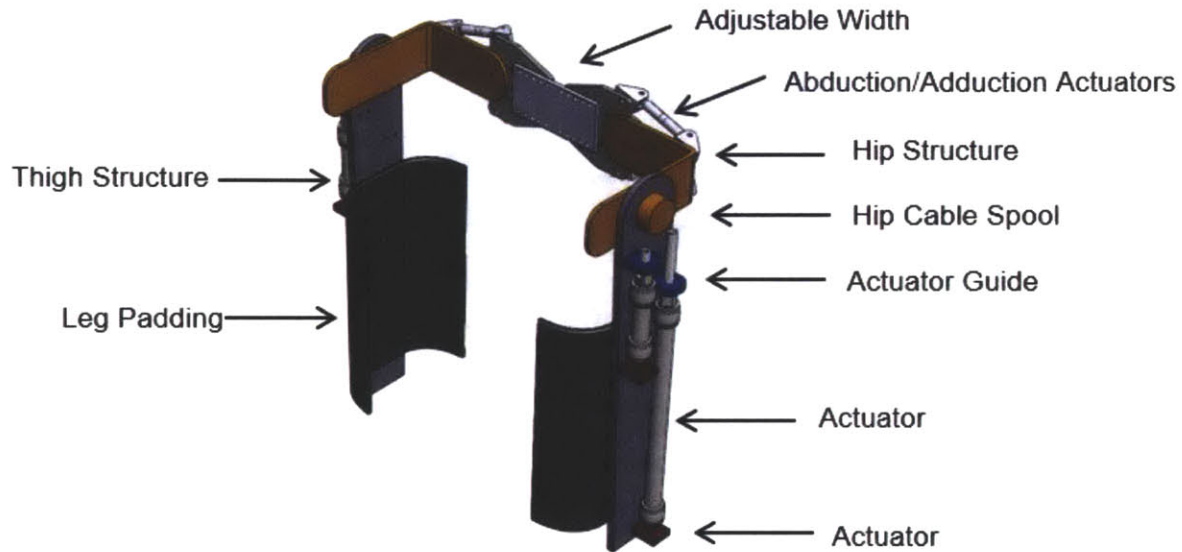


Figure 3.14 – Early concept where antagonistic actuator pairs pull on a single spool (orange cylinder)

#### 3.3.2.1 Dual Spool Design

The dual spool design allowed each spool to be optimized for each actuator. The diameter of the spool could then be reduced to the radius that would produce the minimum torque required for a particular actuator. Since a smaller spool has a shorter perimeter, a shorter actuator can move the spool through its required range of motion, resulting in a more compact assembly. Figure 3.15 is an early concept of the dual spool design with each actuator and spool pair independently optimized.

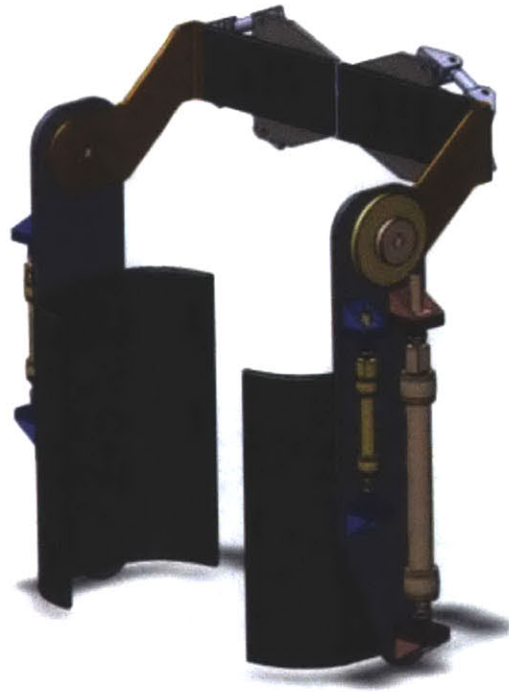


Figure 3.15 – An early concept of the dual spool design with appropriately sized actuators

### 3.3.2.2 Dual Cam Design

The spools can be designed as cams to further reduce the actuator length. Since the largest torques occur at the greatest angle, the radius of the spool can be decreased as the angle decreases. The resulting system can still achieve the torque range required with a smaller perimeter, thus requiring a shorter actuator stroke length. This results in a more compact actuator assembly by reducing the required actuator length by four times the stroke length eliminated.

Cams are typically designed following the fundamental law of cam design: the cam function must be continuous across the first and second derivatives of displacement across the entire interval. Effectively, the jerk function needs to be finite over the entire interval (Norton 1999). The purpose of this principle is to prevent discontinuities that could create large spikes in force that could cause excessive wear or result in a loss of contact between the cam and the cam follower. The cable serves as the cam follower in our design. The loss of contact with the cable is less of a concern,

but the design needs to have a predictable torque profile that minimizes force spikes that could reduce the fidelity of the simulator.

The cams will then be attached to a shaft fixed to the waist brace. A roller will guide the cable from the cam to the vertical actuators. In the dual spool design, one actuator is typically longer than the other because the ROM requirements are asymmetric. For example, the hip flexion actuator must control torque for 90 degrees and the extension actuator only needs to control torque for 20 degrees. Reducing the required stroke length of the flexion actuator reduces its length and consequently decreases the size of the actuator assembly. Weight can be reduced by also making the smaller spool a cam but that will also increase cost and system complexity.

The design chosen was a dwell-rise-dwell-fall, for the flexion cam following a cycloidal displacement profile (Equation 3.5 ).

$$a = C \sin\left(2\pi \frac{\theta}{\beta}\right) \quad 3.5$$

Where  $c$  is the magnitude of displacement and  $\theta$  is the independent variable and  $\beta$  is the size of the segment. Cycloidal displacement had a simple equation for the profile that still satisfies the fundamental law of cam design, though it can produce higher accelerations than some polynomial cam designs. Accelerations are not as critical in this design because there is no cam follower and a slight increase in acceleration will not contribute significantly to wear. The simple profile streamlines the torque calculations needed for active control. A potential cam profile for a 20 mm hip flexion/extension actuator (joint range of motion: 90 degrees, torque: 32 N m) is described below. Figure 3.16 is a CAD rendering of that cam concept.

1. Initial dwell at a 15 mm radius for 90 degrees
2. Cycloidal rise to a radius of 21 mm over 90 degrees
3. Dwell at 21 mm for 90 degrees
4. Cycloidal fall to 15 mm over 90 degrees

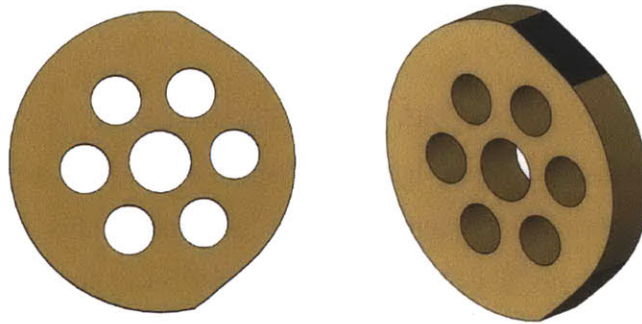


Figure 3.16 – Prototype cam concept with weight saving holes

This design assumes that the maximum torque is required at the maximum range of motion for the designated design. The main disadvantages of this design are the added manufacturing complexity and reduced adjustability. The reduced adjustability stems from the radius decrease at lower angles. It is not possible to produce the maximum torque at a smaller angle because of the shortened moment arm at that position. If a space suit has the same maximum torque that we specified, but it occurs at a lower range of motion, it will not be able to be simulated with adequate joint torque. The decision was made to use two constant radius spools optimized for each actuator in the antagonistic pair. The small improvements in compactness were not worth reducing the adjustability of the system.

### **3.3.2.3 Spool designs to control slack cable**

During the implementation of the spool design, it is important to consider slack cable when a joint is moved past one of the actuator's active ranges. Excess slack in the cable could result in the cable unseating from the spool, disabling the actuator from providing any torque. Two methods for dealing with the slack were considered: a retractable spool design and an extended cable guide design.

### **3.3.2.4 Retractable spool design**

A method evaluated to avoid the folding of a slack actuator is to spring load the spool to prevent cable slack. This design uses a torsion spring to rotate to coil excess wire. The spring is coiled around the keyed shaft used for torque transmission. Pins engage the coil with the spool, and a

spring anchor is fixed to the shaft. The spool has a keyway that will allow it to engage when the actuator is activated, but allows the spool to rotate backwards to coil the spring.

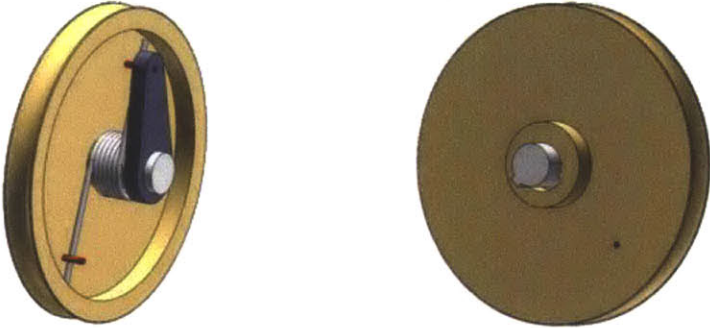


Figure 3.17 – Front and back view of spool concept

This design is a relatively simple method to remove slack from the line. It does not require sliders to move the actuators. However, it does increase complexity of the spools with few additional parts. An exploded view details the assembly components. The design also requires an increase in width of the spool (seen below), but the use of a smaller torsion spring in the mock up device minimizes the thickness increase.



Figure 3.18 – Exploded view of retractable spool (A). Side view of Spool (B).



A prototype of the spool concept is shown below. The spool and spring lock were 3D printed with ABS. A torsion spring spools the cable (not pictured), and the keyed shaft limits motion to a necessary range of 120 degrees.

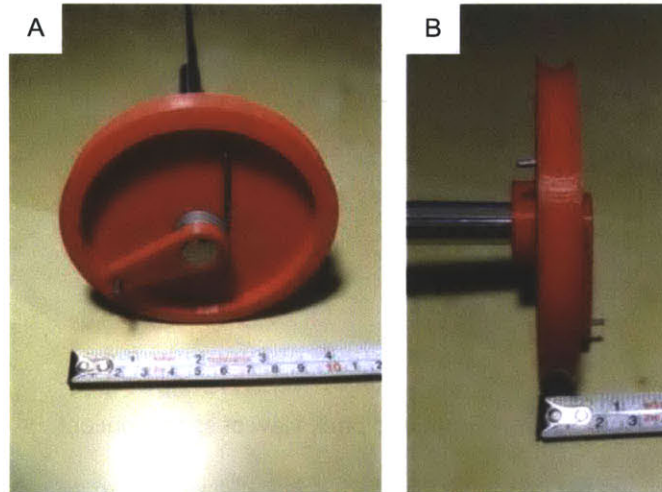


Figure 3.19 – Retractable spool prototype front (A), side (B)

### 3.3.2.5 Extended cable guide design

A second option to control the slack cable was to extend the cable guides so the slack cable is contained inside of the guides and does not derail. The biggest concern about this design is the guides protruding so far from the spool that they interfere with the operator. The vertical actuator travel distance for the final design was a maximum of 4.3 cm in a single direction so a large guide was not needed. The extended guide design was overall simpler and lighter than the retractable spool concept. Figure 3.20 is a rendering of the final spool with cable guides.

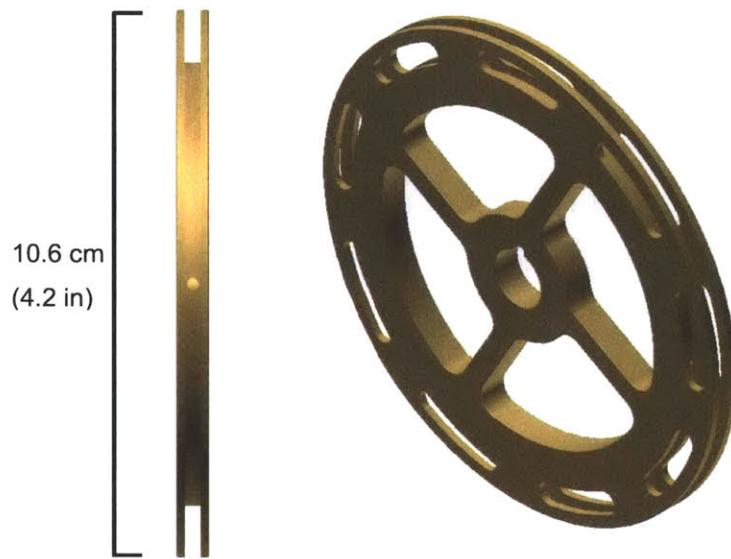


Figure 3.20 - Final spool with extended cable guides

### 3.4 Actuator assembly

Customizability of the EVA S3 is of high importance for fit and for function. From the early stages of design, the spools were planned to be easily interchangeable in case a user needed to change the radius of a spool to accommodate a suit design outside the range of the requirements. The concept is to have a keyed shaft that the spools can slide over and then be locked in place by a retaining ring. The shaft is partially keyed to lock in the relative positions of the two spools and the shaft collar (Figure 3.21). The torque arm (orange) attaches to the extension fixed to the backpack frame of the exoskeleton. The opposite end of the shaft is not keyed and is fit into a bearing so that it can rotate freely with respect to the thigh support structure. Figure 3.21 is an exploded view of the components of the prototype spool assembly. A keyed shaft collar bolts into the torque arm and holds the keyed shaft. Figure 3.22 is the final design of the spool assembly. The shaft collar and torque arm are combined into a single aluminum component. The low friction nylon disc is also replaced with a Teflon spacer that provides space for the mechanical safety stops. The potentiometer and its mount can also be seen. Snap rings on either end of the keyed shaft hold the assembly together and can be removed to quickly change spool sizes if needed.

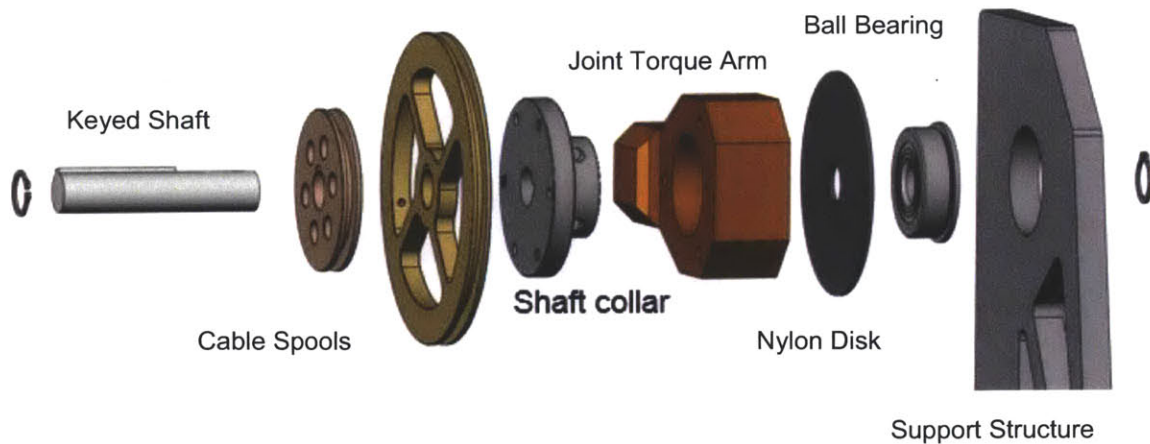


Figure 3.21 – Detail of prototype spool assembly

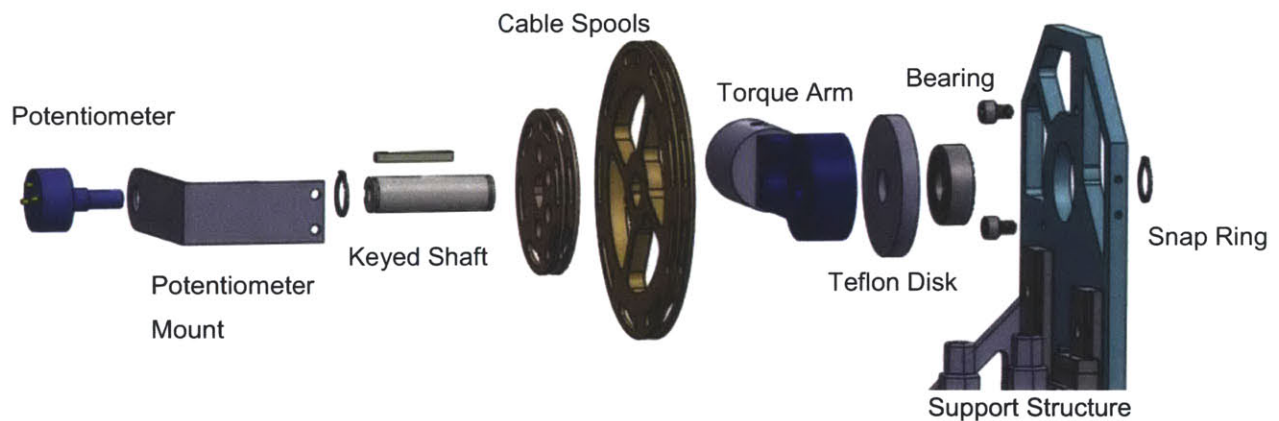


Figure 3.22 – Detail of final spool assembly

The prototype actuator assembly included the two actuators and the spool assembly mounted to a large aluminum structure (the grey plate in Figure 3.23). This structure has three slots machined in each side for webbing straps to loop around the legs. In the final version the webbing holes were removed when the structure was redesigned to bolt to the TROM leg brace. The leg brace would serve as the interface between the user and the hip flexion/extension actuator assembly. The removal of these strap holes enabled the removal of the structure below the extension actuator (gold actuator, right side of Figure 3.23).



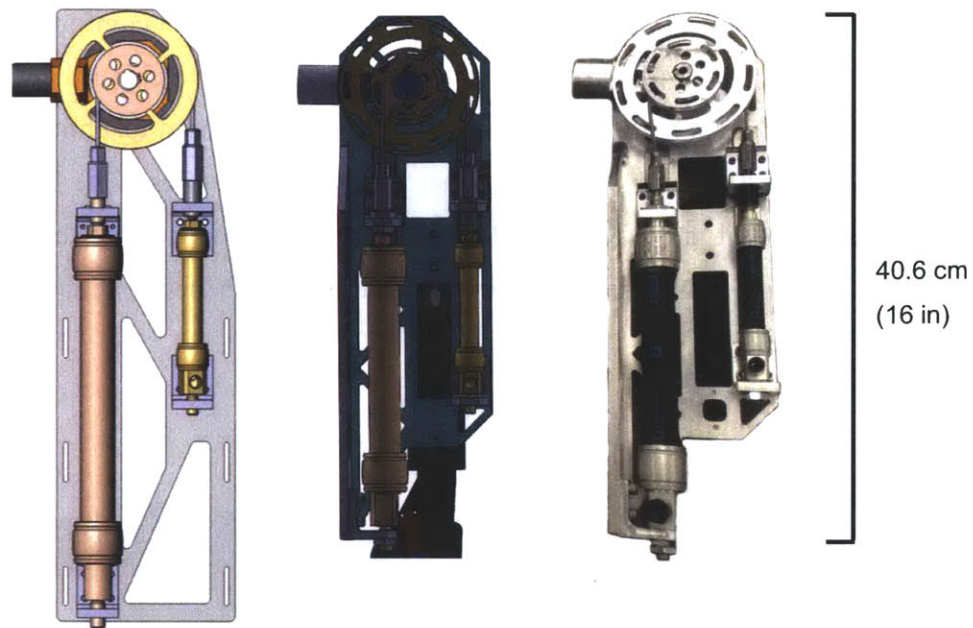


Figure 3.23 – Renderings of prototype I hip flexion extension actuator assembly (A) and final hip flexion/extensions assembly (B)

Additional structural changes included adding cutouts to the structure to allow for size adjustments of TROM leg brace, and a structural reinforcement to reduce the overall thickness of the structure and allow the bottom of the flexion actuator to be mounted to it so it would avoid conflicts with the knee joint of the EVA S3.

### 3.5 Fitting the Human Operator

#### 3.5.1 Exoskeleton/body interface

Once the basic actuator methods were selected and the rough size of the exoskeleton hip joint was known, the method to fix the exoskeleton to the body could be determined. Below are some components off the shelf (COTS) options for hipbelts to secure the exoskeleton that were considered. The hip belt could either be secured to the frame for padding or serve as part of the structure. The Osprey Bioform belt (Figure 3.24 A) is designed to support downward loads in hiking packs; this belt is well padded and would protect the hip from any rubbing. Climbing harnesses (Figure 3.24) are used to support vertical/forward loads and distribute the force to the thighs as well. Climbing harnesses were viewed as more secure on the user because of the thigh

straps; however the waist padding was not viewed sufficient for operator comfort. Kidney belts for motorcycle racing (Figure 3.24 B) offer back support and protection and breathability but are not designed to support loads. Figure 3.24 D shows a hip stabilizer used to limit hip motion after surgery. This brace is stabilized with a band that rides above the waist. The DonJoy hip ROM appears to have a firm fit and is well padded but there were concerns that the metal joint that connects the upper and lower segments would restrict hip abduction/adduction freedom of movement.

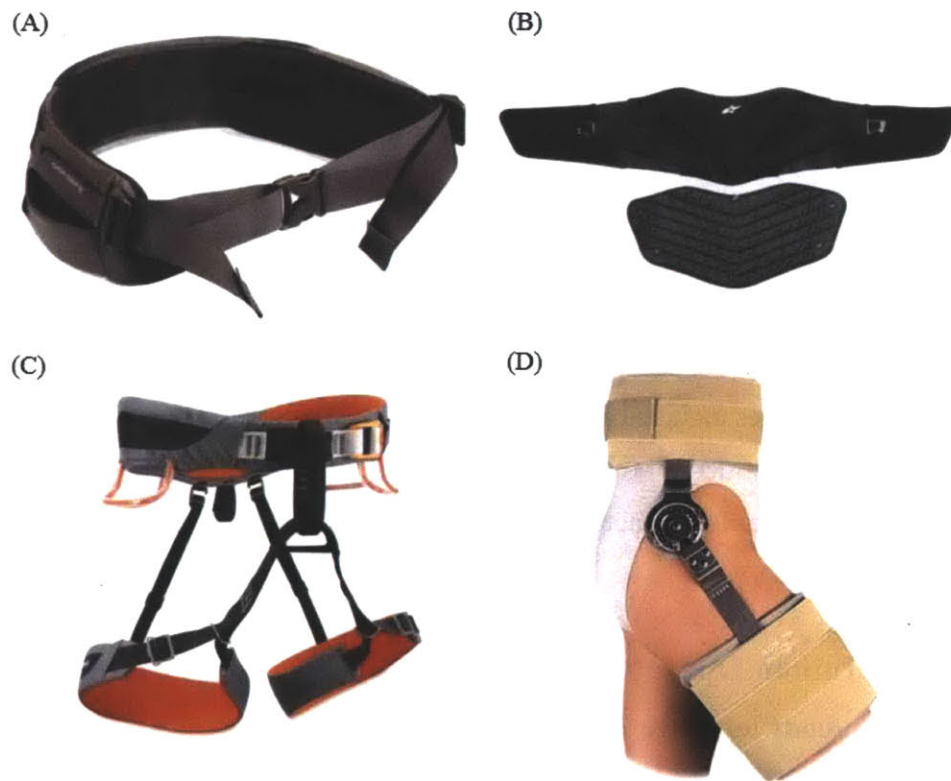


Figure 3.24 – Potential COTS options to secure the EVA S3 hip to the operator. (A) Osprey Bioform Hipbelt (REI 2012). (B) Alpinestars Touring Kidney Belt (Alpinestars 2012). (C) Black Diamond Climbing Harness (REI 2012). (D) Donjoy ROM hip brace (DonJoy 2012).

The hiking hip belt was viewed as the best option; however, there were still concerns about the ability of a simple belt to adequately secure the EVA S3 hip joint to the operator. After further investigation, the idea of using an external frame hiking pack was proposed. The storage compartment portion of most external frame backpacks can be removed, leaving just the waist and

shoulder straps attached to the frame. The shoulder straps can help stabilize the waist belt and prevent downward slippage while gravity prevents the belt from inching higher. The frame also provides a solid structure to mount components and is already connected to the waist belt in a manner that avoids uncomfortable pressure points. From a systems level view, using an external frame pack makes sense because some structure was already necessary to provide a location to mount onboard controls and power, as well as to possibly attach upper arm components of the exoskeleton. This choice saved additional engineering work as well as cost as the price of the backpack selected is about 160 U.S. dollars (Kelty 2013). Figure 3.25 is an image of a Kelty Trekker 65 external frame backpack, the backpack selected to be the base structure for the EVA S3 hip.



Figure 3.25 – Kelty Trekker 65 external frame backpack (Kelty 2013).

### 3.5.2 Sizing and adjustments

A good fit is important for comfort and predictable joint torques in the EVA S3. The hip design concept evolved from adjustments based on adjustable, interlocking plates to a design based on telescopic cylinders with set pins. The final design retained the telescopic tube concept and adjustments to where the hip abduction/adduction actuator assemblies bolt to each other on an 80/20 extruded aluminum rail.

Figure 3.26 shows an early concept for adjusting the width of the exoskeleton. The idea was to machine a ribbed plate (grey/blue) to interlock with grooves and a matching bolt pattern in the actuator mount plate (brown). This had a bolt pattern spacing that allowed adjustments in discrete



steps of 1.27 cm (0.5 in). This idea was eventually discarded because of the weight and bulk when compared to the telescopic cylinder concept shown in Figure 3.27.

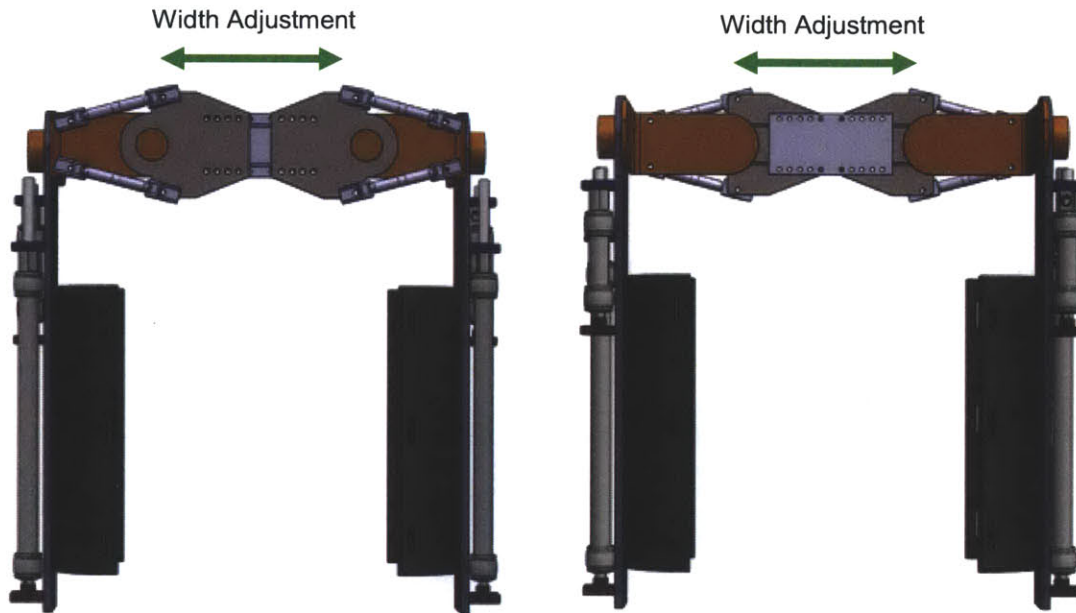


Figure 3.26 – Early concept with interlocking plate adjustments. Bolts could be moved to adjust the width in half inch increments

The telescopic tube concept allows adjustment in hip width, back to hip joint center, and hip joint height for flexion and extension. This design also adjusts in 1.27 cm (0.5 in) increments but is significantly lighter and more compact than the interlocking plate concept. The commercial availability of telescopic tubing in multiple materials reduced manufacturing time because the only modifications from commercial stock that need to be made are cutting the tubes to length and drilling holes for the locking pins that fix the tube locations with respect to each other.

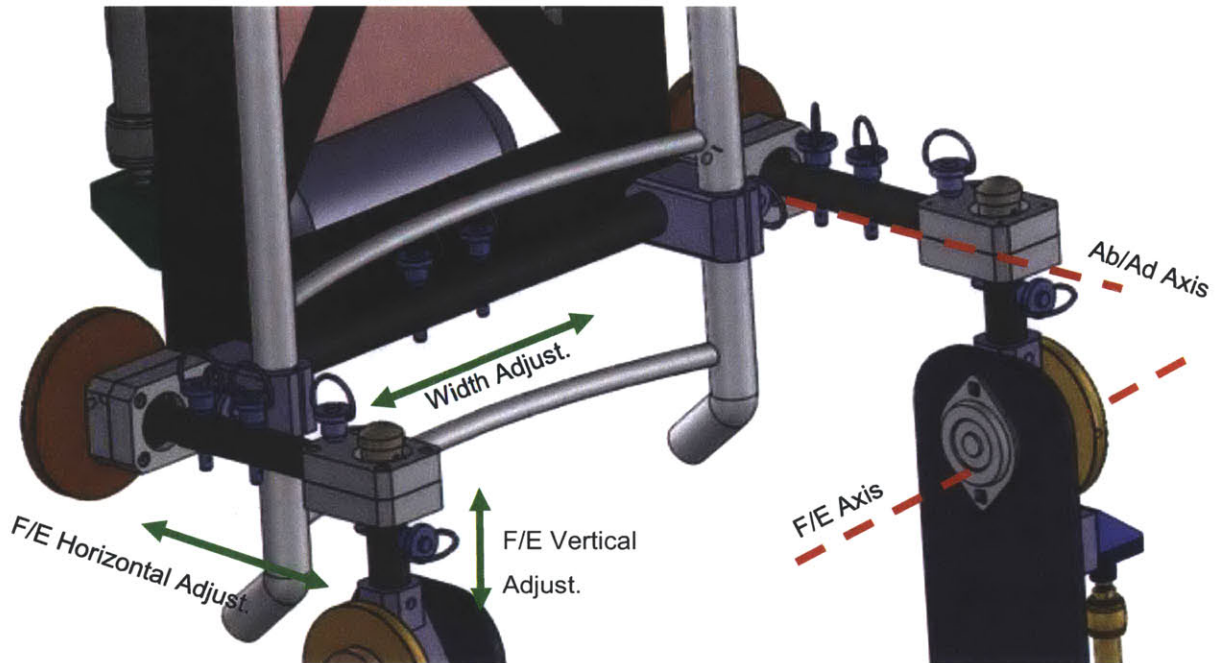


Figure 3.27 – Telescopic pole concept for hip joint alignment

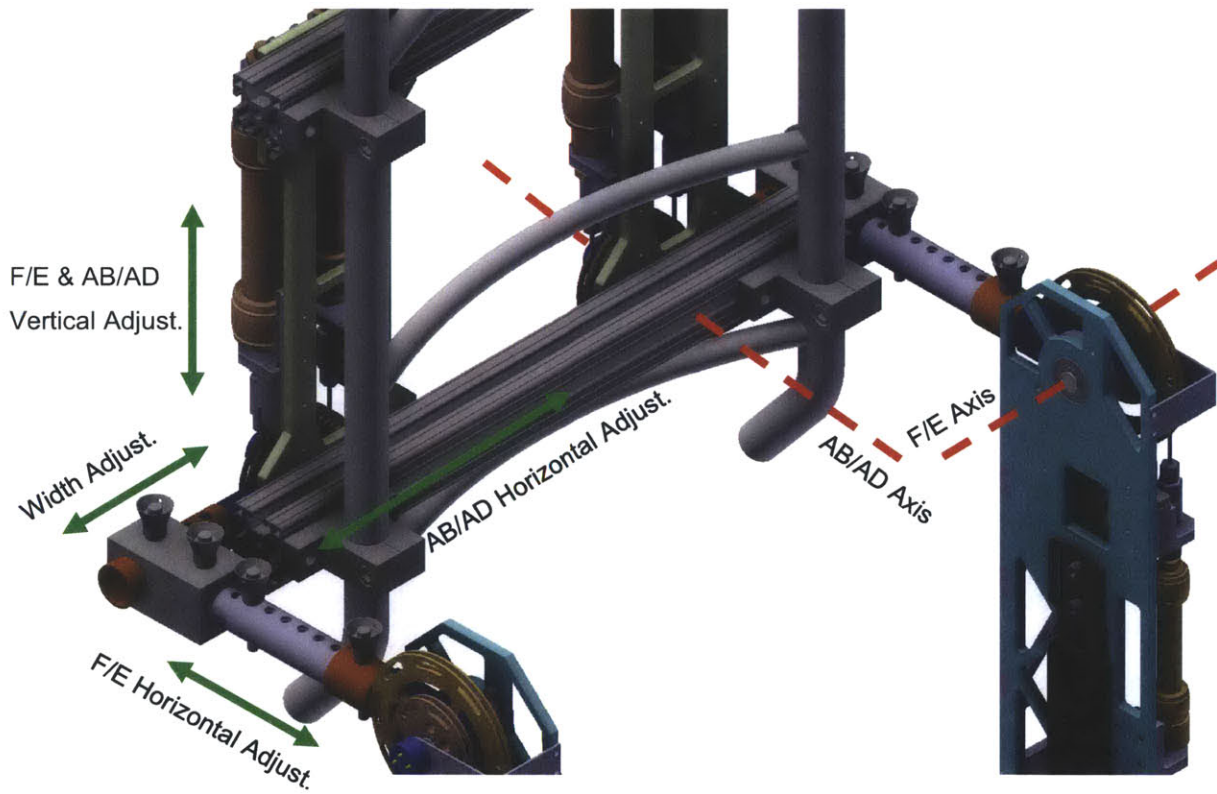


Figure 3.28 – Telescopic cylinder and sliding rail combination for hip joint alignment in final design

Figure 3.29 demonstrates how adjusting the hip abduction/adduction mount location along the 80/20 rails allows the hip abduction/adduction axis to be aligned with that of the EVA S3 user. This adjustment relies on clamping forces of the bolts along the rail so alignment holes are not needed and it can be adjusted at continuous rather than discrete intervals. The entire hip abduction/adduction assembly moves with this adjustment so that no cable length changes are needed with adjustment. In earlier designs, the actuators were mounted in a fixed location to the backpack and required cable length adjustments when the spool locations were moved to accommodate different hip sizes (see Figure 3.30).



Figure 3.29 – Simplified model showing horizontal adjustment of hip abduction/adduction axis center

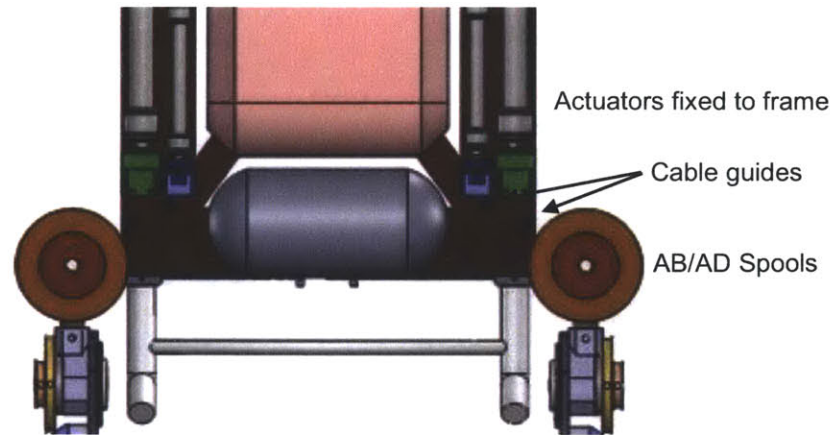


Figure 3.30 – Concept where abduction/adduction spools are adjustable but the actuators are fixed to the backpack frame.

Another continuous adjustment is for the vertical location of the hip abduction/adduction and flexion/extension axis. The clamps that hold the 80/20 crossbars to the backpack frame can be loosened to slide the hip components vertically with respect to the backpack frame (Figure 3.31). Bolt holes were added along the side of the hip abduction/adduction assembly to increase the available range of vertical adjustment.



Figure 3.31 - Simplified model showing a vertical adjustment of hip abduction/adduction axis center. This adjustment also changes the vertical alignment of the hip flexion/extension center

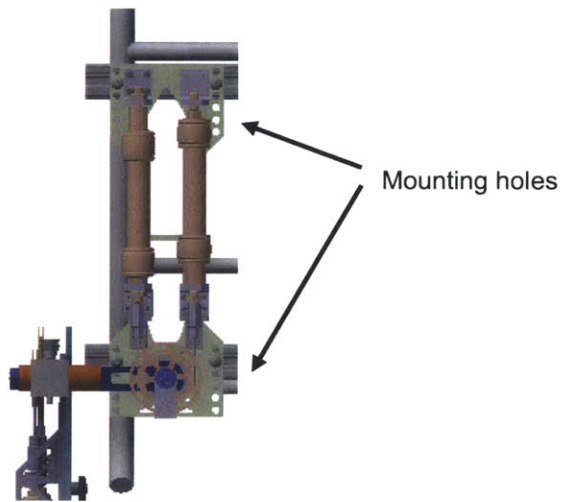


Figure 3.32 – The final design also included mounting bolt holes to increase range of vertical alignment



### 3.6 Material Selection

Plastics, composites, steels, and aluminums were considered for the construction of the EVA S3. Three major properties influence the material selection for EVA S3 components. First, material density must be considered so the EVA S3 can achieve the goal of being considerably more lightweight when compared to full space suits. Second, material strength is important to reduce the bulk of the structure and so the EVA S3 will not break under self-imposed loads. Third, corrosion resistance an important consideration because of the potential test environments of the EVA S3 may be in locations where the exoskeleton could be exposed to water. In addition to weight, strength, and corrosion resistance, two other considerations were added as the project progressed: manufacturability and cost.

Plastics were primarily used for parts being prototyped. Many parts of the EVA S3 hip prototype were 3D printed with orange acrylonitrile butadiene styrene (ABS) plastic (see the orange components in Figure 3.33 B). These structures could withstand the light loads encountered during fit checks. All major ABS parts were replaced with machined aluminum components in the final EVA S3 hip joint.

Composite materials were used in two places, “greave” armor protecting the knee and shin of the operator in the exoskeleton knee (Figure 3.33 A), and the telescoping composite poles used in the prototype of the hip component (Figure 3.33 B). The greave was constructed of 2 layers of standard carbon fiber weave oriented at 0-90° and 45° with a 1/8 inch Nomex honeycomb core sandwiched between another 2 layers of carbon fiber weave oriented at 0-90° and 45°.

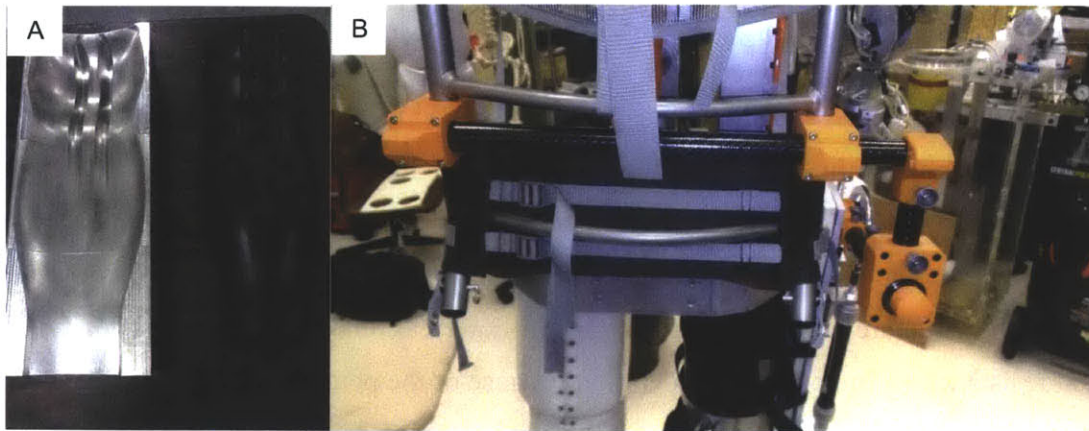


Figure 3.33 – Composite structures. The carbon fiber greave and aluminum mold (A). Carbon fiber telescopic tubes in the hip prototype (B).

Telescopic carbon weave tubes were selected for the hip prototype to accommodate sizing and to support the thigh components. The tubes were cut to size and locking pins were used to fix the size of the tubes. The carbon tubes were very light at 0.077 lb/ft however, drilling the adjustment holes required special tooling, making it more challenging to resize tubes during prototyping and potentially complicating the construction of replacement parts once the EVA S3 was delivered. After the final redesign of the EVA S3 hip, the back carbon poll was replaced with more versatile ½ inch 80/20 extruded aluminum. The 6 inch long tubes on the side of the exoskeleton were replaced with extruded aluminum. The weight penalty for this replacement was justified by the ease that end-users can make their own sizing tubes or replacement parts if needed.

Steel is a heavy but strong material that comes in seemingly endless varieties. Stainless steel was used in the torque transmission shaft of the spool assemblies. Steel was selected over aluminum for this component to minimize the angle of twist of the shaft. Shaft twist between the spools and the structure or the spools and the potentiometer reduces the accuracy of the angle readings and torque transmission for a specified joint angle. Hardened 400 series stainless steel was used to comprise the slider rails of the linear motion carriages to reduce wear.

A majority of the structural components such as the spools and the support structure were made from 6061 T6 aluminum. 6061 T6 aluminum has a density of 2.7 g/cc (0.0958 lb/in<sup>3</sup>) and a typical yield strength of 255 MPa (37000 psi) (MatWeb 1996-2013). 6061-T6 aluminum is affordable,

easily machined, and very corrosion resistant. An alternative to 6061-T6 aluminum often used in aircraft construction is 7075 T6 aluminum. This metal has a slightly higher density at 2.8 g/cc (0.102 lb/in<sup>3</sup>) and a typical yield strength almost double that of 6061-T6 at about 462 MPa (67000 psi). The high strength to weight ratio of 7075 series aluminum was preferred. However, finite element analysis (FEA), of concept designs indicated that the strength of 6061 would support the necessary loads. While some structural dimensions could have been decreased if constructed of 7075-T6, 6061-T6 aluminum is usually half the price (\$129.93 vs. \$276.72 for a 5” by 1’ rod) and has better welding and corrosion characteristics.

### 3.7 Finite Element Analysis for Structural Design

During the design process the spool cable guides were lengthened to eliminate the problem of cable derailment. All spools were tested via FEA analysis to ensure that they would not fail under the design loads. A spool design for the hip abduction/adduction actuators is shown in Figure 3.34

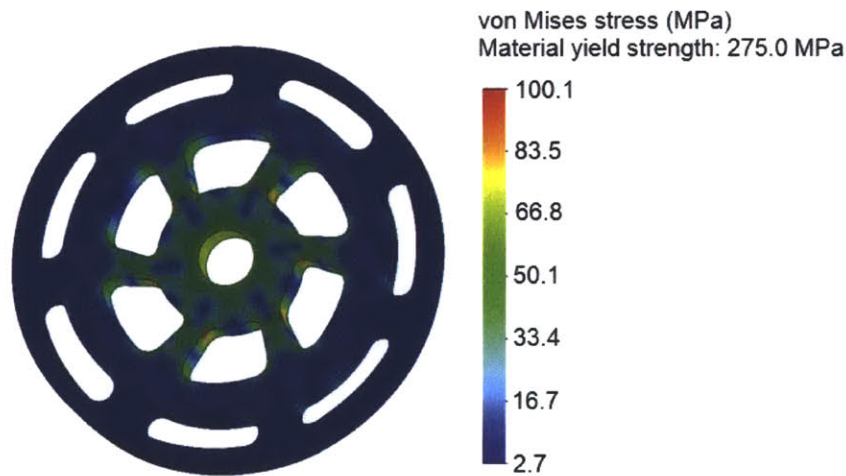


Figure 3.34 – FEA of the hip rear spool shows the von Mises stress does not exceed 101 MPa.

The weight saving cutouts of each spool were iteratively adjusted based on the results of the FEA analysis. A 1.8 factor of safety was specified as the minimum for the spool components. The most complex iterative design using FEA checks was the hip actuator assembly structures. Each structure design was loaded under the worst case scenario where both actuators are applying the maximum theoretical force to the actuator mounting brackets. For the hip flexion/extension

structure that was a load of 1500 N (337 lb) and 630 N (142 lb) on the flexion and extension actuator brackets respectively. This loading condition is shown in a rendering of a concept design in Figure 3.35.

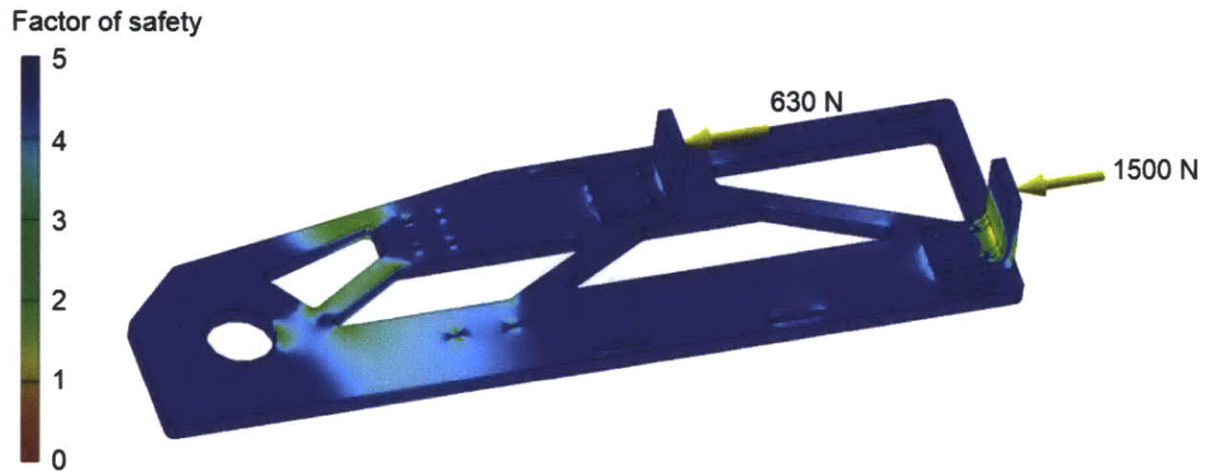


Figure 3.35 – Loading condition on the prototype hip flexion/extension actuator assembly structure

The hip flexion/extension actuator assembly structure thickness was safely reduced from 0.953 cm (0.375 in) to 0.635 cm (0.25 in) aluminum plate with the geometry alterations seen in Figure 3.36. A stiffener was added perpendicular to the primary structure. This stiffener also allowed the bracket for the 20 mm diameter actuator to be mounted horizontally to create more clearance between the hip flexion/extension assembly structure and the potentiometer mounted near the knee joint (not pictured).





Figure 3.36 – Factor of safety FEA profile of a hip flexion/extension actuator assembly structure design iteration

The results of this simulation indicated that material could be removed from the area near the top of the structure and around the smaller actuator mount. The FEA analysis also indicated a stress concentration where the stiffener ends. The stiffener tapers off the joint axis to provide clearance for the support bar that attaches the hip flexion/extension actuator assembly to the EVA S3 hip backpack. The solution, shown in Figure 3.37, makes use of a steel slider rail to be both a guide for the actuator and reinforcement for the structure. To save weight, unnecessary structure above the joint has been removed and additional cutouts above and below the small actuator mount were added.

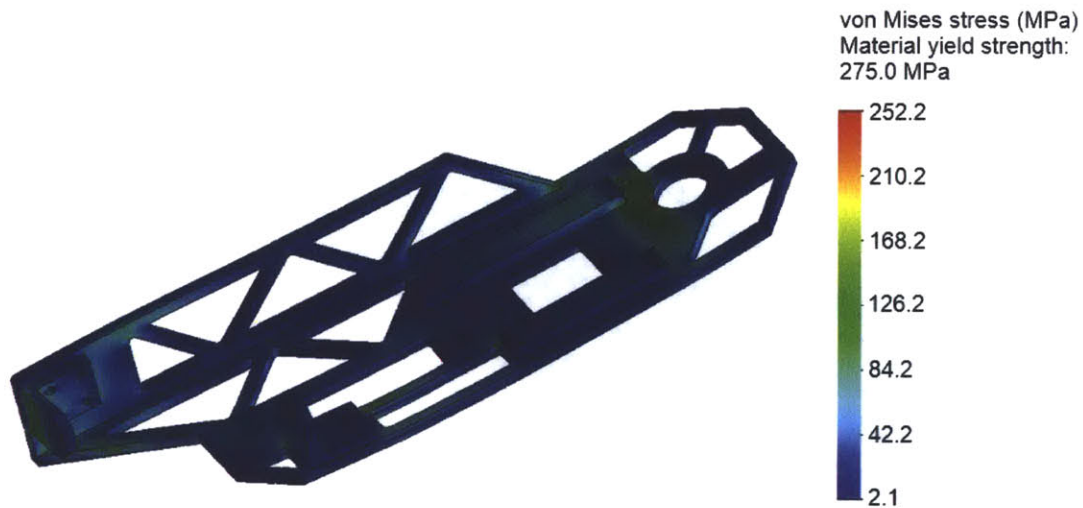


Figure 3.37 – von Mises stress in the final hip flexion/extension actuator assembly structure design.

FEA was used to validate designs and reduce weight through an iterative process of repeated alterations and simulations. Any simulation can only be as good as the inputs and initial conditions. Care was taken to check force loads and fixtures. Outcomes were predicted using simple hand calculations before a design underwent an FEA simulation.

### 3.8 Construction and Design Revisions

The EVA S3 was created with an iterative design philosophy. In order to effectively assess a design before creating the final product it was necessary to build a partially complete prototype to validate the fit and function of the EVA S3 hip. This also gave us the opportunity to test manufacturing methods and check tolerances. Figure 3.38 shows the design of the prototype EVA S3 hip and backpack system.

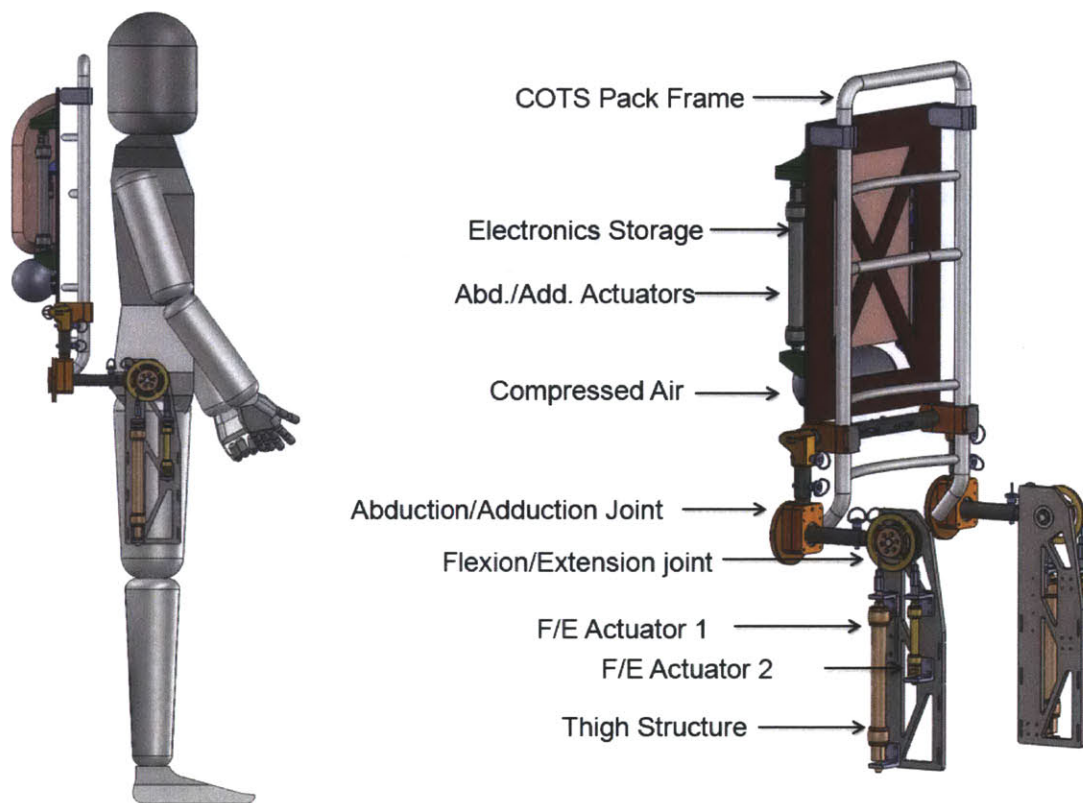


Figure 3.38 – Prototype hip and backpack design

As a prototype used to check design concepts and fit, it was not necessary to build to every component of the prototype design. Some components had repeatable concepts, such as the actuator assemblies; therefore only the flexion/extension actuators were fully constructed. For the same reason it was only necessary to build one side. The electronics storage and compressed air tanks were also omitted as they were not critical influencers of the joint design. Some components (bright orange in Figure 3.39) were 3D printed out of ABS to save machine time. Prototyping was valuable for improving mounting and assembly methods. Figure 3.39 A shows prototype components ready for assembly. In Figure 3.39 B the spool assembly prototype helped confirm the alignment of the spools with the actuators and that the fit tolerances would minimize play in the assembly but still allow free rotation of the spool assembly.



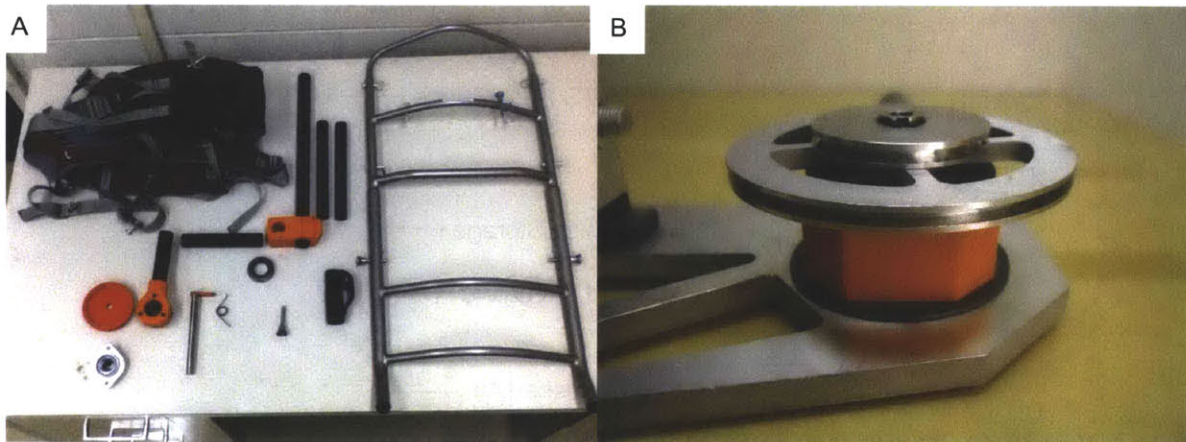


Figure 3.39 – (A) Some prototype components ready to be assembled.(B) The assembly of the prototype spool.

Important structural components that could not be made out of ABS for the prototype, and parts to be used in the final design were made were manufactured in the Edgerton, and Aero/Astro student machine shops using a water jet (Figure 3.4 A), lathe, saw, break, and CNC mill (Figure 3.4 B). Welding of the support structure in the final design was performed by Central Machine Shop.

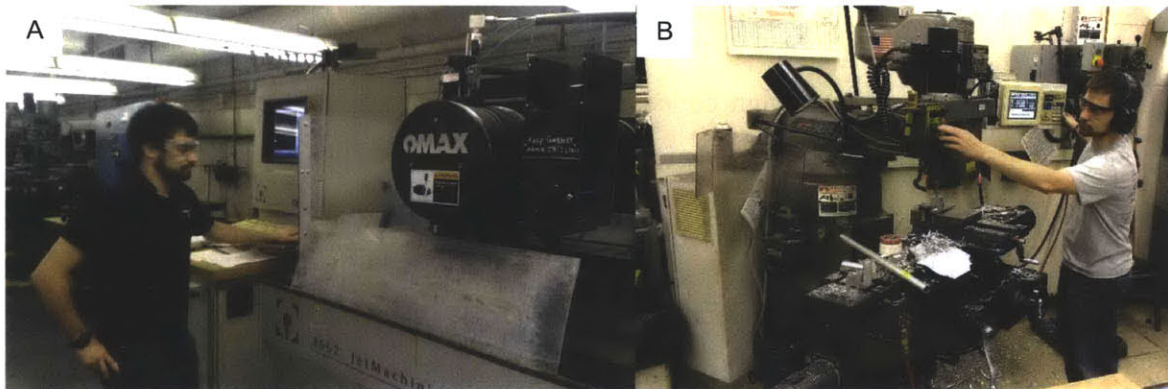


Figure 3.40 – Manufacturing EVA S3 components using a water jet cutter (A) and a CNC mill (B)

Table 3.6 describes the tests and checks the prototype underwent, the results observed and the improvements implemented in the final design. Many of these test were qualitative and provided information that would be impossible to get from a CAD model.



Table 3.6 – Tests, results, and actions taken during the prototype testing.

Prototype Test	Result	Action
Effectiveness of cable guide rails	Cable sometimes derailed from spool	Guide rail height on spools doubled
Linear carriage guide and sliding cylinder friction	Too much friction in sliding cylinder	Replaced sliding cylinder with another linear carriage guide
Play in structure	Excessive play in concentric bearing and tube for hip ab./ad. joint	Redesign hip ab./ad. joint
Play in spool assembly	Minimal play observed	Kept concept, improved spool compactness
Unactuated resistance	Excessive resistance felt in hip ab./ad. joint	Change hip ab./ad. joint location
Inflation/deflation speed of actuators	Cycle time too slow for gait cycle	Increase air tube diameter and use different solenoid valves
Manufacturability of components	Multiple issues with composite tubing	Replace composite tubing with aluminum tubing
Tube sizing clamp strength	Relative slippage between tubes when force is applied	Use locking quick release pins to hold tubes in place

Figure 3.41 is a side view of the constructed prototype being worn by a subject. This was part of a fit check to see where there is room for improvements. The next section will discuss the fit check in more detail.



Figure 3.41 – The prototype secured to a subject

## 3.9 Integration and Testing

### 3.9.1 Qualitative Testing

The purpose of qualitative testing is to assess characteristics that cannot be measured by computer simulations or robotic testing. These qualities are comfort, general mobility, and ease of donning and doffing. Feedback from qualitative testing allows an engineer to identify possible improvements that are difficult to find any other way. This was the chief justification for building an early hardware prototype of the EVA S3 hip components. Figure 3.42 shows two types of qualitative tests: A fit check (A) and a general mobility test (B).

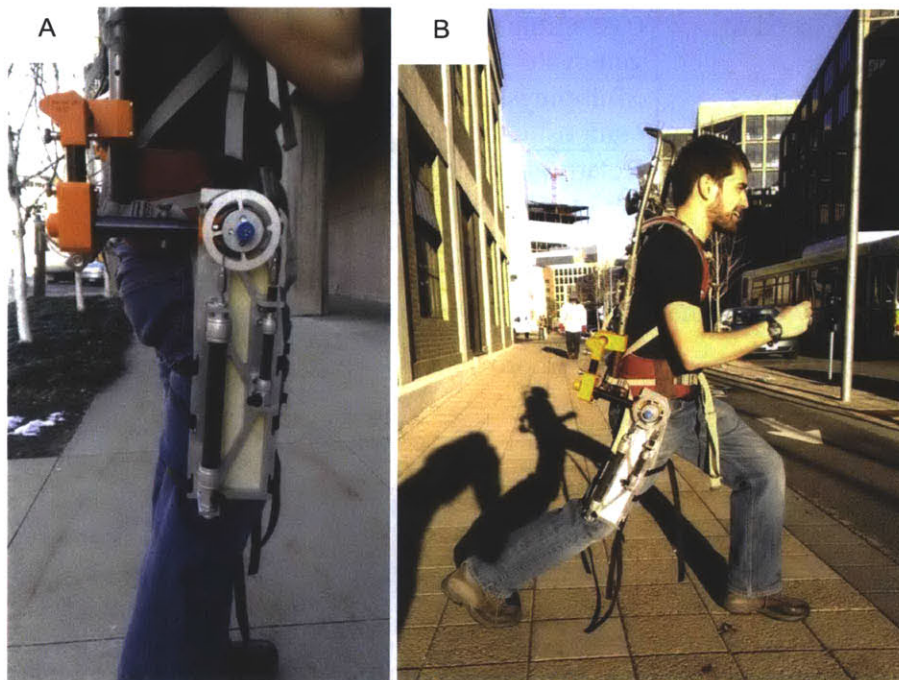


Figure 3.42 – A qualitative fit check (A) and a general mobility test (B)

The fit check, Figure 3.42 A, was important to validate and change the size of the structural beams and adjustments. It is difficult to use solid models in computer software to fit people, even with models of 5<sup>th</sup> and 95<sup>th</sup> percentile men and women. How the device will sit on the body and how much padding will compress was unknown until verified through fit checks. The fit check also helped inform if the method to secure the exoskeleton was adequate. After the check in the figure, structural support lengths were adjusted. The strap method was deemed inadequate to secure the

lower leg of the exoskeleton. The next version of the EVA S3 hip was designed to bolt directly to a leg brace that runs the length of the whole leg for a more secure fit. The general mobility test, Figure 3.42 B, demonstrated that this EVA S3 hip prototype had very good hip flexion/extension axis alignment. The exoskeleton moved freely. The dominating encumbrance felt was from the weight and inertia of the exoskeleton itself rather than mechanical interference. The hip abduction/adduction joint of this prototype was incomplete and did not have actuators attached to it. However, its representation here was still enough during qualitative testing to show mechanical interference, primarily due to the misalignment of the hip abduction/adduction axis of the prototype and that of the human hip. Figure 3.43 shows the hip abduction/adduction of this early prototype. Note how the axis runs beside the hip.

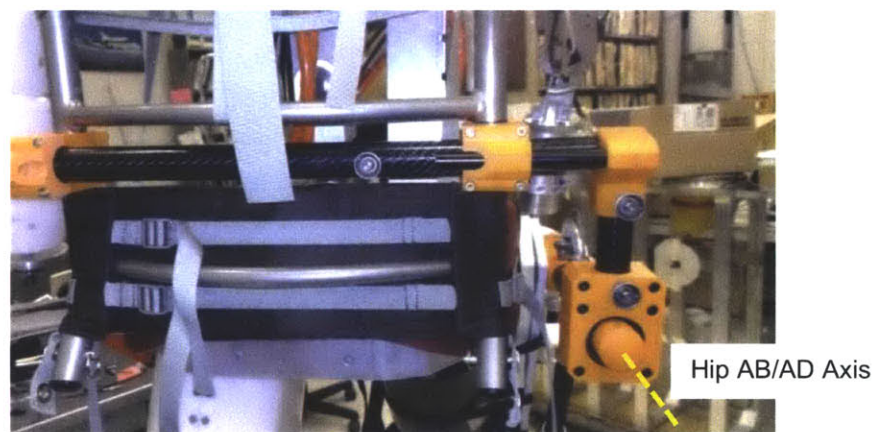


Figure 3.43 – A rear view of an early EVA S3 prototype

This test demonstrated the need to increase the adjustability of the axis of rotation of the hip abduction/adduction joint of the EVA S3 to properly align with the axis of the human hip. These changes are described in Section 4.1.1

Subjective testing of ease of donning and doffing is least effective at the component level. As a separate entity, a component is lighter and is not constrained by other attachments. Donning and doffing impressions for the full EVA S3 are described in Section 4.2.



### 3.9.2 Robotic Space Suit Testing

The Robotic Space Suit Tester (RSST) was used to develop and validate the control system for the EVA S3. The RSST, pictured in Figure 3.44, is a hydraulically actuated robot designed and built by Sarcos Inc., and was originally designed to quantify joint torques for advanced space suit mobility development for NASA. NASA loaned the RSST to MIT for use in support of student EVA research projects. The RSST has 12 articulating joints on its right side, and each joint contains a potentiometer to measure joint angle and a strain gauge load cell to measure joint torque. During the early 2000s the RSST was used extensively by MIT researchers to create joint torque database for the EMU (Schmidt, Newman et al. 2001) and more recently has been used to characterize aircraft pressure suits (Meyen, Holschuh et al. 2011) and space suit simulators (Duda, Newman et al. 2011).



Figure 3.44 – The Robotic Space Suit Tester (RSST)

Parameters such as sensor gain calibrations are altered in the Simulink program that runs the robot. The RSST records data in MATLAB. Program errors and faulty controller boards prevented the robot from executing Simulink commands to follow sinusoidal motions. Actual movements of the RSST joints were controlled manually by rotating knobs on controller boards (Figure 3.45).

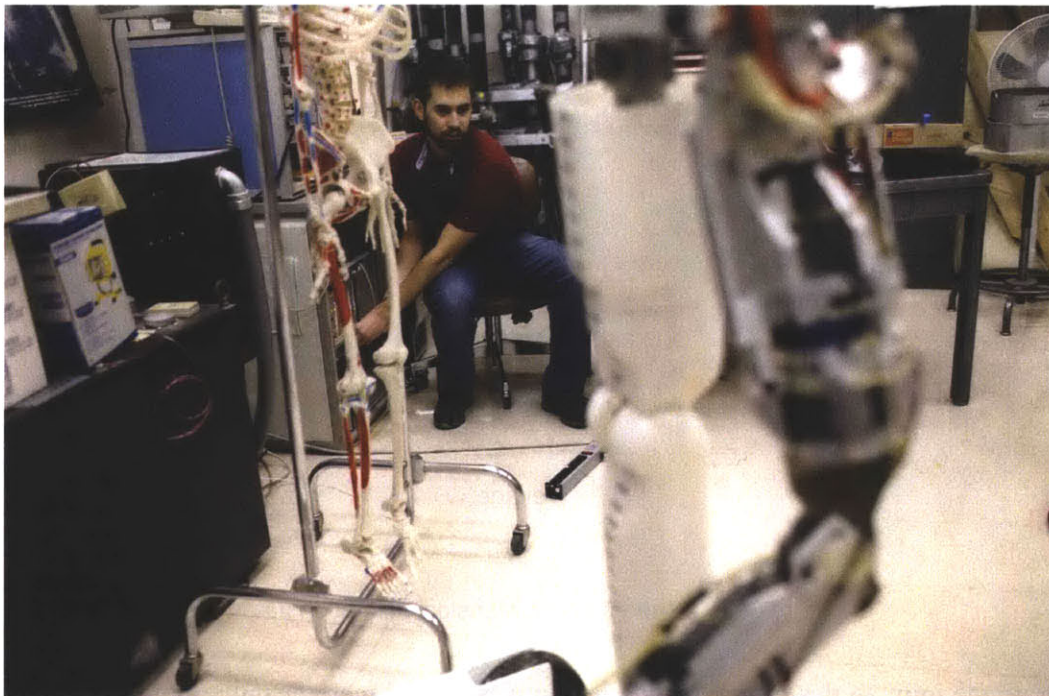


Figure 3.45 - Manual control of the Robotic Space Suit Tester

### **3.9.2.1 Calibration and quality control**

Before testing, the robot was calibrated to ensure the accuracy of the results. The torque sensors of the robot were calibrated by moving a joint to a pre-defined angle and adding successively heavier weights and a fixed point along the limb. The torque for each setup was calculated by multiplying the weight by the horizontal distance from the joint (perpendicular to the vertical force vector from the weight). The voltage of each strain gauge was recorded and the points were fit linearly to determine the relationship between torque and voltage (see Figure 3.46).

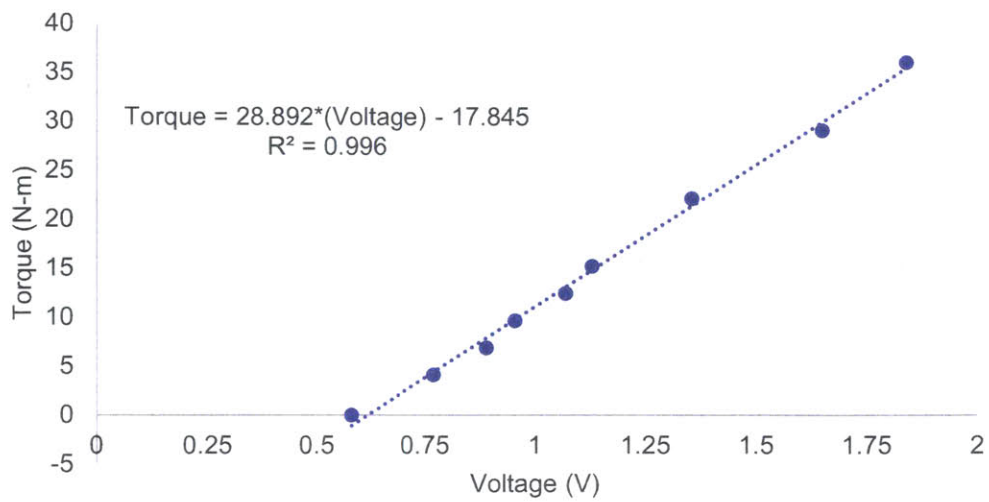


Figure 3.46 – Knee flexion/extension calibration data

To calibrate the joint angles of the RSST, the leg was moved incrementally and the position read from a protractor. The calibration curve was derived from a linear fit between the measured angle and the voltage read from the RSST potentiometer.



Figure 3.47 – Method for determining joint angle using a protractor and a plumb line

### **3.9.2.2 Robotic Testing Procedure**

First, torque-vs.-position curves must be obtained for the RSST alone. This curve, representing the torque due to the RSST weight, will be eventually subtracted from the data obtained so that the data includes torque due to the EVA S3 alone, not due to the EVA S3 plus the weight of the RSST.

During testing, the left lower body of the EVA S3 is mounted to the RSST (Figure 3.48). The EVA S3 joints cannot be mounted and validated individually because the weight of the components below a joint also affects the torques that are felt at that joint. It is necessary for the control system not only to apply a specified torque but also enough torque to offset any excess weight of the exoskeleton.

First, the EVA S3 potentiometer for a joint is calibrated to match the joint angle reading of the RSST. Next, one actuator from the joint's antagonistic pair is calibrated. This calibration process records the torque read by the RSST for a variety of pressures at several positions. This calibration is important because we have found that the torques transmitted through the exoskeleton to the robot often vary. Then the maximum torque generation for the maximum range of motion is verified. Next, the other actuator goes through the same process and this information is used to fit corresponding relationships between pressure, position, and transmitted torque.

These relationships are used to create a preliminary control algorithm that varies the actuator pressure based on the position and the desired torque output from the EMU joint torque data. The control system is then moved slowly through the operational range of motion at 1 degree increments to validate torque values and make further adjustments.



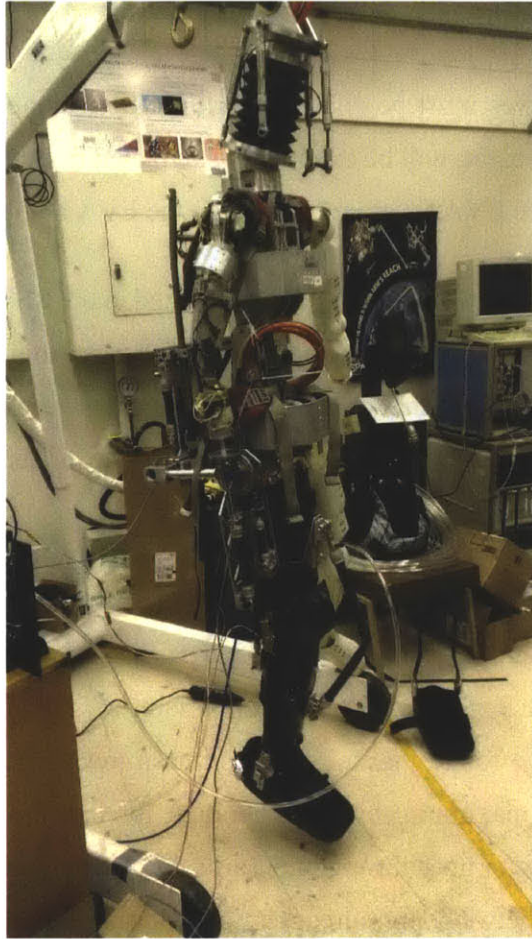


Figure 3.48 - Right lower body of EVA S3 mounted to the RSST

Once the calibration of actuator pairs at static locations is complete, the control system's response to fluid motions is recorded. The joint being tested is actuated three times through its functional range of motion at a rate of about 0.5 Hz. The range and speed of motion is approximately executed by turning a knob on the controller board. These trials are each repeated three times for a total of 9 cycles through the range of motion. If any changes were made to the fitting of the EVA S3 or the control system between trials, the trials were repeated.

### **3.9.2.3 Data Processing**

The desired curve for each joint motion is torque vs. angle. Two datasets were needed: the recorded torque with the S3 active, and the torque due to the weight RSST alone ("unsuited robot")

torque). Unsuiting robot torque is subtracted from the torque measured during S3 testing, and the resulting curve is the torque due to the S3:

$$\tau_{SS} = \tau_{meas} - \tau_{US} \quad 3.6$$

where  $\tau_{SS}$  is the torque due to the EVA S3 (what we wish to know),  $\tau_{meas}$  is the torque measured when the EVA S3 is worn on the RSST, and  $\tau_{US}$  is the torque measured when the RSST is unsuited. For both the suited (

Figure 3.49) and the unsuited data (Figure 3.50) we cycled the RSST limb through the range of motion three times.

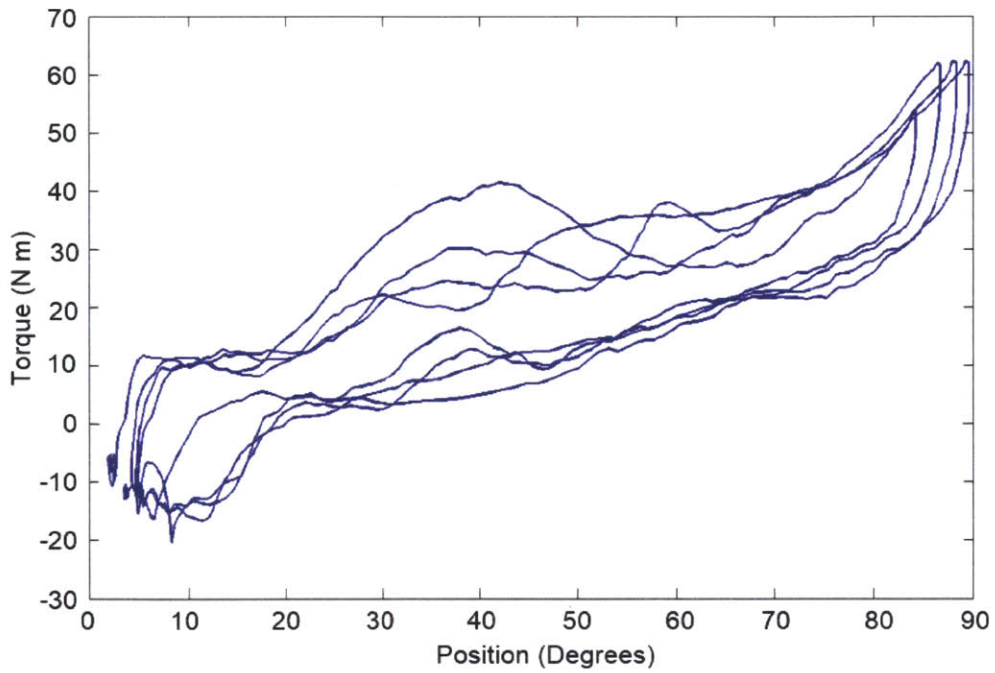


Figure 3.49 – Torque vs. angle, net measured value for RSST knee for three cycles

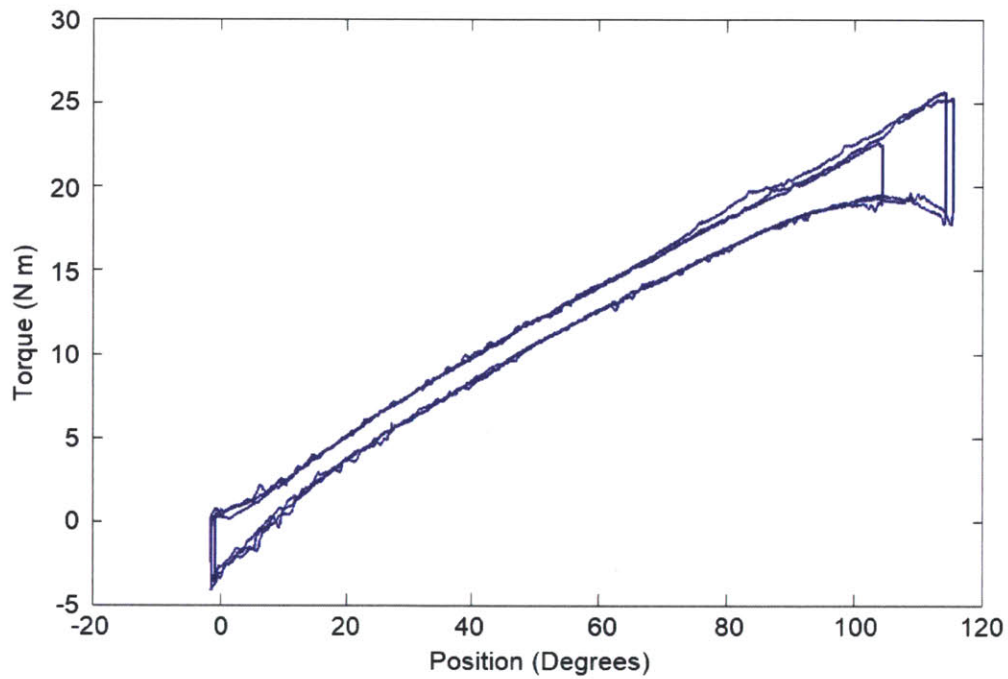


Figure 3.50 – Torque vs. angle plot of the unsuted RSST knee for three cycles

The unsuted data set was averaged, such that one set of numbers was subtracted from the suited data. We did not average that data, so that we could better see the consistency of our measurements. An example of the resulting processed data can be seen in Figure 3.51.

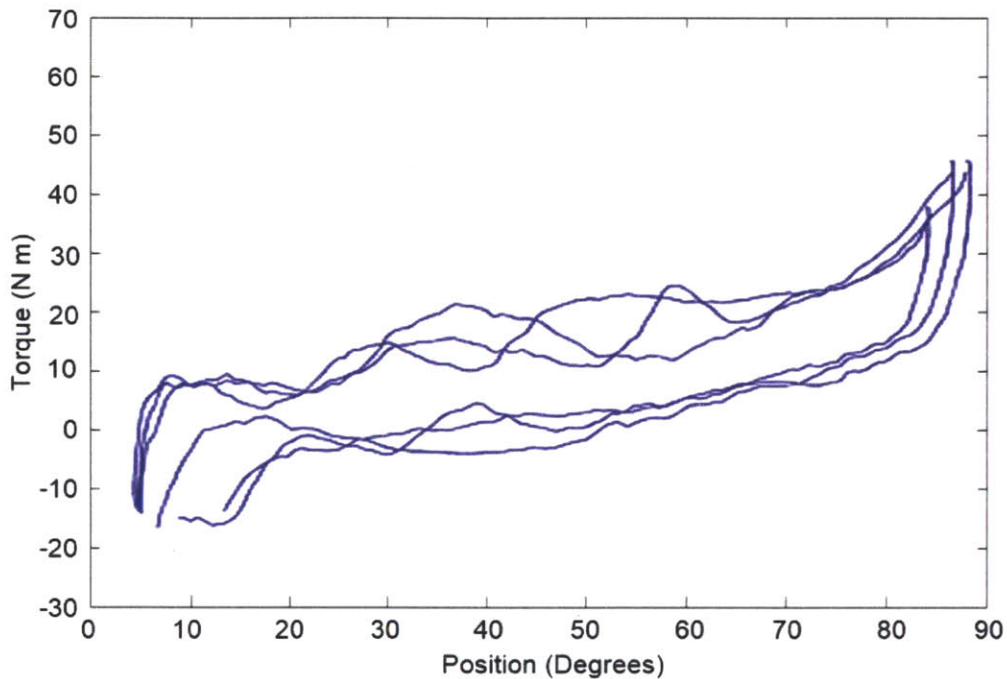


Figure 3.51 – EVA S3 Knee torque vs. angle for four cycles

There is a time component that should be considered as well. Specifically, whether unsuited or suited:

$$\tau = I\ddot{\theta} + mgl \sin \theta \quad 3.7$$

where  $\tau$  is the torque of the RSST (suited or unsuited),  $I$  is the RSST limb moment of inertia,  $\ddot{\theta}$  is the angular acceleration of the limb,  $m$  is the mass of the limb,  $l$  is the distance from the joint to the center of gravity, and  $\theta$  is the angle of the limb at any given time.

This equation poses a number of logistical difficulties. First, we do not know the moment of inertia or mass of any limb of the RSST. We know the mass of the S3, but do not know how that alters the moment of inertia when mounted to the RSST. Finally, we do not explicitly measure angular velocity or acceleration. While these can be derived from the position and time measurements, these derivations made our noisy data considerably noisier, such that it was unusable.

If the rate of movement of the limb is kept constant, then the simple data processing scheme (Equation 3.6) holds true. Thus, we attempted to maintain a constant angular rate when cycling

the limb through the range of motion, and to keep the same rate when cycling the unsuited robot and the suited robot.

### **3.10 Summary of Methods**

The design of the EVA S3 hip was constrained by requirements and optimized to achieve the design goals. The primary requirements were specific torque generation and range of motion requirements selected from the review of the joint torque database. Overall design goals included lightweight, low bulk, customizability, fit, and cost. The progression of the exoskeleton benefited greatly from a “design, prototype, test and repeat” philosophy. Over ten designs were created in the computer aided design (CAD) program SolidWorks. Early physical prototypes were created using cardboard and 3d printing was used for the rapid prototyping of mechanism such as the retractable spool. One major prototype was constructed halfway through the project cycle to test the concepts and a whole unit and perform fit checks. These fit checks were critical in informing future design and communicated issues that were not clearly understood with virtual CAD models. The quantitative testing procedure was conducted by mounting the EVA S3 components to MIT’s Robotic Space Suit Tester (RSST). Before testing, repairs and a calibration procedure were performed to protect the validity of the results. The recorded data was processed by subtracting the weight of the unsuited robot so the results would include only data attributed to the EVA S3.

## 4. Results and Discussion

### 4.1 EVA S3 Architecture

#### 4.1.1 Hip and Backpack Design

The hip portion of the EVA S3 consists of four actuator assemblies mounted to a Kelty Trekker 65 external frame backpack (Boulder, CO), with the cloth storage compartment of the backpack removed and the hip padding and shoulder straps remaining in place. Figure 4.1 is a rendering of the final EVA S3 hip and frame design, including the backpack frame, hip abduction/adduction and hip flexion/extension actuator assemblies, and the DonJoy TROM leg brace (Vista, CA) that comprises the structure of the knee joint. The padding and straps of the backpack are not pictured.

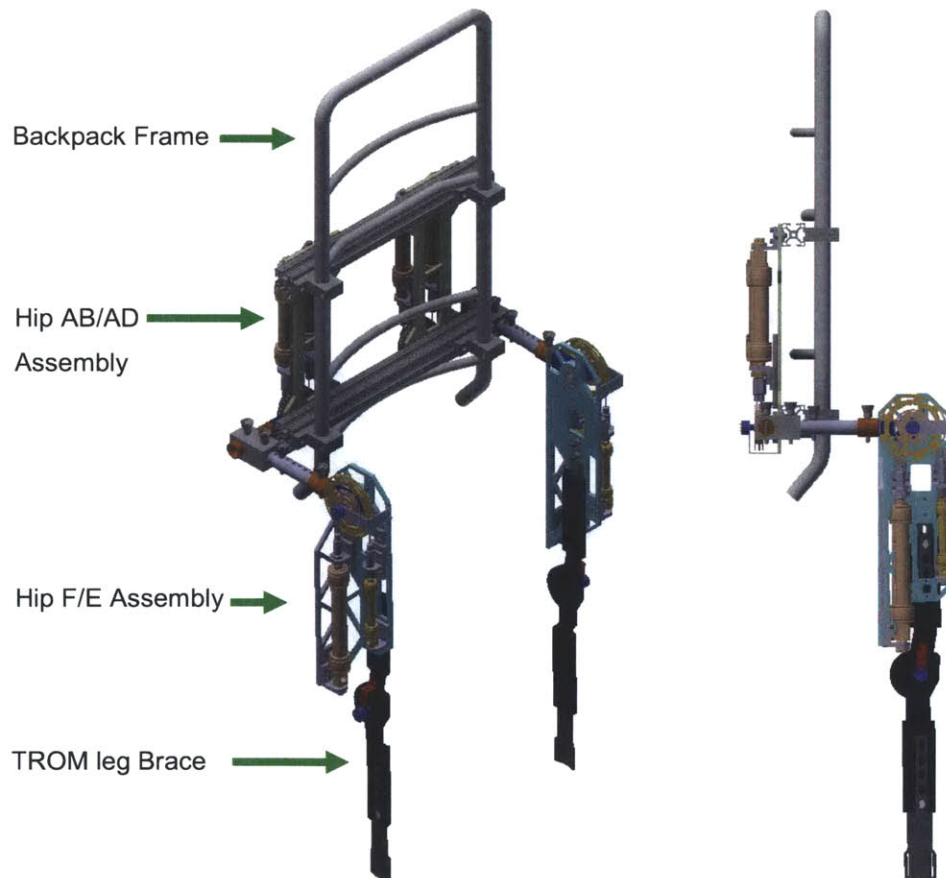


Figure 4.1 – Renderings of the EVA S3 hip and backpack components



The hip abduction/adduction actuator assemblies each include two FESTO 20 mm diameter, 90 mm long, pneumatic muscle actuators. Each actuator is attached to a spool that can apply up to 43 N-m of torque over 45 degrees in abduction and 45 degrees in extension. The torque is applied to an L-shaped connector arm that extends forward to the hip flexion/extension assembly.

Figure 4.2 details the actuator assemblies mounted to the back of the EVA S3. Two 80/20 extruded aluminum crossbars are clamped to the backpack frame. Hip abduction/adduction actuator assemblies are bolted to the 80/20 crossbars.

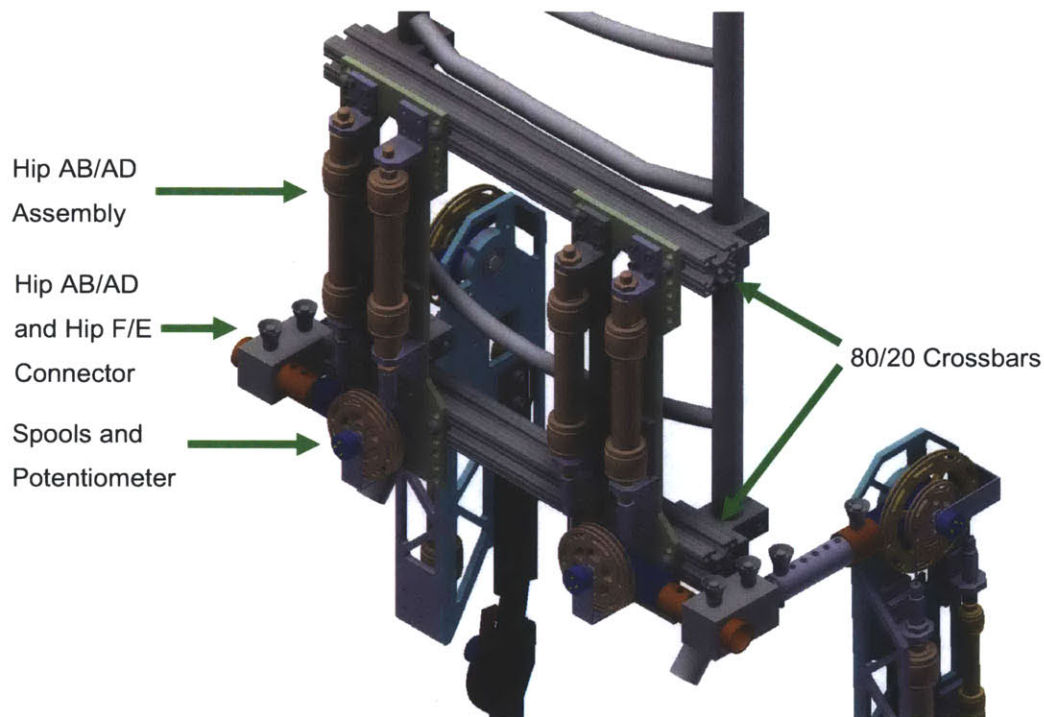


Figure 4.2 – Rendering of the EVA S3 hip abduction/adduction actuator assemblies

The hip is highly adjustable in order to align the axis of each exoskeleton joint with the corresponding axis in the human hip. Figure 4.3 illustrates the adjustment mechanisms included in the design to improve the fit of the hip joint components.



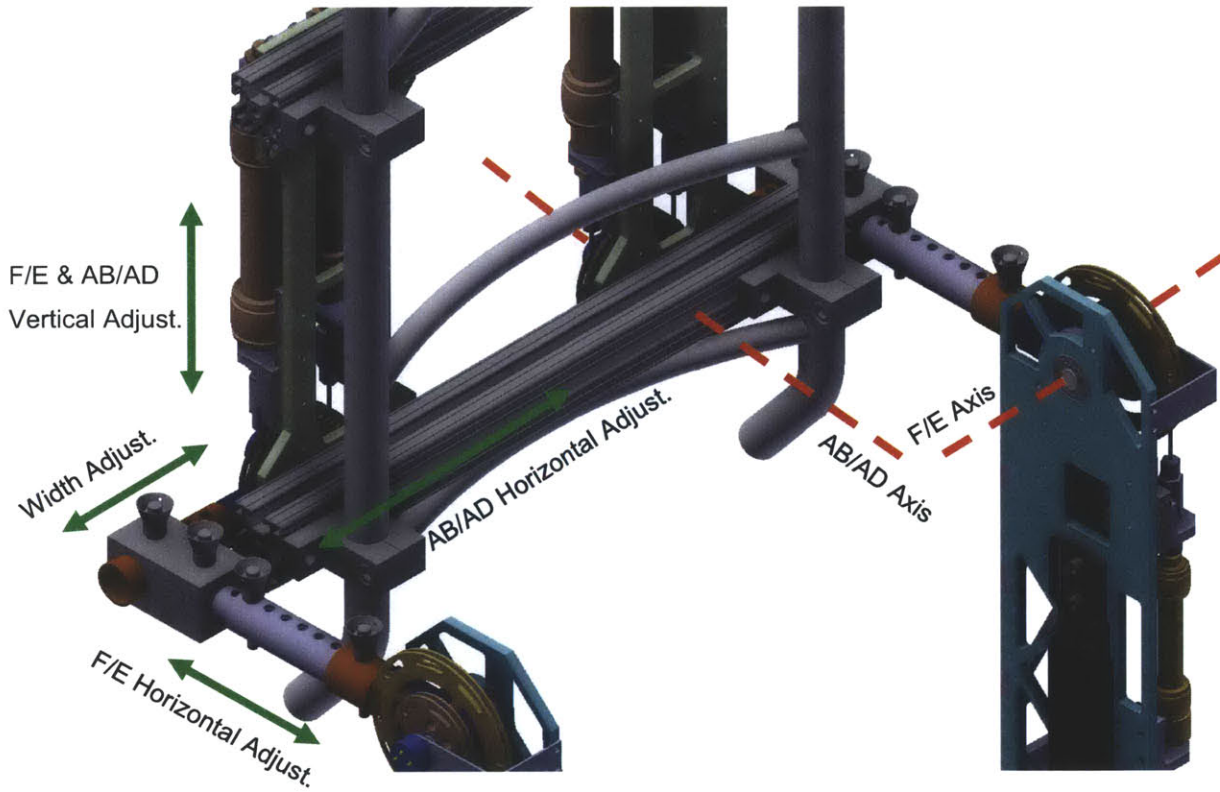


Figure 4.3 - Rendering of hip flexion/extension position adjustment system excluding padding

The vertical alignment of the hip joint is achieved through two mechanisms. The main vertical adjustment is achieved by changing the bolt locations where the hip abduction/adduction actuator assembly bolts onto the 80/20 beam. There are 6 bolt holes spaced 0.5 in apart for a total of 3 in of vertical adjustment. The fine adjustments for vertical alignment are achieved by loosening the clamps that fix the 80/20 beams to the back pack frame and by sliding them up or down with respect to the backpack. Horizontal alignment of the abduction/adduction axis is achieved by sliding the hip abduction/adduction actuator assembly horizontally along the 80/20 cross bar and tightening the mounting bolts once it is in place. A secondary width adjustment exists to bring the

hip flexion/extension assembly closer to the subject's body. Figure 4.4 is a photograph of the completed backpack with hip abduction/adduction assemblies mounted to it.



Figure 4.4 – The completed backpack with hip abduction/adduction actuator assemblies

The hip flexion/extension assembly bolts to the extension bracket of the TROM leg brace (Figure 4.5). This extension bracket can be slid in and out of the TROM leg brace to vary the distance between the knee and hip flexion/extension joint. A similar attachment at the bottom of the TROM connects to the ankle joint (not pictured) and allows for distance adjustments between the knee joint and the ankle joint.

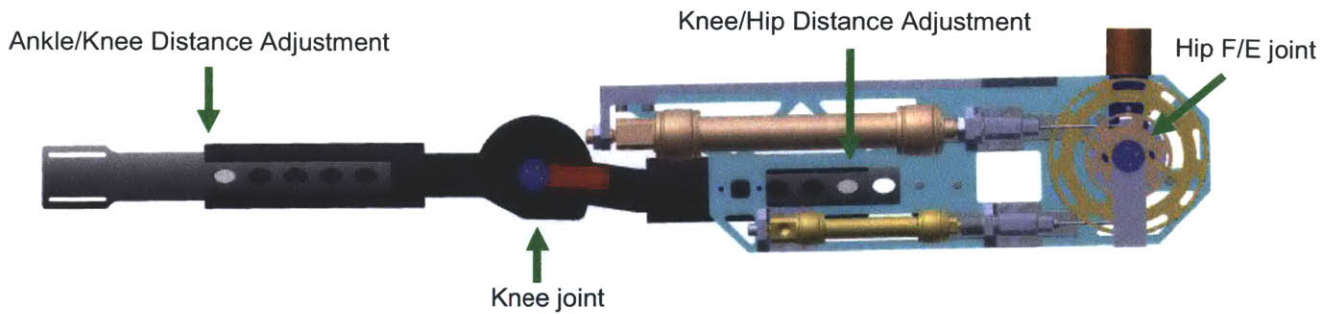


Figure 4.5 – Rendering of hip F/E joint assembly detailing ankle, knee, and hip distance adjustments

The hip flexion/extension assemblies each include a 20 mm diameter, 130 mm long actuator paired with a spool to create 31 Nm of torque over 90 degrees of flexion, and a 10 mm diameter, 62 mm long actuator paired with a spool to produce 28 Nm of torque over 20 degrees of flexion. The actuators and their mounting points can be seen in Figure 4.6. The large actuator is mounted to the side of the structural reinforcement to make room for the knee joint. The small actuator is mounted directly to the main structure. The ends of the actuators that connect to the cables are mounted to linear ball-bearing carriages to reduce frictional losses during contraction. The potentiometer that measures position is fixed in place by a bracket mounted to the main structure.

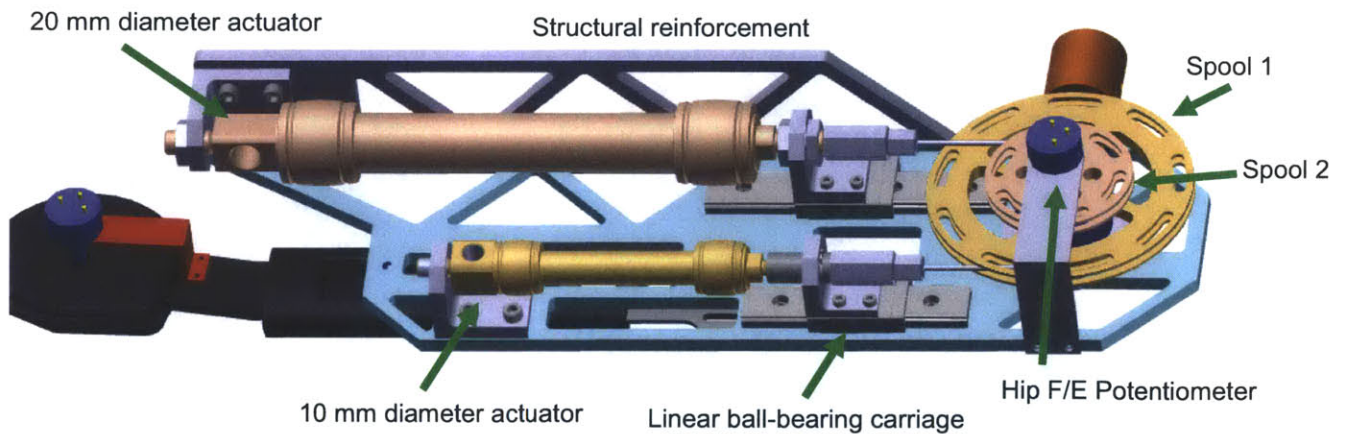


Figure 4.6 – Rendering of hip flexion/extension joint assembly

Figure 4.7 is a photograph of the completed hip flexion/extension actuator assembly before being connected to the EVA S3. Figure 4.8 A and B are front and back images of the hip flexion/extension assembly being worn by a subject.





Figure 4.7 – Completed hip flexion/extension assembly

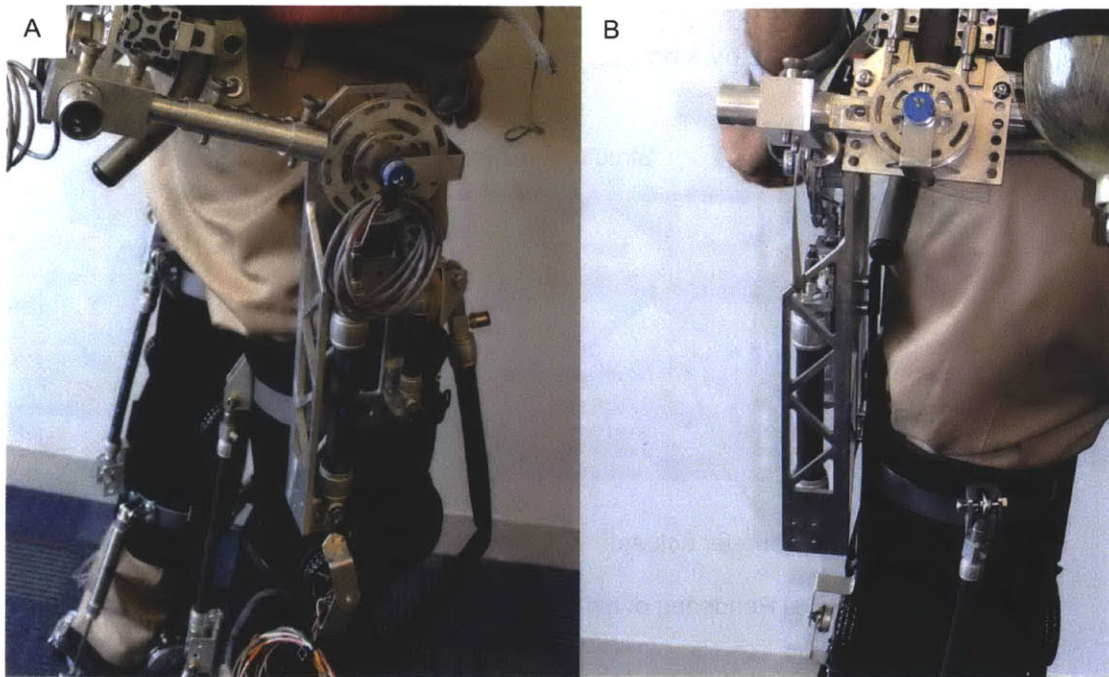


Figure 4.8 – Detail of hip flexion/extension actuators with a subject wearing the EVA S3. Seen from the side (A) and back (B)

Figure 4.9 is an image of the assembled hip and backpack components from behind. A mock compressed air cylinder is also mounted to the backpack to represent the proposed mounting location for a future EVA S3 that carries its power and control system on a backpack. Note how the hip joints are following the subject's adduction motions.



Figure 4.9 – Rear view of EVA S3 hip assembly on a subject.

#### 4.1.2 Knee Design

The EVA S3 knee is comprised of two primary structures a DonJoy TROM leg brace and a carbon fiber greave. In Figure 4.10 the greave is the carbon fiber structure that appears similar to a shin guard that extends over the knee. The leg brace is the thin black structure on either side over the greave.



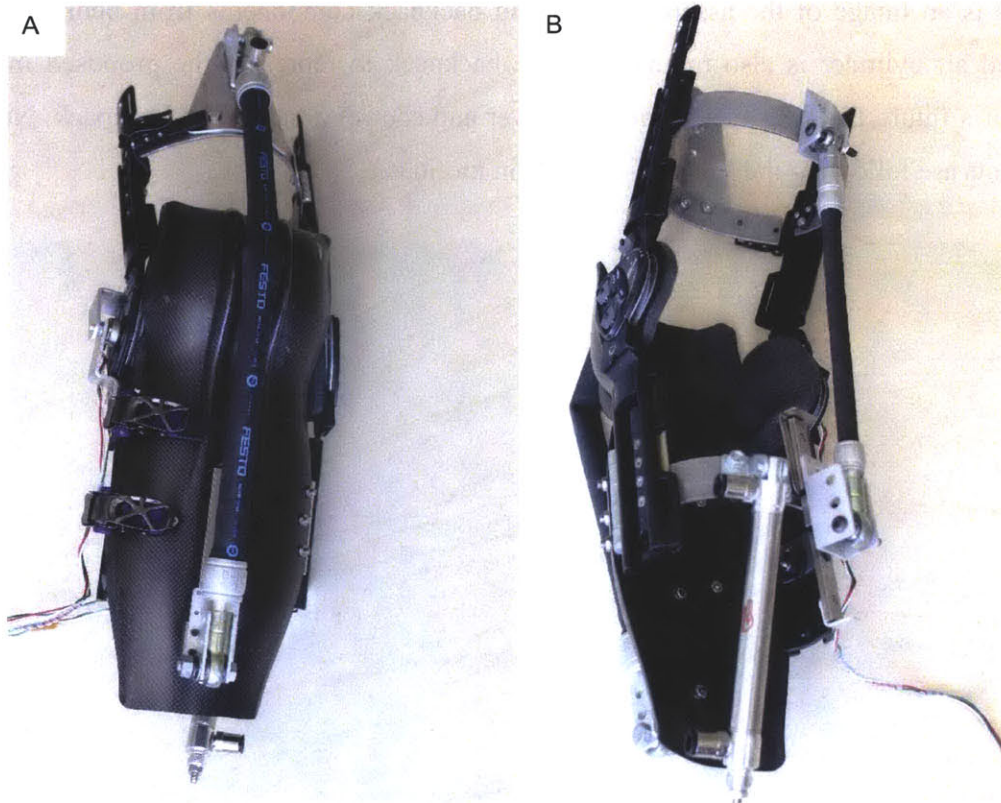


Figure 4.10 – The EVA S3 knee component front and back.

The groove serves a dual purpose in this design. The first is to provide a structure to mount the actuator and connect the sides of the leg brace. The second is to be the contact point between the actuator and the knee joint, so that the torque can be transferred through the EVA S3 structure and the operator. The groove has ridges molded into the structure that guide the actuator around the front of the knee. To reduce weight, the groove is constructed out of a composite sandwich of carbon fiber weave with an epoxy matrix, and a Nomex honeycomb core (details in Appendix A). The actuator ridges and curved shape of the groove further stiffen the structure.

The DonJoy TROM leg brace is commercially available and used to stabilize the leg and limit the range of motion of the knee after an injury or surgery. The brace is attached on the lateral side with snowboard binding clasps to steel brackets in the upper part of the leg (as seen in the top of the knee joint in Figure 4.10) and to the groove (Figure 4.11 A). The medial side is hinged so that when the clasps are opened, the groove and front actuator swing to the lateral side to facilitate donning of the device.

The TROM leg brace can limit the knee motion by either locking it in a particular position in 10° increments from 0° to 90°, or by limiting the lower bounds of motion at 10°, 20°, 30°, or 40° and the upper bounds at 80°, 70°, 60°, or 50°. The 90° limit serves as a safety to protect the operator of the EVA S3. The adjustable limits are available if necessary but are unlikely to be used. Extending from the leg brace knee joint is a slotted structure and a corresponding black anodized aluminum bracket that extends the overall length of the leg brace. Push buttons engage holes in the aluminum brackets to enable size adjustments. The leg brace sizing bracket is visible in the upper parts of the leg brace in Figure 4.10 and in the connection between the knee and ankle components in Figure 4.12 B.

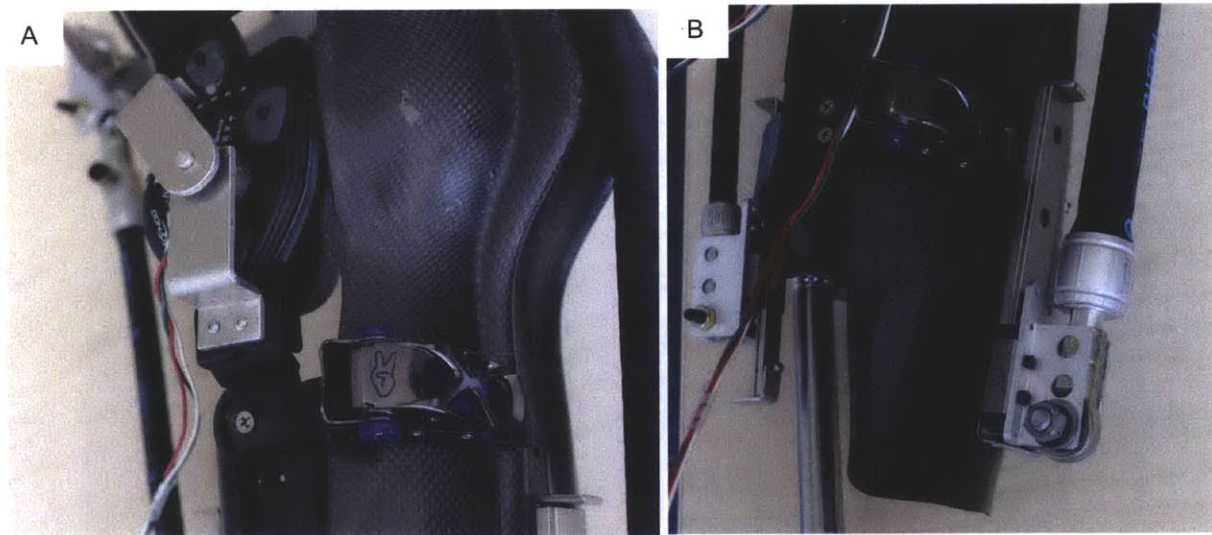


Figure 4.11 – Detail of the binding clasp (A) and slider rail (B)

The knee angle data is recorded by a potentiometer mounted to the lateral side of the knee joint. In Figure 4.11 A, the potentiometer mounts are visible as aluminum brackets mounted just over the point of knee rotation. The axis of the potentiometer is the small shaft protruding through the top bracket.

Figure 4.11 B shows the slider rail mounted directly to the groove. The purpose of this slider rail is to allow the actuator to slide downward when the knee is straightened to reduce actuator bunching that can lead to wear as described in Section 3.3.



The EVA S3 knee and ankle are being worn by a team member in Figure 4.12. Black foam padding is fastened to the subject before donning the knee joint. The comfort padding is visible on the thigh and calf of the subject in Figure 4.12 A, and is also visible above the top of the greave in Figure 4.12 B. In both photos, the actuators are unpressurized.



Figure 4.12 – Side and front view of the EVA S3 knee.

Overall, the impressions of the completed knee joint were positive. The use of a composite greave helped reduce the weight. The DonJoy TROM leg brace allows for 5 inches of brace height adjustability above and below the knee. Donning is achieved by simply ratcheting the straps into place.

However, there are numerous issues in addition to the need to improve simulator fidelity that came up during testing that leave room for improvement. The first is that the slider rails, designed to prevent the kinking of the unpressurized actuators, reduced kinking, but did not completely

eliminate it. In Figure 4.12 A, the rear actuator can be seen as kinking. A solution to this would be to increase the length of the slider rails, however, length is limited by the dimensions of the smallest subject. The rails cannot be made much longer or they would jab the top of the operator's foot or the back of their ankle. Furthermore, the slider rails are constructed of high strength steel and are significant contributors to the weight of the EVA S3.

Another concern is the durability of the DonJoy TROM knee brace joint itself. The joint is made of multiple layers of metal pinned together. The range of motion limiter buttons act as stops in the joint mechanism to prevent motion beyond a certain angle. During qualitative human assessment, one of the knee joints seized, apparently jammed by a limiter button after some of the layers were wedged apart by the top edge of the greave.

### **4.1.3 Ankle Design**

The EVA S3 ankle is an extensively modified DonJoy MaxTrax ROM walker. Snowboard binding straps were added to secure the foot in place. The ankle position data is derived from a potentiometer mounted to the outside of the joint. TROM leg brace brackets are bolted to the ankle rotation joint and fit into the leg brace used for the knee joint. A double acting pneumatic cylinder resists motion in both dorsiflexion and plantar flexion. All structural components, except for the pneumatic cylinder are pictured in Figure 4.13.

Early versions of the ankle design consisted of a low profile device that would fit inside the shoe. To ease the donning and doffing process, a step-in design was considered that initially looked at a foot securing method similar to mountaineering crampons. The DonJoy ankle brace was selected for its sturdy structure and ease of donning. Please see Appendix A for more details about the evolution of this design.

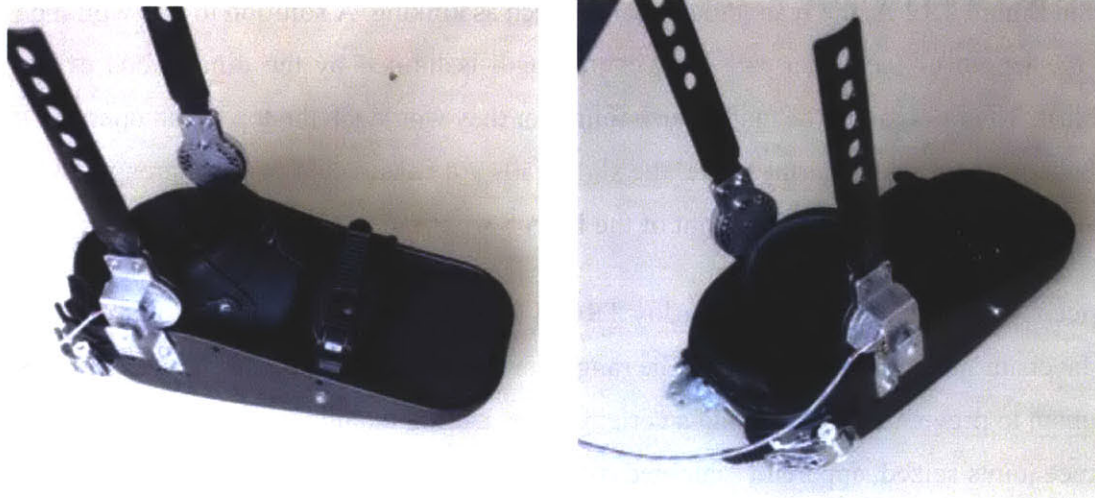


Figure 4.13 – The EVA S3 ankle without the rear pneumatic cylinder

A detailed photograph of the EVA S3 ankle, integrated with the knee joint and worn by a team member can be seen in Figure 4.14. One of the pneumatic cylinders is visible behind the operators left foot (to the viewer's right). A double acting pneumatic cylinder was chosen in this instance because the ankle requirements did not require high torque generation (only -2 to 7 Nm).

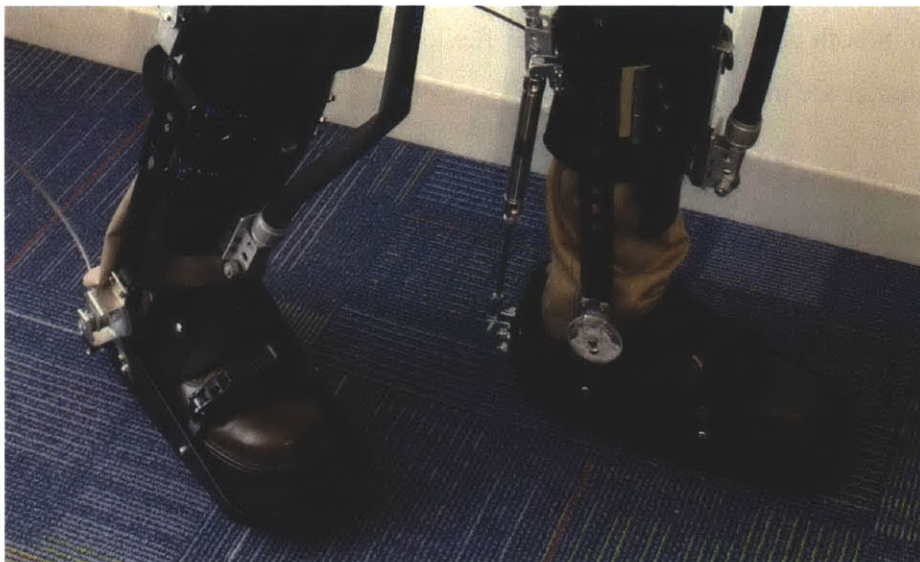


Figure 4.14 – Both EVA S3 ankles worn by a human subject. The pneumatic cylinder can be seen behind the ankle on the right.



The ankle portion of the EVA S3 is simple to put on because of the large foot hold and comfortable snowboard straps. The biggest challenge may be aligning the point of rotation of the ankle exoskeleton with that of the operator. For people with very small feet, their ankle rotation point is slightly behind the rotation point of the ankle brace. This can be remedied by putting a foam spacer behind the heel of the subject and the heel of the brace. Multiple spacers will be needed as sizing varies, not just with the foot size, but also with the subject's footwear selection.

#### 4.1.4 Upper Body Design

The EVA S3 upper body (Figure 4.15) is a shoulder and elbow exoskeleton with passive resistance controlled by torsion springs. Two DonJoy Quadrant shoulder braces were modified for this purpose. The braces are anchored to the body with shoulder straps, and a large Velcro lined cummerbund.

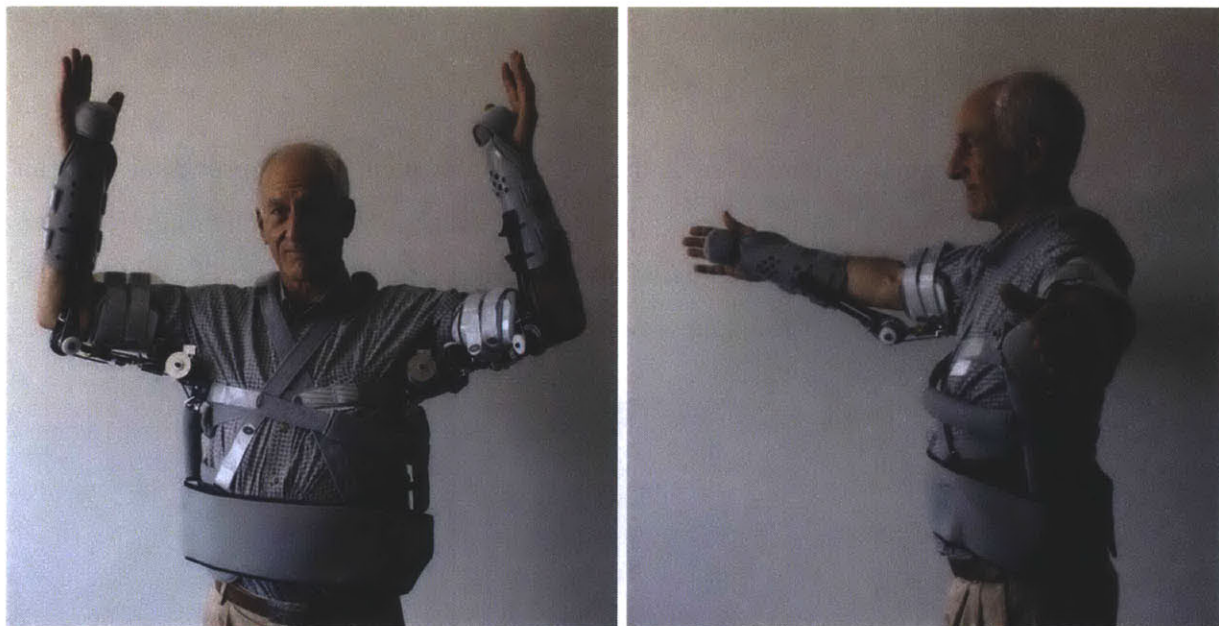


Figure 4.15 – The upper body passive exoskeleton.

The shoulder joint has two points of rotation located below and in front of the arm pit (Figure 4.16 in red circle). There is one point of rotation in the elbow joint (Figure 4.16 in green dashed circle).

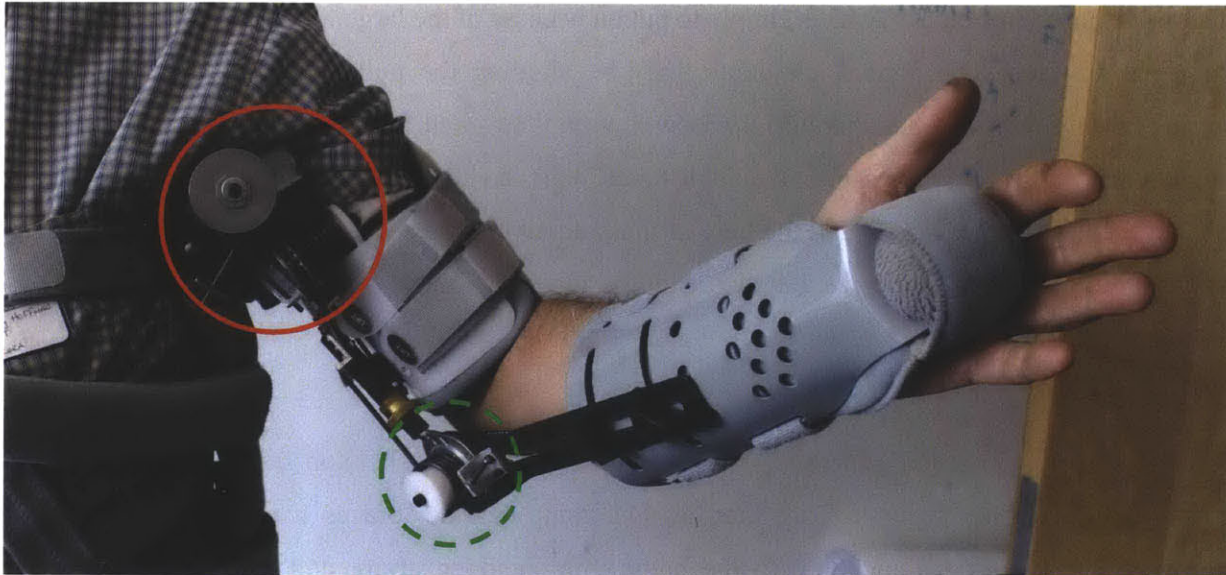


Figure 4.16 – Detail of passive shoulder (red circle) and elbow joints (dashed green circle).

#### 4.1.5 Pneumatic and Control System Design

At the heart of the control system is an Atmel STK600 development kit processor, and an AT32UC3C0512C 32-bit microcontroller (Figure 4.17). Each microcontroller controls two actuators on one joint. The current configuration uses two microcontroller boards. An additional 6 microcontrollers can be added for simultaneous operation of all active leg joints.

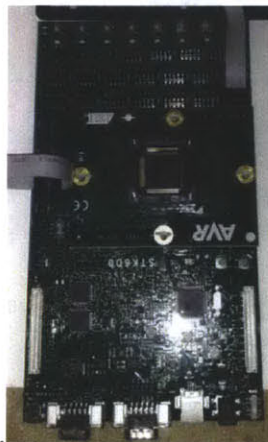


Figure 4.17 - Amtel STK600 processor and AT32UC3C0512C 32-bit microcontroller.

The simulation parameters are set using a laptop computer that loads the information into the microcontroller board. The microcontroller sends and receives signals from the breadboard, which is used primarily for signal conditioning. Figure 4.18 is a simplified control system diagram. The control system is a proportional controller. The potentiometers provide joint location and filters are used to determine the direction of motion. The position and direction data is then translated into a desired torque based on the EMU suit data. That torque is converted into a desired pressure based on a pressure to torque conversion table supplied by FESTO. That command is then sent to the solenoid valve that adds or releases air from the actuator.

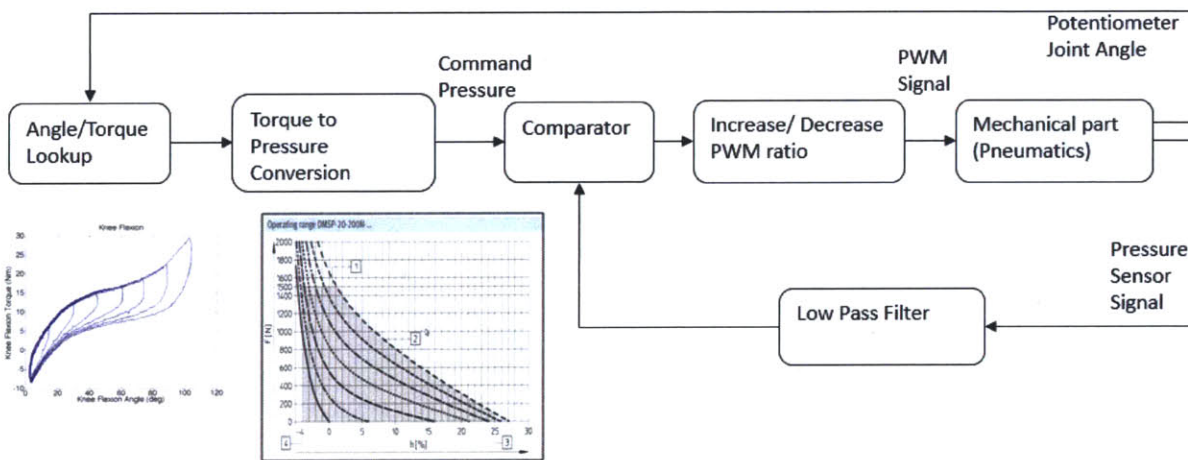


Figure 4.18 – Simple control system diagram.

Figure 4.19 is a schematic detailing the actuator pressure control system. This is how the system reaches a desired pressure and maintains it. The desired pressure is determined by the the control scheme shown in Figure 4.18. A command signal is then sent to a solinoid valve to either input pressure into the actuator from the air source or to exhaust air from the actuator. A pressure sensor provides feedback to the microcontroller on the current pressure level.



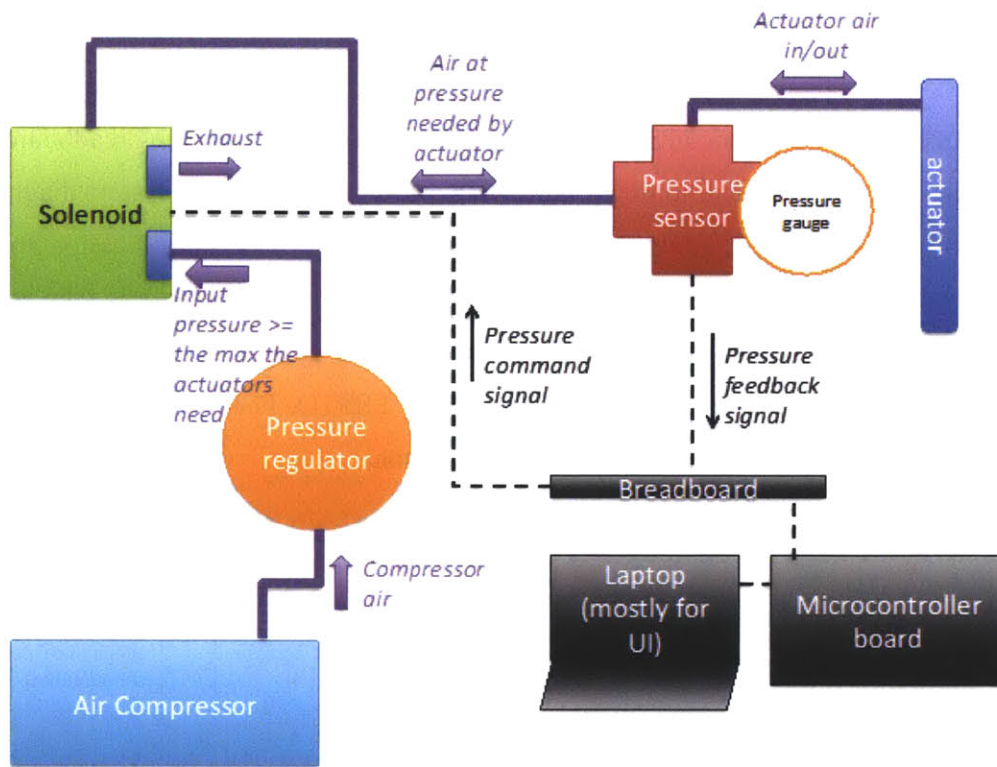


Figure 4.19 – Pneumatic control system diagram.

The final construction of the pneumatics pathway is shown in Figure 4.20. The connectors and tubing for all of the 20 mm diameter actuators and the bi-directional ankle actuator is 6.63 mm (0.25 in) in diameter. The two 1 cm diameter actuators (used in the posterior knee position and the anterior hip flexion position) use 3.18 mm (0.125 in) tubing and connectors.

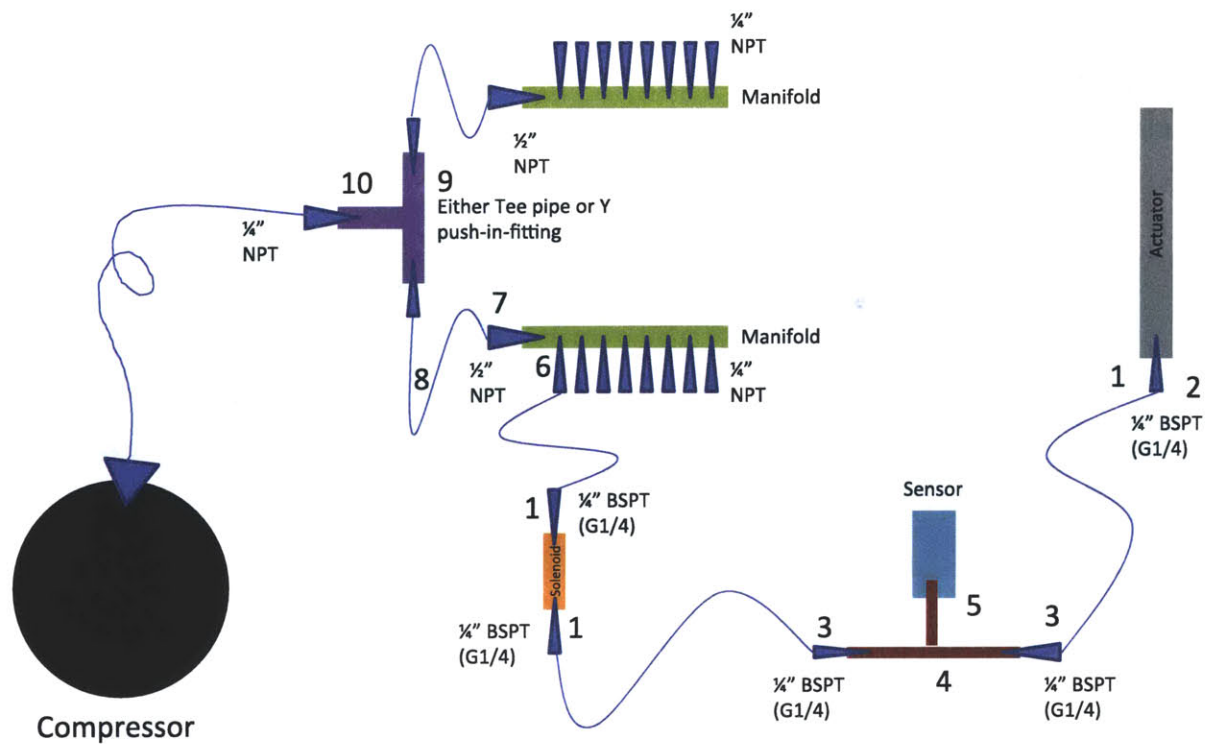


Figure 4.20 Pneumatic pathway design.

Table 4.1 – Labels corresponding to Figure 4.20.

Number	Explanation
1	Male thread to actuator (1/4" BSPT); Push fitting to tube 3/8" OD (1/4" ID)
2	For ankle actuator: Male thread to actuator (1/8" NPT); Push fitting to tube 3/8" OD (1/4" ID); McMaster #5779K115
3	Push fitting to tube 3/8"; Female thread 1/4" BSPT
4	Tee fitting, 3 male 1/4" BSPT
5	Tee: male; Sensor: female
6	Push fitting to tube 3/8"; Male thread 1/4" NPT
7	Male thread 1/2" NPT; Push fitting to tube 1/2" OD
8	Tube size = 1/2"
9	Two, 1/2" push-in-fitting pipes with 3/8" NPT male
10	Female 3/8" NPT

The pneumatics and control equipment was mounted to an ABS plastic board. Sixteen solenoid valves (one for each actuator) were bolted together in an array and received air pressure from two manifolds. Eight solenoids were attached to each manifold (see Figure 4.21).

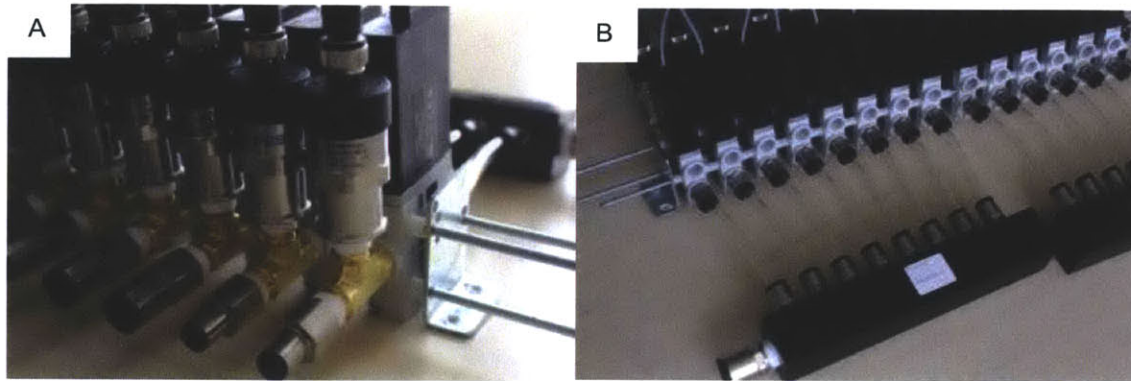


Figure 4.21 – The solinoid stack (A), and the manifold air pressure inlet (B)

Small circuit boards were soldered to replace the breadboards for signal conditioning (Figure 4.22 A). Each joint requires one of these boards. In the next iteration of the EVA S3 design these boards will be part of a printed circuit board to save space. Figure 4.22 B shows the final layout of the microcontrollers, circuit boards, manifolds, and solenoids. These components were bolted to a sheet of ABS plastic for easy transport. The control system assembly should be placed on a table near EVA S3 testing. Air cables and position sensor cables connect to the control system assembly through the EVA S3 tether.

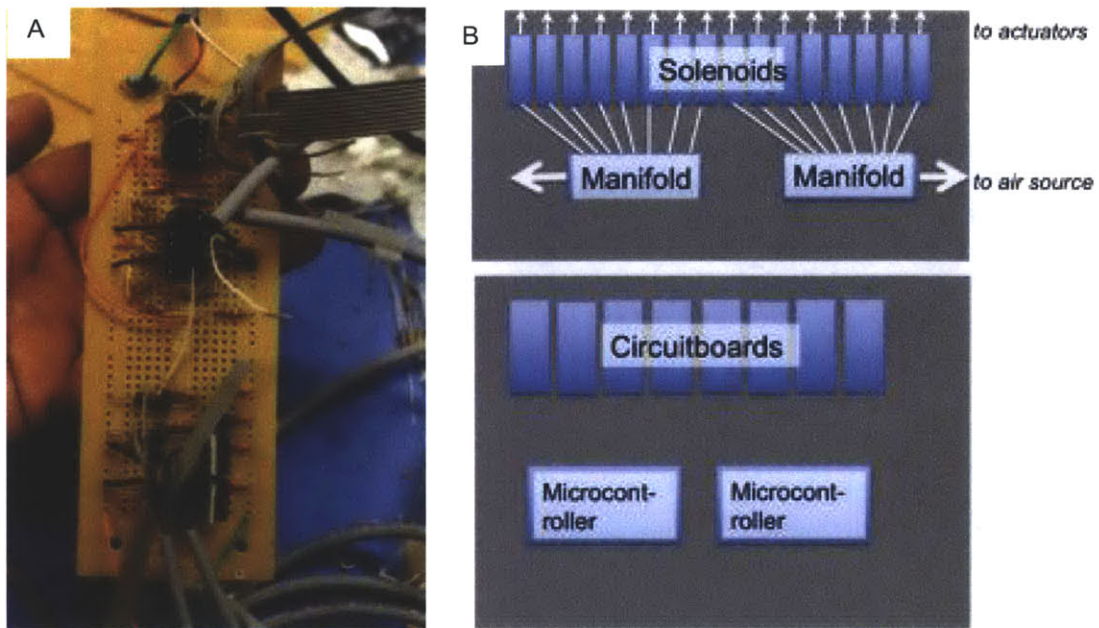


Figure 4.22 – (A) Signal conditioning circuitboards. (B) Pneumatics and control system assembly layout.

#### 4.1.6 Integrated Design

The fully integrated EVA S3 is shown in Figure 4.23. The TROM leg brace connects the ankle, knee, and hip flexion/extension joints and secures those components to the leg. A connecting bar extends from the hip flexion/extension actuator and connects to the hip abduction/adduction assembly mounted to the backpack frame. A compressed air cylinder is worn where it would be



mounted to the backpack. Air lines and valves are not connected as the tank serves only to represent what could be added in the future. The final weight of the EVA S3 is 26 kg (57 lb).



Figure 4.23 – Side and back views of the integrated EVA S3.



## 4.2 Fit and Human Use

Human testing of the EVA S3 is outside the scope of this thesis. However, unpowered fit and mobility checks were done in order to assess the function of the design. We also tested the donning method to create a procedure for putting on the device.

1. Strap on the arm braces (Figure 4.24). Attach one arm brace at a time. Place the subject's head through the shoulder strap of one arm brace and position the brace under the subjects arm pit. Then fasten the cross-chest straps and the lower cummerbund. Then adjust the bicep and forearm straps. Repeat this with the opposite side, securing the straps on top of the straps from the first brace. Test shoulder flexion/extension, abduction/adduction, and elbow flexion/extension motions to confirm that there are no pinch points. Adjust straps as necessary.



Figure 4.24 – Donning the upper body of the EVA S3.

2. Don the backpack with only the hip abduction/adduction actuator assemblies attached (components as shown in
3. Figure 4.7 – Completed hip flexion/extension assembly

4. B). Place the backpack over the straps for the EVA S3 upper body (Figure 4.25 A). Make strap adjustments for comfort as needed.
5. Secure the knee and ankle assemblies. This can be done one leg at a time as shown in Figure 4.25 B. Add comfort padding to the upper and lower leg. Help the subject don the knee and ankle straps by holding open the foot straps and the knee greave so the subject can step into the assembly. Align the ankle with the ankle rotation point of the EVA S3 and use a heel spacer if necessary. Tighten the ankle, greave, and upper leg straps.



Figure 4.25 – Donning the EVA S3. (A) Adding the backpack. (B) Adjusting the knee and ankle assembly.

6. Connect hip flexion/extension assembly to the knee joint structure and the hip abduction/adduction actuators (see Figure 4.26 A). The upper bracket for the TROM leg brace is bolted to the bottom of the hip flexion/extension assembly. First, insert that bracket into the guides of the TROM leg brace part of the knee assembly. Adjust the height using the grey push button on the upper part of the TROM. Next, connect the upper portion of

the hip flexion/extension assembly to the hip abduction/adduction assembly by inserting the hip abduction/adduction extension bar into the connecting bar and securing it with locking pins.

7. Adjust the sizing of the EVA S3 (Figure 4.26 B). Ask the subject if there are any uncomfortable areas or pinch points. Adjust sizing or add padding as needed. Next, confirm the alignment of each EVA S3 joint to the joint axis of rotation of the subject. These adjustments can be made by adjusting bolts, moving locking pin positions, or push button adjustments. A description of each sizing mechanism can be found in Section 4.1.

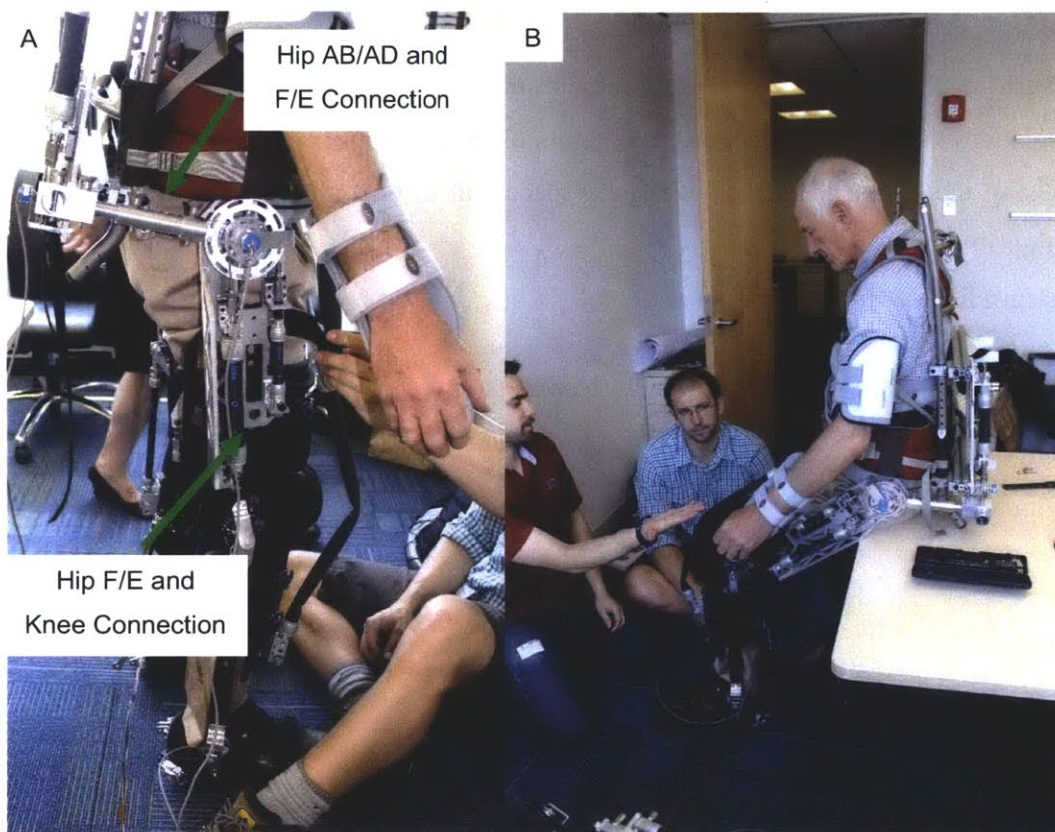


Figure 4.26 –Attaching the hip flexion/extension component (A). Donning the EVA S3 from a seated position (B).



Once the exoskeleton is donned, the following steps are required to prepare for human subject testing of the EVA S3

1. Connect the lower body joints electrically and pneumatically. Connect the potentiometer wires from the ankle, knee, and hip joints directly to the microcontrollers or to a bus as part of a longer tether. Insert the pneumatic air tubes corresponding to the ports on each actuator.
2. Set up the controller and air supply. Plug the controller power source into an outlet. Plug in the compressor for the air supply or attach a compressed air supply to the system inlet regulator.
3. Turn on the controller and compressed air supply. The default configuration is for all solenoid valves to be closed and actuators to be unpressurized.
4. Using the laptop interface, select the space suit to be simulated and initiate the control algorithm.
5. Begin EVA simulation activities.

The most important part of any human testing is ensuring subject safety. Several risks have been identified for human testing. These risks and mitigation strategies are listed in Table 4.2.

Table 4.2 – Risks and mitigation strategies for human testing of the EVA S3

Risk	Mitigation
Pinch points/sharp edges	In all cases, the interface between the EVA S3 and the human subject includes significant padding to prevent contact between the subject and any pinch points or sharp edges.
Fast removal	The EVA S3 lower body includes snowboard-binding-type attachment straps, which have a quick-release mechanism. These straps are used along the leg, and the hip component uses a standard backpack hip belt. Based on these components, the EVA S3 is removable in less than one minute to allow for emergency access to the subject and/or removal of the subject to another location.
Actuator pressure	<p>The actuators are never pressurized above 105 psi, so that even if the actuator were to fail, it would not cause significant stress on the skin of the test subject. In any case, the padding between the S3 and the subject's skin would protect the subject from any high velocity air jets, should an air leak occur.</p> <p>If a pressure canister (air tank) is used rather than an air compressor, selection should be conducted in accordance with the ASME Boiler and Pressure Vessel Code.</p> <p>The software includes a physical “kill switch” to depressurize the actuators.</p>
Accidental hyperextension	By designing the lower body using COTS athletic/rehabilitation braces, the EVA S3 has a built-in safety against hyperextension. The exoskeleton portion of the knee and ankle joints do not allow hyperextension because of the mechanics of the joint. The hip flexion/extension and abduction/adduction are limited by the range of the actuators; that is, the actuators cannot be stretched beyond a very limited range of motion.
Software malfunction	Software safeguards have been incorporated to prevent unexpected system behavior; in particular, all actuators can be immediately depressurized using one keystroke. This ensures that the actuators cannot move the S3 in such a way as to result in injury.
Actuator and component heat	Due to the fast flow rate and high pressure of the air in the actuators, the metal components touching the McKibben actuators can become hot. Padding is incorporated between the EVA S3 and the subject's skin; however, it is recommended that external shielding also be incorporated so that hot surfaces would not be accidentally touched by the subject or the experimenter.



## 4.3 Simulator Results

### 4.3.1 Prototype Test Results

The EVA S3 team built prototypes of the EVA S3 knee and hip components and the accompanying pneumatic hardware and control system. Prototype testing allowed us to verify and improve concepts, hardware, and testing procedures. Joint prototype testing was performed at MIT's Man Vehicle Laboratory (MVL). The pneumatic hardware and controls were first validated independent of the joint prototypes in a tabletop test. Figure 4.27 shows a close up view of the valves, controller electronics, gauges and actuators used to control pressure. Next, the pneumatics were installed in the joint prototypes and the joints were mounted to the Robotic Space Suit Tester (RSST) for testing. The hip flexion/extension prototype joint was tested at varying static pressures, and the knee prototype joint was tested with an early version of our active control system.



Figure 4.27 – Pneumatic control system and hardware.

#### 4.3.1.1 Prototype Hip Results

The prototype hip flexion/extension portion of the exoskeleton was mounted on the RSST in tandem with the prototype knee joint (Figure 4.28). Inflation and deflation of the actuators was tested, as well as the resistance to movement with fixed inflation and deflation points.

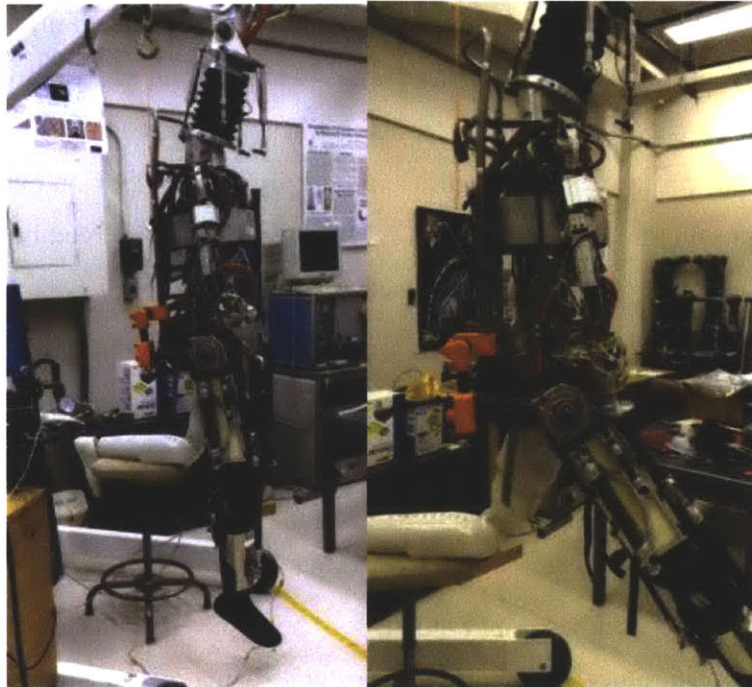


Figure 4.28 – Prototype hip and knee joints mounted to the Robotic Space Suit Tester.

A plot of that torque vs. angle data at 20 psi actuator inflation is shown in Figure 4.29. This plot shows the torque imposed on the hip flexion/extension joint when both actuators are inflated.

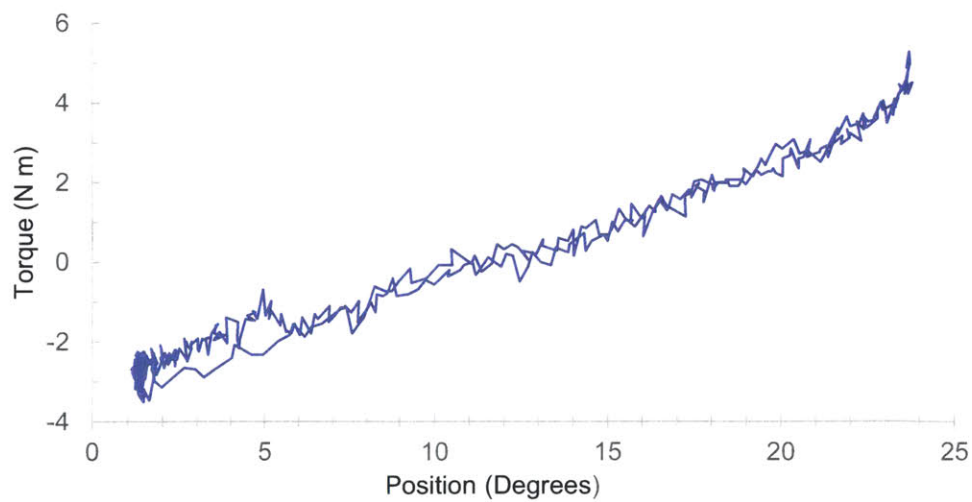


Figure 4.29 – Hip flexion/extension at 20 psi.

The pressure is 20 psi, approximately 1/5th of the final design pressure. Full pressurization was not tested because this prototype was still in the early stages and had many components that were made out of 3D printed ABS and had the potential to fracture. Active control was not valuable at this point because the prototype had significant play in the hip flexion/extension link arm, potentially reducing torque transfer to the RSST. No hysteresis is observed because this was an isobaric test and the control system had not yet been implemented.

#### **4.3.1.2 Prototype Knee Results**

The active control system experimentation began during the prototype knee testing. The knee joint was strapped to the knee of the RSST (Figure 4.30 A and B) and activated as the RSST knee was manually controlled through a range of motion of about 90 degrees (limitations noted below). The pneumatic control system receives joint angle as the input and then actively adjusts the corresponding pressure in either the anterior or posterior actuator to generate the desired joint torque. A potentiometer mounted to the prototype knee provides exoskeleton position information to the control system (Figure 4.30 C).

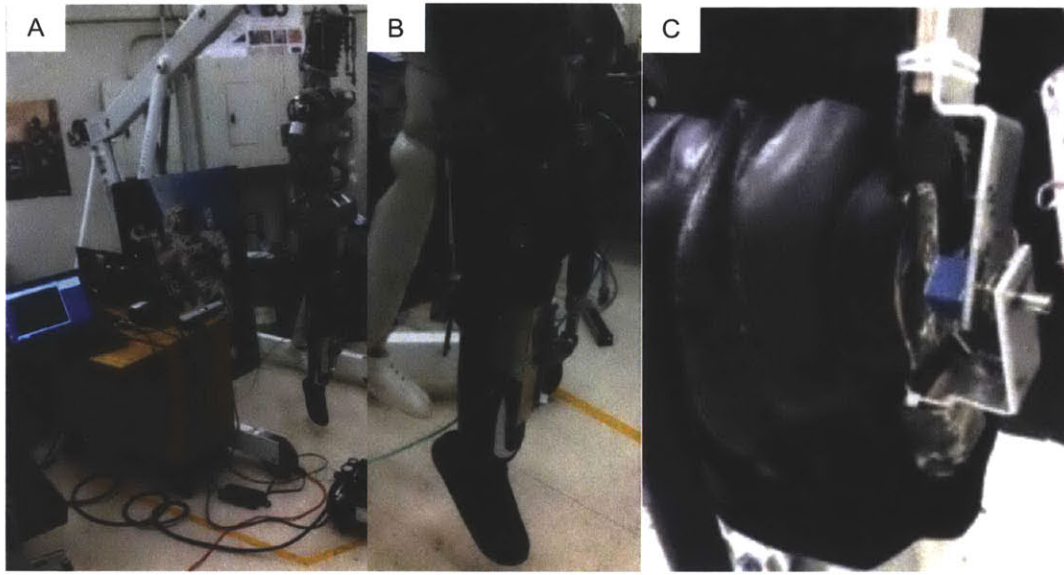


Figure 4.30 – RSST and control hardware (A), Prototype knee mounted to the RSST (B), Detail of potentiometer (blue) mounted to prototype knee joint (C).

The RSST records torque information from calibrated strain gauges within the joint and records its true position from an internal potentiometer. Collected data is recorded based on the torque and position that the RSST senses. The control system makes adjustments based on estimated torques and the angular position of the EVA S3 knee joint. To help calibrate the control system and verify resistance generation, both actuators were statically pressurized as the prototype knee was moved through a range of motion. These static tests (results in Figure 4.31) were conducted unpressurized and at 138, 276, and 414 kPa (20, 40, and 60 psi).

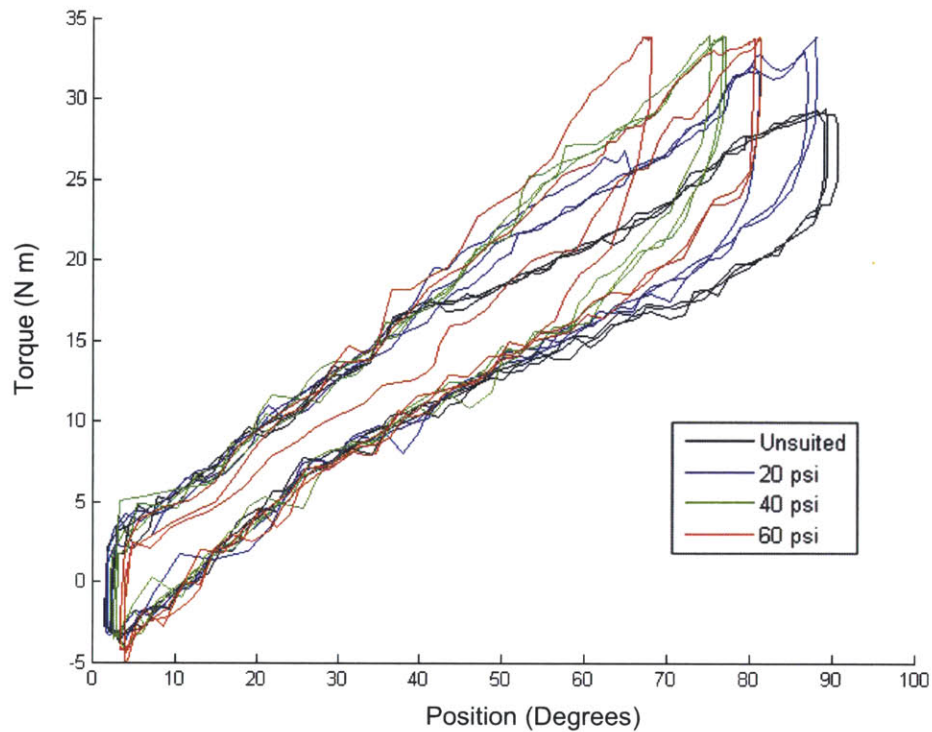


Figure 4.31– Knee torque vs position for statically pressurized actuators at 0, 138, 276, and 414 kPa (0, 20, 40, 60 psi)

The limb was robotically moved from 0 to 90 degrees but the maximum angle was often less because the torque was capped at approximately 33 N m due to a self-imposed limitation on the hydraulic pressure (and thus “strength”) of the robot limbs. The hydraulic pressure limitation was in place during the static testing because of a small hydraulic leak that developed in the elbow joint of the RSST (see Appendix C).

The goal of the first active control experiment was to replicate the EMU knee torque data shown in Figure 4.32 A. The torques measured by the robot for the controlled actuation and the unsuited RSST data plotted in Figure 4.32 B. The unsuited robot data can be removed as described in section 3.9.2.3.



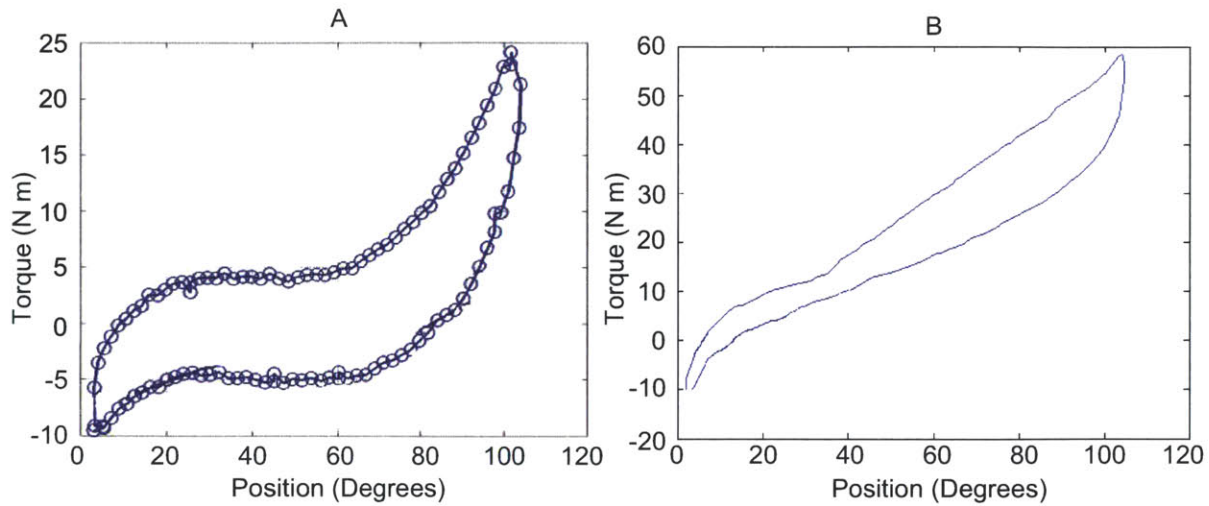


Figure 4.32 - (A) EMU requirements graph (in blue) that we are attempting to replicate (Schmidt, Newman et al. 2001) (B) Test using controlled actuation. Data, in blue, plotted with torque-vs-angle of the robot alone (green).

In the initial data, joint hysteresis is clearly visible and maximum torque exceeds that of the EMU space suit. In this initial test we were able to reproduce the range of torque and angle, but have not achieved matching torques. One potential contributor to the large torque amplitude difference is the mechanical placement of the actuators. The slider rails were installed to take up the slack of the actuators when they were depressurized. It is necessary that the slider stopper is located exactly at the point where the actuator begins to become activated. This was not the case for this first prototype. The other reason for the torque level difference could have been because the control system at this point was relatively rudimentary. An advanced version of the control system was implemented in the final design.

### 4.3.2 Final Test Results

This section details the results from testing the final EVA S3 and control system before it was delivered to NASA. Testing followed the testing protocol outlined in section 3.9.2.2, with some exceptions that will be noted when relevant. The performance of the system did not satisfy all testing goals at this early stage in development; however, the EVA S3 can continue to be improved through software tweaks and hardware adjustments at NASA or at institutions who wish to use the EVA S3 for research.

### 4.3.2.1 Final Hip Flexion/Extension Results

Hip flexion and extension data was collected following the procedure outlined in section 3.9.2.2. The robot hip torque collection was inoperable at the time of final testing, so a replacement 350 Ohm strain gauge was applied to the joint torque lever and calibrated to record torque values. The torque data was collected using National Instruments cDAQ system and LabVIEW 2010. Further details of this modification are listed in Appendix C. Figure 4.33 shows the results from active control testing of the hip flexion/extension joint. The weight of the RSST has been removed from the data as described in Section 3.9.2.3.

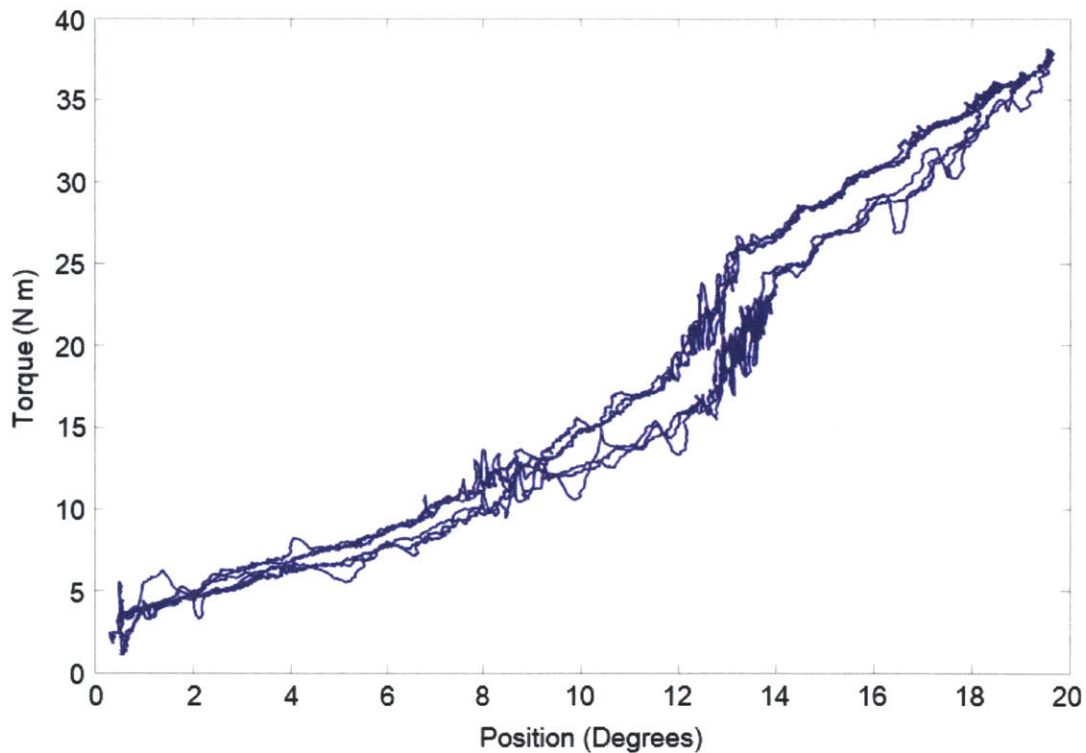


Figure 4.33 – EVA S3 hip flexion/extension torque vs. angle

Due to the limited torque range (see Section 3.1) the range of motion of the hip testing was limited to a range that matched the torque generation capabilities of the hip flexion/extension joint. However, by limiting the range of motion, the anterior actuator was not used at all. Therefore, only the ascending motion of the joint was actively controlled. The control scheme was altered to only replicate torque values when the joint angle was increasing. Hysteresis could not be simulated

with only an ascending profile. Figure 4.34 compares our results for this limited range of the ascending curve to actual hip flexion/extension data (Frazer 2003).

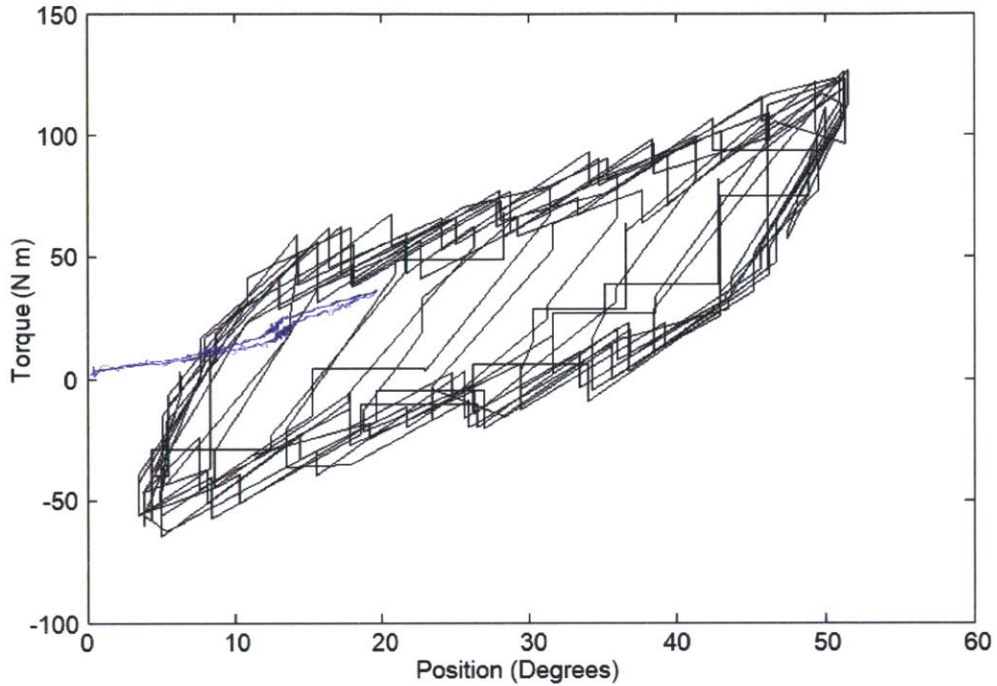


Figure 4.34 – EVA S3 hip flexion/ extension torque vs. angle (blue) overlaid on EMU torque data (black) (Frazer 2003)

As seen in Figure 4.34, the hip flexion/extension joint is not able to simulate the full range of torques. This is also the case with hip abduction/adduction and is described in the next section. These limited torque values are expected based on the reduced design requirements (see Section 3.1).

In addition, play was observed between the exoskeleton structure and the RSST, increased by play in the extension bars connecting the abduction/adduction hip component to the flexion/extension component. Thus, the onboard potentiometers read different angle values than the RSST internal embedded potentiometers. This made it difficult for the control system to produce the exact torques from the EVA S3 potentiometer readings, and resulted in decreased fidelity. Since we were only able to simulate an approximately 20° range of motion, the decreased fidelity caused by the play in the extension bars diminished data fidelity.

#### **4.3.2.2 Final Hip Abduction/Adduction Results**

Hip abduction/adduction testing was performed following the protocol described in Section 3.9.2. As with hip flexion, due to the expected limited torque range based on incomplete requirement data (see Section 3.1). The range of motion of the hip was limited to simulate the EMU in a range of motion that could simulate the torque generation capabilities of the joint. However, by limiting the range of motion, we found that the lateral actuator was not used at all. Therefore, only the ascending motion of the joint was controlled and only the descending control scheme was replicated. The ascending and descending control scheme was not executed, and hysteresis was not simulated.

Figure 4.35 is the EVA S3 hip abduction/adduction torque vs. position data. The data range is between 8.75° and 12° with resistive torque ranging from 9.5 N m to 23 N m. The EVA S3 hip abduction/adduction performance is compared to hip abduction/adduction torque data recorded from NASA's EMU space suit in Figure 4.36.

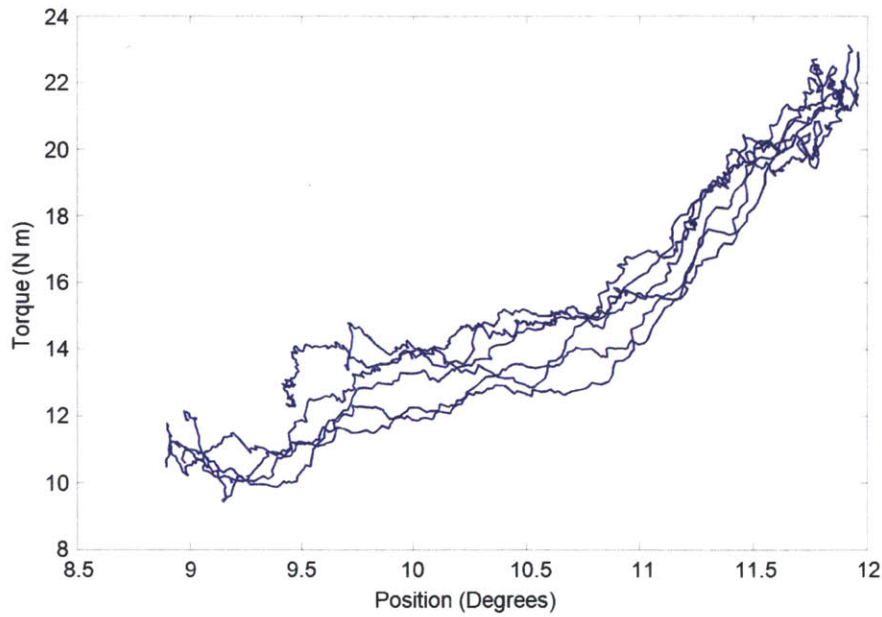


Figure 4.35 – EVA S3 hip abduction/adduction torque vs. angle

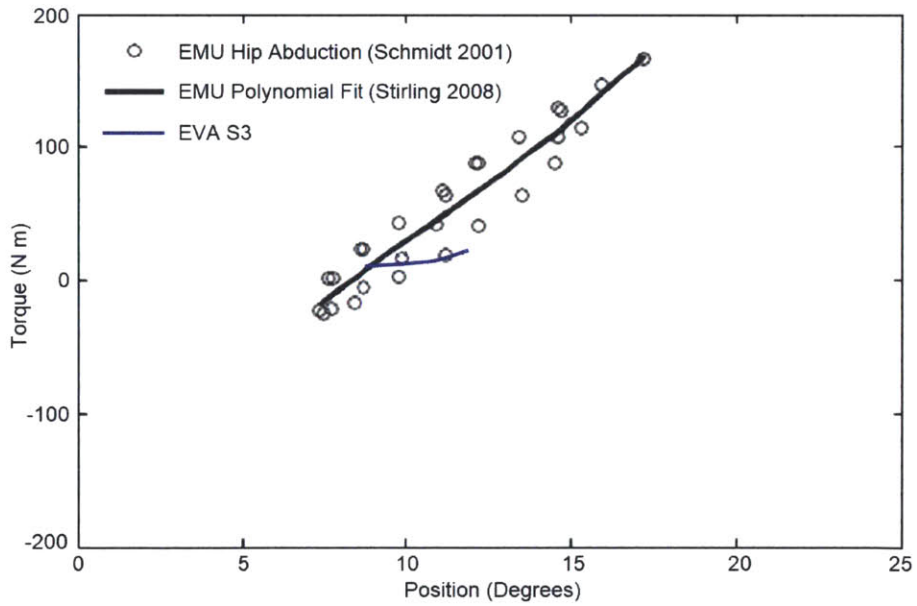


Figure 4.36 – EVA S3 abduction/adduction torque vs. angle (blue) overlaid onto the EMU data (grey) from (Stirling 2008) and (Schmidt, Newman et al. 2001)

The most notable limitation in the hip abduction/adduction test data is its limited range of motion and torque capability as a result of the design requirements. The abduction/adduction joint was



limited to simulating a 5° range of motion where the EMU has similar torque values to the maximum torque that could be generated by the design.

As described in the hip flexion analysis, the connection bar between the abduction portion of the hip and the flexion portion of the hip was twisting and bending. This was causing the hip abduction potentiometer reading to differ from the RSST potentiometer reading, such that the commanded torques were incorrect. These inaccuracies were magnified due to the very limited scope of our data collection. The twisting of the bar connecting the flexion portion to the abduction/adduction portion resulted in potentiometer errors of at least 5°; thus, it was extremely difficult to control within this range.

An unstable system often resulted when the position of the leg would push the potentiometer into a range where resistive torque was required. The torque would be applied, resulting in a change in the relative position between the connecting bar and the actuator assembly. This resulted in a change in the measured angle even though the actual angle of the RSST had not changed. The new angle would require a new torque output, which would then change the potentiometer angle and that would in turn, command another torque output. As little as a few degree perturbation of measured joint angle resulting from a torque change could induce this cycle.

#### **4.3.2.3 Final Knee Results**

The EVA S3 knee was tested using the protocol in section 3.9.2. Torque vs. angle data of the actively controlled knee joint is shown in Figure 4.37

This data is processed and the weight of the RSST has been removed as described in Section 3.9.2.3. The plot includes three cycles of data through a joint range of approximately 5° to 90°. The resistive torques range from -15 N-m to 45 N-m. Figure 4.38 is a comparison of the EVA S3 knee torque vs. angle data and the EMU knee data that we were simulating.

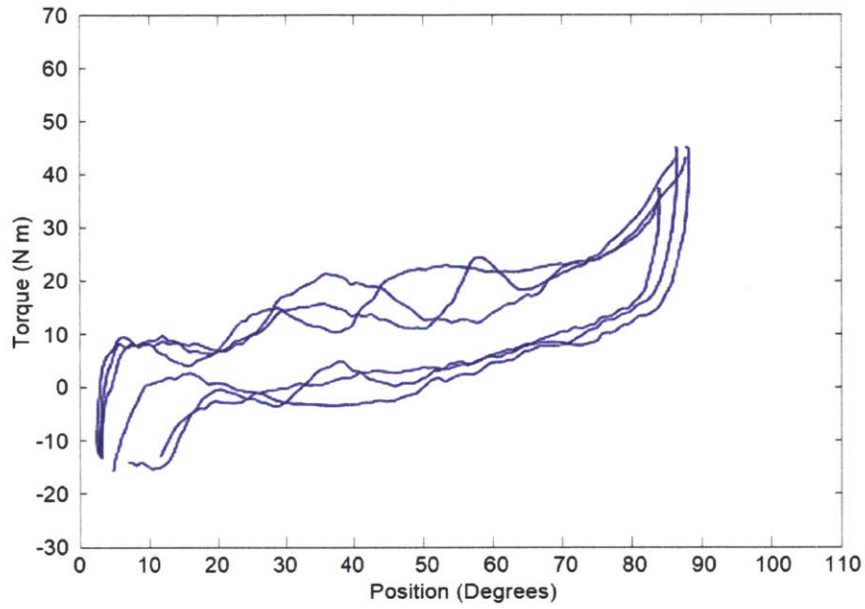


Figure 4.37 – EVA S3 Knee torque vs. angle for three cycles

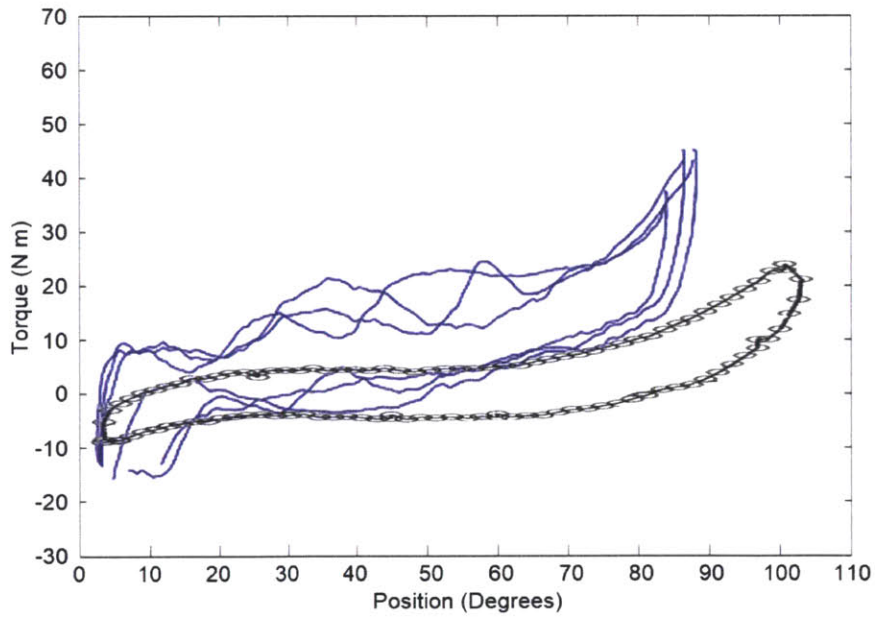


Figure 4.38 – EVA S3 knee torque vs. angle (blue line) overlaid onto the EMU data (grey circles)  
(Schmidt, Newman et al. 2001)

The knee joint was designed for the full range-of-motion. Given the lowest torque (approximately -10 Nm in full extension ( $0^\circ$ ) and the highest torque of approximately 25 Nm at full flexion ( $100^\circ$ ),

actuator sizes were selected to ensure they would meet the range of motion and torque requirements. During knee characterization, flexion angles greater than approximately 30° would not simulate low enough torques even with the actuator completely depressurized. The additional torque not accounted for in the design and actuator selection was from the weight of the ankle component of the EVA S3. Attempts were made to counteract the torque by pressurizing the posterior actuator; however, at high angles of flexion, the posterior actuator was freely moving along the linear ball-bearing carriage. Since the actuator does not engage the stopper at that angle, it does not produce any torque. The angle is limited by the actuator stopper settings, and the torque is limited by the choice of actuators themselves. Future designs will need to include an estimation of the torque needed to offset the weight of other exoskeleton joints and a factor of safety to account for the uncertainty in the final weight of a joint early in the design process. The orientation of the EVA S3 application will also need to be considered. Using the EVA S3 a vertical treadmill like the eZLS may require control system and hardware adjustments due to different force vectors due to the weight of the exoskeleton in a horizontal position.

#### **4.3.2.4 Final Ankle Flexion/Extension Results**

The EVA S3 ankle was tested according to the procedure described in Section 3.9.2 except that RSST ankle joint was inoperable and was only used as a structure to mount the ankle joint. The angle was measured by the potentiometer mounted to the ankle brace. The torque was calculated by the force transmitted to a load cell that was mounted to a cantilevered L-bracket used to pull the ankle through the desired trajectory (Figure 4.39).



Figure 4.39 - View of ankle test setup. An L-bracket was used to manually move the ankle, since the RSST actuation was not working

The ankle was actuated manually through a  $-45^{\circ}$  to  $5^{\circ}$  range of motion. Ten cycles of data are plotted in the torque vs. angle plot in Figure 4.40. A comparison of the EVA S3 ankle data to EMU ankle data taken at 29.6 kPa (4.3 psi) is presented in Figure 4.41.

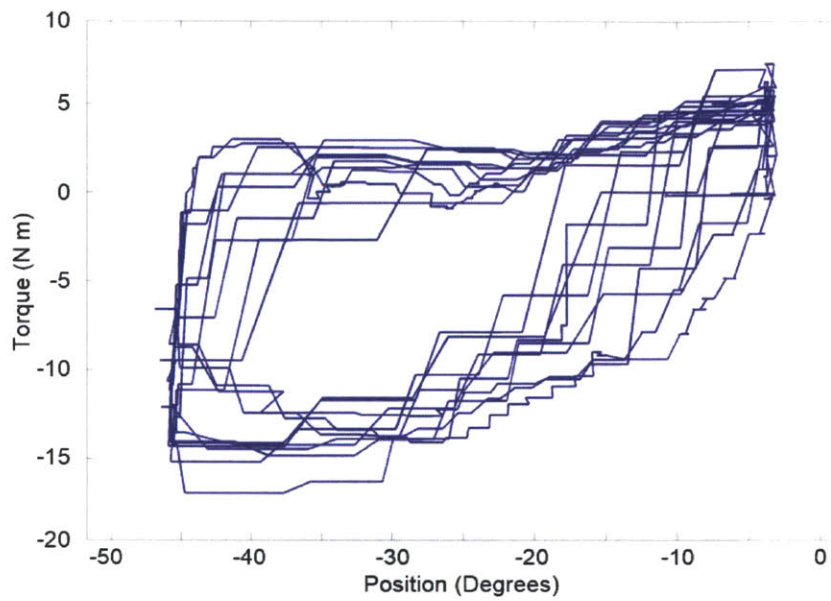


Figure 4.40 – EVA S3 ankle flexion torque vs. angle over ten cycles

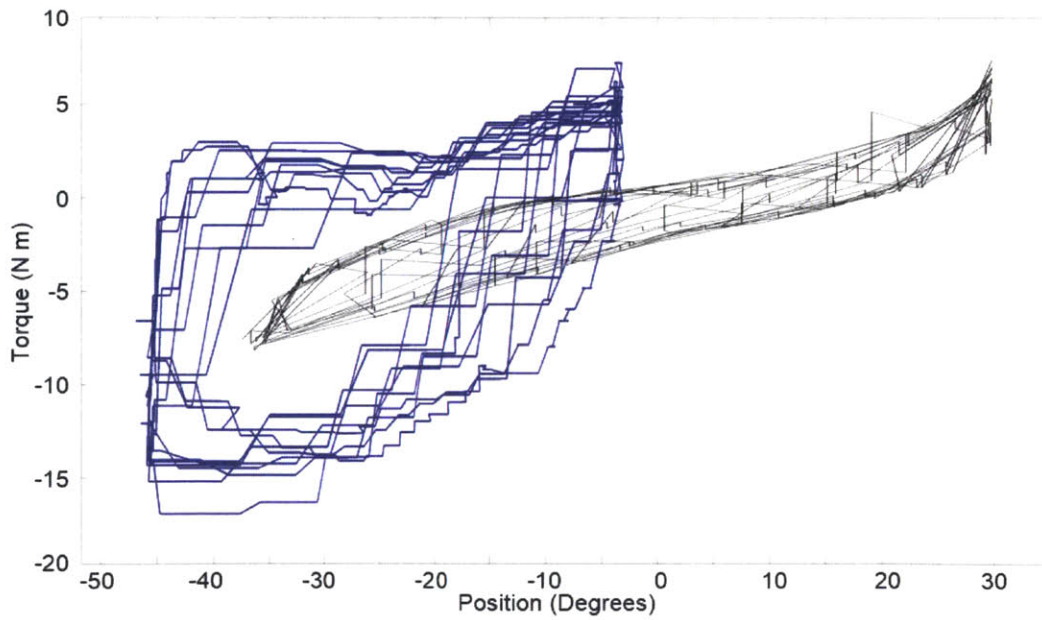


Figure 4.41 – EVA S3 flexion/extension torque vs. angle (blue) overlaid onto the EMU Data (grey) from (Frazer 2003)



The S3 ankle curve compared with the requirements data is shifted approximately  $10^\circ$  to the left. This is due to the range of motion limits of the actuator. A new actuator is needed with a longer stroke length to simulate the full range of motion.

The EVA S3 ankle curve demonstrates excessive hysteresis. This may be due to stiction in the ankle joint. This property can be improved by reducing the friction in the ankle joint by adding Teflon washers, lubricating the joint, or rebuilding it with low friction bearings.

Finally, the torque values for the lower angle ranges are too low. As with the knee, this is in part due to the weight of the system, which was not taken into account when the actuator sizing requirements were developed.

## **5. Conclusion**

### **5.1 Thesis Summary and Contributions**

This thesis describes the creation of the Extravehicular Activity Space Suit Simulator, referred to as the EVA S3. The purpose of this device is to simulate the feel of a space suit by replicating the joint torques felt by the operator. Gas pressurized space suits resist joint motion because of pressure, torque, and volume effects (Holschuh, Waldie et al. 2009). The restriction posed by these suits affects how astronauts work in the environment of space. Space suits are heavy, expensive, and in limited supply. The goal of the EVA S3 is to provide a light, cost effective, and attainable space suit analogue to improve EVA research and training, and to aid in the development of new space suits.

The EVA S3 builds upon previous research to develop effective space suit joint torque simulators. The ATA-MIT simulator used springs and dampers to simulate the resistive knee torques of NASA's EMU space suit (Schaffner 2007). MIT developed another space suit simulator for the knee that employed the spring like characteristics of fiberglass beams to simulate the Apollo A7L series of space suits (Carr and Newman 2008). The novel aspect of the EVA S3 is the application of an active control system and actuators in order to more accurately simulate multiple types of space suits. In 2011, a team from Aurora Flight Sciences and MIT completed the first knee prototype of the EVA S3 from a modified knee brace and pneumatic McKibben actuators (Duda, Newman et al. 2011). This thesis presented the advancement of the EVA S3 from a single joint to a full body exoskeleton with 8 actively controlled degrees of freedom and 6 passively controlled degrees of freedom. Actively controlled joints include knee flexion/extension, ankle flexion/extension, hip flexion/extension and hip abduction/adduction. Passively controlled joints include shoulder flexion/extension, shoulder abduction/adduction, and elbow flexion/extension.

Chapter 1 motivates this research with the background of joint torques and space suit simulators. Also in chapter one is the problem statement, hypothesis, and success criteria. Chapter 2 details the history of exoskeleton development and the state of the art of wearable robots. The methods used to develop the EVA S3 are in Chapter 3 including requirements development, prototyping, and design evaluation. The final design, results from validating the EVA S3 on the robotic space

suit tester (RSST), and discussion are presented in Chapter 4. The current chapter, Chapter 5, details the contributions, limitations, and future work of the EVA S3.

The major contributions of this thesis to previous work are

1. First full body space suit joint torque simulator (excluding costumes and other “bulk” simulators)
2. Assessed the feasibility of using McKibben actuators (pneumatic muscles) in a space suit simulator
3. Design and construction of an actuated hip joint and possibly the first adduction/abduction exoskeleton joint actuated with McKibben actuators

## 5.2 Hypothesis Evaluation

Three hypotheses were developed at the beginning of this research effort, namely:

Hypothesis 1: A programmable exoskeleton using pneumatically powered actuators can effectively simulate space suit joint torque profiles and has advantages in fidelity over passive space suit simulators. This hypothesis will be verified if the EVA S3 can

- Match each joint to Extravehicular Mobility Unit (EMU) joint torque data within a root mean square (RMS) error of 10% for the hip, knee, and ankle joints.
- Achieve the range of motion (ROM) requirements outlined in the survey of studies of space suit joint mobility.
- Simulate patterns of hysteresis often observed in space suit joint torques.

Hypothesis 1 was not proven during this research project. The performance of the EVA S3 did not reach an RMS error of 10% for any of the joints. The performance of both the hip flexion/extension and abduction/adduction joints was limited by incorrect design requirements. The ankle joint generated the required torque magnitudes, but did not achieve the range of motion requirements because of limitations in actuator stroke length. The knee joint, which has undergone the most development as a multi-year effort, came closest to achieving the desired results. The knee joint

achieved a similar hysteresis pattern and achieved the required range of motion, but the magnitude of the torques were elevated by about 10 N m.

Hypothesis 2: A programmable exoskeleton can be designed to weigh significantly less than the EMU to allow testing research environments that are not submerged (such as NASA's Neutral Buoyancy Laboratory) or require attachment to a crane or other support.

- This weight will be defined by what is considered acceptable for backpacking: approximately 27.2 kg (60 lb).

Hypothesis 2 is confirmed by our results. The final weight of the EVA S3, excluding the pneumatics and control system is 26 kg (57 lb).

Hypothesis 3: The cost of a fully programmable exoskeleton will be significantly cheaper than a space suit, which could allow for greater researcher access to space suit like constraints. This can be tested by

- Determining if the whole cost of materials and development for an effective space suit simulator is 10% of the cost of a production space suit.

Hypothesis 3 is confirmed by comparing the total cost of the grant to the cost of the Small Business Innovation Research (SBIR) Phase II grant that funded the project to the approximate cost of one EMU space suit. The grant amount was \$600,000 (SBIR.gov 2013). A significant portion of this was research, design, and personnel costs. ILC Dover estimated that almost 20 years ago, a spare EMU cost 2 million dollars (ILC Dover 1994). More recent estimates place the cost near 12 million dollars (Freudenrich 2011). Development cost for a next generation suit are estimated to be between 300 and 700 million dollars (Harris 2001). While this iteration of the EVA S3 did not achieve the desired performance levels, we estimate the modifications needed are to improve it will be less than \$100,000. Once appropriate modifications are made, it should be able to simulate the current EMU as well as the future generations of suits yet to be developed. \$700,000 is about 5.8% of the current EMU price and is an even smaller fraction when compared to the number of suits it could simulate. This satisfies our 10% criteria for Hypothesis 3. The EVA S3 appears to be a much cheaper and versatile option for basic research or training.

## **5.3 Limitations**

During the design process, an incomplete version of the space suit torque and range of motion performance database was mistaken as the final database. Joint torque requirements for the hip were developed from this incomplete database, resulting in a design optimized for reduced torque values. The values used for hip flexion/extension and hip abduction/adduction were from a NASA suit performance comparison study that used a fish scale type method for measuring joint torque. The requirements did not include data collected from robotic space suit testing, which records much higher and more precise torque values. Overall the control system is not simulating joint torques to the desired simulator fidelity of 10%. Until the hardware adjustments described in Section 5.4.1 are made, the EVA S3 cannot accurately simulate the joint torques of a specific spacesuit.

The goal of the EVA S3 is to be a space suit joint torque simulator. The EVA S3 does not attempt to accurately simulate the bulk of a space suit. The bulk of a space suit is important for some operational studies, especially when a task requires moving in tight spaces or manipulating small objects. Costume space suits have been used to simulate space suit bulk but they do not accurately simulate the joint torques experienced by the explorer and the resulting metabolic load from those torques.

The completed EVA S3 is a tethered system, with the compressed air supply, control circuitry, and solenoid valves separate from the exoskeleton. The tether restricts the test environment to a treadmill, stationary tests, or movements over a contained area such as the volume of a motion capture facility. Future work includes the possibility of miniaturizing some components and mounting them in a backpack.

## **5.4 Future Work**

### **5.4.1 Device Modifications**

The EVA S3 is still a research and development device and a number of improvements can be made to increase its performance. The hip actuators and spools need to be replaced to increase to



force generation capabilities. This will require using actuators of a larger diameter and reinforcing the thigh actuator assembly structure.

Another improvement to the hip design is to reduce the play in the connecting bar between the hip flexion/extension assembly on the thigh and the hip abduction/adduction assembly mounted to the backpack. Decreasing the tolerances between quick release pins and holes in the connecting bar may reduce play. The sizing mechanism could also be redesigned with material and structure to increase the rigidity of the connector.

The weight of the hip actuator assemblies could be reduced by building the support structure out of carbon fiber reinforced composite sandwich panel, similar to the knee greave. Development of such a structure was considered in this iteration of the EVA S3 but was forgone in favor of an aluminum structure because of limitations in time and resources necessary for proper analysis and construction of such a structure.

The hip, knee, and ankle joints can also be enhanced with hardware adjustments. The knee joint can be improved by adjusting the actuator slider stopper location to account for the weight of the EVA S3 leg components. The passive spring system in the upper body can be replaced with an actively controlled system. The foot restraint for the ankle joint is a large ankle brace in order to accommodate most foot sizes. A quick release system to swap out foot restraints for ones designed for people with medium and small feet will reduce the bulk of the system and make it easier for people with smaller feet to walk. The stroke length of the rear pneumatic cylinder also needs to be increased.

The pneumatic system can be changed from a tethered system so that it can be carried. The current system relies on an air compressor to supply air at 120 psi for operation. An EVA S3 that can be carried in the field would include a Self-Contained Breathing Apparatus (SCBA) tank to store air near 34500 kPa (5000 psi). The EVA S3 backpack has already been designed with tank mounts but additional piping and valves will need to be added. Circuit boards will also be miniaturized into printed circuit boards in order to save space on the backpack frame.

The performance of the pneumatics and control system can be improved in future work. Some issues discovered include noise, response rate, and simulation fidelity. The aural noise is a result

of the solenoid valves cycling to control actuator pressure. With only 2 solenoids active, the noise produced required the use of hearing protection. Two solutions have been identified for the noise problem. The most cost effective solution is to isolate the solenoids in a sound dampening box. A second more effective but costly solution is to replace the solenoids with an electronically controlled variable pressure regulator. These pressure regulators, described in Appendix A, create almost no audible noise but were not used in this iteration of the EVA S3 because of a cost of \$1000 each (16 total would be needed).

The response rate is primarily limited by airflow and the response time of the control system and solenoid (or pressure regulator in a future system). The current limiting factor is airflow. Approximate flow rate per actuator required to achieve 2 Hz gait cycle is 25 L/min. A tube with an inner diameter of 5 mm can exceed this flow rate at our working pressures.

Additional testing and tweaking of the control system will also be needed to improve simulator fidelity. One alteration that may be extremely helpful is to place force sensors in line with the actuators to feed accurate force readings to the control system. The current system uses look-up tables to determine forces based on the properties of the McKibben actuators. This can result in increased error and is a reason why the current system requires significant robotic testing to adjust the control parameters to achieve the desired torque and range of motion curves. Once this alteration is made, the time to develop control algorithms for additional space suits will be reduced.

#### **5.4.2 Research Applications**

Human testing of the EVA S3 was outside of the scope of this research project. After some modifications are made, the EVA S3 will help answer a variety of interesting research questions.

Future work to integrate the EVA S3 with the eZLS vertical treadmill would allow physiological studies to be conducted on the metabolic cost of space suit EVA operations in a simulated reduced gravity environment. EVA S3 use in conjunction with NASA's ARGOS weigh offload system would create research opportunities to study tool use, and EVA operations in a simulated microgravity environment while under space suit mobility constraints.

The EVA S3 can help study the tradeoff between space suit joint stiffness and operational metabolic costs. It is important to understand how incremental increases in space suit performance affect EVA performance, and consequently the ultimate goal of exploration, scientific return. The EVA S3 can be programmed to different joint mobility levels and performance can be assessed. It is possible that there is a point where a slight gain in mobility, vastly increases astronaut performance and other points where a gain in mobility yields a much smaller performance increase. This information will help engineers and policy makers decide in what joints to invest to improve the mobility, and to what performance level this mobility must be improved. Perhaps the research will show only slight EVA performance with a certain increase in mobility and provide justification for focusing research on other suit components. Or perhaps there is a huge EVA performance bonus (and a corresponding scientific return bonus) by increasing mobility to a level that requires more investment innovative suit designs, such as mechanical counter pressure space suits.

## **5.5 Broader Impacts**

The technology for the EVA S3 can be applied outside the field of space suit simulation. A majority of exoskeletons are designed for augmentation in order to help a weakened person to regain mobility or to further strengthen a physically fit person. The EVA S3 control system can be adjusted to provide torque, but to be truly effective as an augmentation device several hardware changes would need to be made as well. The actuators for the EVA S3 are designed to mimic space suit joint torques. These actuators would need to be selected based upon the torques needed to aid a handicapped person or augment a soldier, based on new design requirements. Additional inputs to the control system may also be needed to signify user intent, such as the EMG and foot force sensors used in the HAL-5 exoskeleton (Suzuki, Mito et al. 2007).

Active control of joint resistance is applicable to both physical training and rehabilitation. The current cost of the system and the equipment required to operate it make it unlikely to be used as an in-home personal strength training device. However, it would be a practical piece of equipment to add to a rehabilitative clinic for stroke victims. One technique used for rehabilitation is called force tunneling. A patient's neuromuscular system can be retrained by using a device that guides a limb to the correct motions by increasing resistance to motions in undesired positions. Researchers at the University of Delaware created a force controlled exoskeleton to guide patient

movements during arm rehabilitation (Mao and Agrawal 2011). The EVA S3 could apply a similar concept for rehabilitation of the lower extremities. The safety of the McKibben actuators that stems from their compliance and well scaled force output makes the EVA S3 especially attractive for such an application. If the EVA S3 as a whole is not repurposed, lessons from the 3 methods of torque transmission and the control system could be applied to a rehabilitation device.

## **5.6 Final Summary**

The EVA S3 is a full-body, programmable exoskeleton designed to give researchers access to realistic space suit joint torque restrictions during research and training exercises in simulated space exploration environments. The focus of this thesis is the design, construction, integration, and testing of the hip joint and backpack for the EVA S3. The final designs of the other joints were also described. Results from robotic testing to validate the mechanical design and control system were discussed along with the planned improvements for the next iteration of the EVA S3. The current EVA S3 consists of a metal and composite exoskeleton frame with pneumatic actuators that control the resistance of motion in the ankle, knee, and hip joints, and an upper body brace that resists shoulder and elbow motions with passive spring elements. The EVA S3 is lighter (26 kg excluding the tethered components) and less expensive (under \$600,000 including research, design, and personnel) than a modern space suit. Design adjustments and control system improvements are still needed to achieve a desired space suit torque simulation fidelity within 10% root-mean-square error. Future work can modify the existing EVA S3 exoskeleton to improve simulation performance, or apply the engineering contributions of this thesis to advance the designs of future robotic exoskeletons for use in human augmentation, simulation, or rehabilitation.





## **Appendices**

### **Appendix A. Development of Other EVA S3 Components**

#### **6.1.1 Knee**

The knee was designed for a 40-year old 95th percentile American male, although the goal of the final product is to be adjustable to fit the entire astronaut population. The reason for selecting this size is to ease integration with the robotic spacesuit tester (RSST) at MIT's Man Vehicle Laboratory during validation and testing. The average sitting knee height of a subject of this size is 60.9 cm (24 in) – a height corresponding to that of the RSST and the EVA S3 knee prototype (NASA 1995).

The prototype design the decision was made to move away from the design from a previous research project that incorporated the pneumatic actuators laterally relative to the knee joint, as this resulted in additional out of plane torques that could present an injury risk. Our alternative approach involves the use of a “greave,” essentially a shin guard, to allow the flexion-inhibiting actuator to be positioned anteriorly relative to the subject's leg, and to prevent the actuator from contacting the subject's leg during flexion. Figure 6.1 shows the detailed CAD model of the prototype knee joint and Figure 6.2 shows the respective joint components.

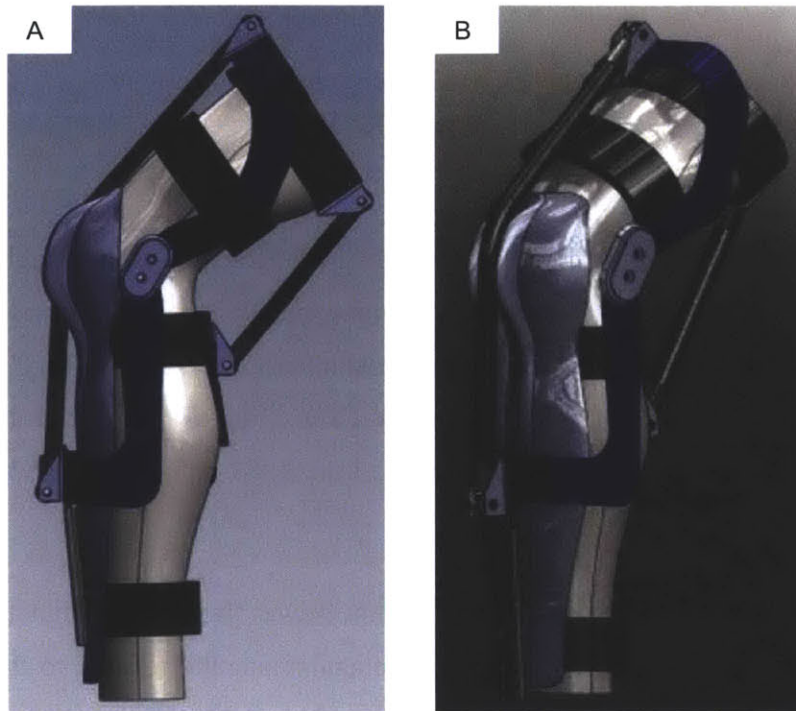


Figure 6.1: (A) Side and (B) Isometric view of detailed EVA S3 knee joint design

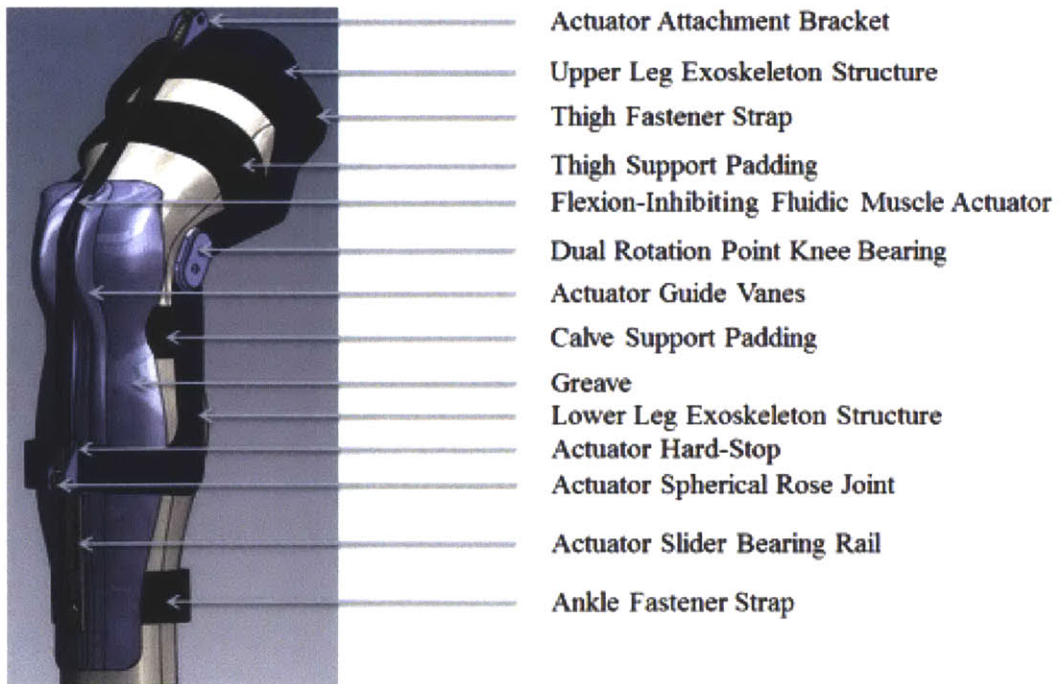


Figure 6.2: EVA S3 knee prototype design with component descriptions and flexion-inhibiting actuator shown

In the earlier EVA S3 knee study, (Duda and Hart 2010), substantial buckling of the pneumatic actuators would occur during certain stages of joint motion, specifically when the actuators are not pressurized and hence not opposing motion. This prolonged buckling cycle could accelerate actuator fatigue that may lead to a puncture, which in turn poses a threat to the subject's safety. By incorporating a slider bearing rail and a hard-stop on one end of each actuator, the actuator is free to slide along the rail when not pressurized, but contracts during pressurization, until it securely catches on the hard-stop, after which point an induced torque is transferred to the system, opposing motion as intended. This solution leads to no buckling of the actuators, thus prolonging overall system life.

The actuator attachment brackets and upper and lower leg exoskeleton structure components of the prototype knee were designed to be fabricated from 6061-T6 Aluminum, due to its light weight and ease of machinability. The final version uses composite materials such as carbon fiber are being considered to reduce the system weight even further. The early prototype incorporated Commercial Off-The-Shelf (COTS) straps, similar to those used in snowboarding equipment, as these components would meet all the above-mentioned requirements. Similarly the thigh and calf support padding requires a thick foam material that ideally wicks away sweat while providing comfort during prolonged operation in the EVA S3.

The McKibben actuators and slider bearing assemblies (shown in Figure 6.3) were sized to accommodate specific elongation and length requirements. We designed for actuators 20 mm (~0.75in) in diameter and attached to the actuator attachment brackets via spherical rose joints to allow for limited rotational motion, should the actuator not be perfectly aligned throughout the knee range of motion.

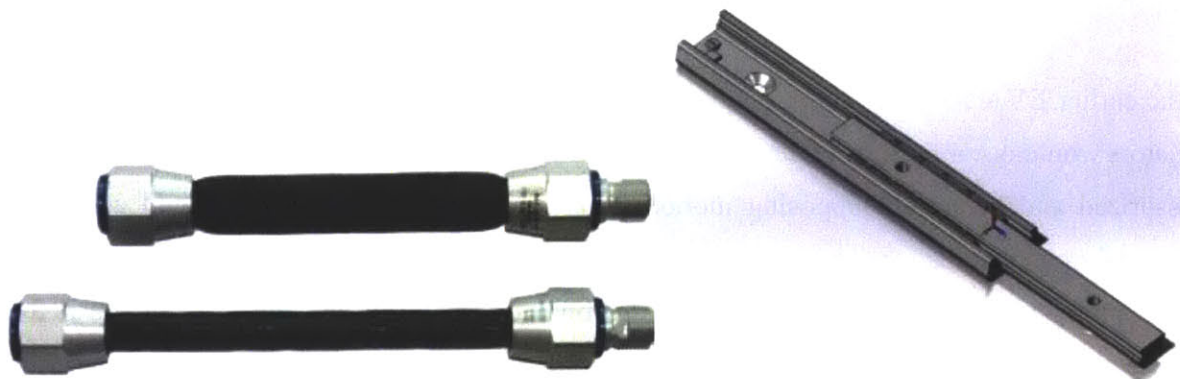


Figure 6.3: Festo Fluidic Muscles and Actuator Slider Bearing Assembly

Figure 6.4 details the greave design. It includes a pair of actuator guide vanes that prevent the actuator from sliding off the front of the greave, and also protects the anterior actuator, should the subject bend down on one knee during planetary EVA simulations, preventing it from being pinched between the ground and the subject's knee. The greave to be constructed of carbon fiber layup, covered with resin, to provide a smooth finish for the actuator to move along and the inside be lined with foam for comfort.

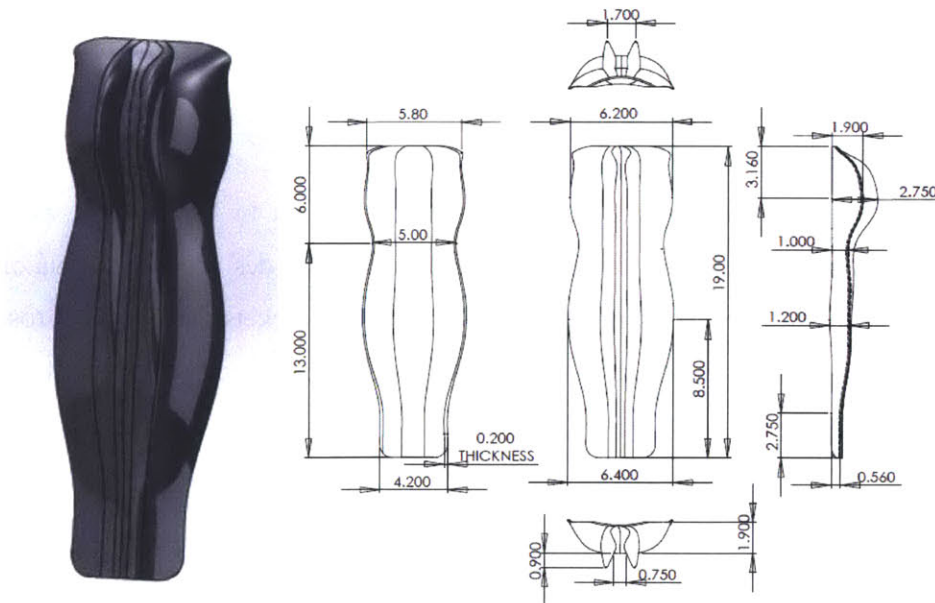


Figure 6.4: Greave design (all dimensions in inches)

The greave that protects the subject's shin and knee from excessive forces generated by the anterior actuator was fabricated by Aurora Flight Sciences. It is made from carbon fiber layups layered with epoxy resin. A mold and plug were created for use in the vacuum curing process are shown in Figure 6.5. Both the plug and mold can be reused to create multiple carbon fiber greaves.



Figure 6.5: (A) Silicone plug with mold sections (B) Silicon plug for use during carbon fiber layups

Figure 6.6 shows the process that was followed during the carbon fiber layup. Three layers of carbon were used – each soaked with epoxy resin prior to installation in the greave mold. In addition, chopped fibers were used to build up the extruded guide vanes of the greave. Once the layers have been fitted into all the cavities of the mold, the silicone plug is inserted to ensure that the carbon fiber layers have the correct shape. Finally, the mold is sealed in an airtight bag and a vacuum of -70 kPa (-20 inHg) and left over night for the resin to cure. **Error! Reference source not found.** shows the fabricated greave after being removed from the mold.





Figure 6.6: The carbon fiber greave layup process

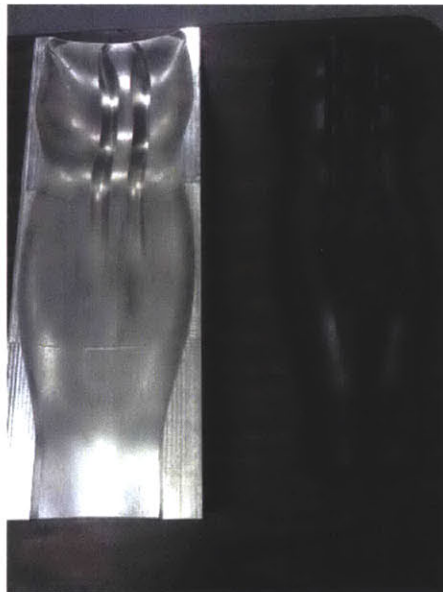


Figure 6.7 – The greave after being removed from the mold



Figure 6.8: S3 prototype donned by subject

After developing this initial design, we determined that a full-leg COTS brace (also DonJoy, see Figure 6.9) would be more useful in terms of integrating the entire leg: hip, knee, and ankle. Due to the telescoping nature of the medial and lateral supports, this brace can be easily connected and integrated with the hip and ankle joints.



Figure 6.9. DonJoy TROM knee brace.

The TROM also offers several other advantages. It is a more minimalist design, providing only lateral support with flexible around-leg straps, which we replaced in most cases with quick-release

snowboard-type bindings. The knee range of motion can be directly limited via hard stops, which provides a safety mechanism should we choose to implement hardware stops. The length of the TROM ranges from 17" to 23 ¼", allowing our system to be adjustable for a wide range of subjects.

Very few design changes were required between the first DonJoy knee design and the TROM-based knee:

- The greave was reinforced and stiffened.
- The greave served as the mounting point for the actuator and strap attachments, and the metal overlay was removed.
- Velcro straps were replaced with snowboard binding to provide quick-release points and a padded, though generally non-compliant, interface with the leg.

The greave was rebuilt as required to create considerable strength with negligible increase in weight. The modified carbon fiber design consists of multiple layers including:

- Three outer layers including 2 sheets of standard weave carbon fiber orientated at 0-90° and 45° angles as well as a strip of unidirectional carbon fiber to reinforce the greave in the longitudinal direction
- Expanding foam that fills the greave channels to create a uniform surface on the inside of the greave
- A 1/8 inch Nomex honeycomb core sandwiched between the carbon fiber layers
- Two additional sheets of standard weave carbon fiber orientated at 0-90° and 45° angles that make up the inside surface of the greave, closest to the subject's leg
- The anterior actuator sliding rail is mounted directly to the carbon fiber greave and the greave is fitted with hinges on the one side and snowboard bindings on the other, which allow it to swivel open during donning/doffing operations.

### 6.1.2 Ankle

Figure 6.10 shows a prototype of the ankle joint with a bidirectional pneumatic actuator mounted to the heel. This prototype was only intended for use in validating ankle control and our choice of actuator, and was modified to allow for a more user friendly interface, i.e. less sharp edges and more additional padding for comfort.



Figure 6.10 – Prototype ankle joint

For the final ankle development, we considered a design utilizing a COTS crampon, to facilitate mounting over any shoe (crampons are adjustable for different shoe sizes.) Crampons, used for ice climbing, include grips and spikes that would have been removed or cut off (Figure 6.11)





Figure 6.11 – Black Diamond contact crampon (BlackDiamond 2013)

This would have been a more minimalist design and only included structure under the subject's heel and over the ball of the foot, with mounting structure in between. This design was eventually rejected for two reasons. First, straps and tread passing only under the heel and the ball of the foot was considered unnatural and possibly uncomfortable for most EVA simulation-type activities. Second, we were concerned that the heel mounting of the actuator would not transfer load properly to the whole foot. The purpose of the S3 ankle joint is to provide a torque similar to that of a given spacesuit boot. Given the light structure between the heel and the ball of the foot, we were concerned that the subject would experience more flexibility in the forward foot than they would in a boot.

We eventually selected the DonJoy MaxTrax ROM Walker ankle brace, still using the heel-mounting strategy. This ankle brace included a full foot bed to be worn over the shoe (Figure 6.12). The foot bed is entirely stiff, so there is no flexion available in the forward-foot, but this was considered to be desirable in terms of simulating the restrictiveness of most spacesuit boots. Should a more flexible spacesuit boot be developed, it may require redesign of the joint's foot bed.





Figure 6.12 – DonJoy MaxTrax ROM Walker

The COTS ankle brace was modified significantly for use on the EVA S3. The interior padding was removed, as were the Velcro straps. The lower leg portion was removed above the ankle hinge joint; instead, the extender bars of the knee brace were attached to the ankle hinge. In this way, the ankle and knee are rigidly attached, and the length between the knee and the ankle may be adjusted as needed.

The final ankle joint utilizes two snowboard bindings for fast donning/doffing as well as a quick-release pin for the actuator, which is needed to physically disconnect the ankle from the knee. The final design is displayed and discussed in Section 4.1.3.

### 6.1.3 Upper Body

Though it was out of the scope of this project to develop actively controlled joints for all body joints, we developed passive joint resistive devices for the upper body joints, in order to facilitate use of the EVA S3 for experimentation and training. In future work, we would replace these passive joints with actively controlled joints to provide the highest possible fidelity.

We explored multiple COTS braces for each passive joint, anticipating that in some cases a satisfactory COTS solution exists that would be compatible with the rest of our EVA S3. This type of research into COTS devices for ROM limitation has been performed before (Mosher, Mitchell et al. 2006). Upper body results from the Mosher study are summarized in Table 6.1.

Table 6.1 – Example COTS braces that might be considered for passive joint resistance (Mosher, Mitchell et al. 2006)

Joint	Goal ROM restrictions	Braces Considered
Shoulder	<ul style="list-style-type: none"> <li>• 150° (adduction/abduction)</li> <li>• 20°/150° (lateral/medial)</li> <li>• 180° (flexion, extension)</li> <li>• 90° (rotation x-z plane)</li> <li>• 120° (rotation y-z plane, lateral-medial)</li> </ul>	<ul style="list-style-type: none"> <li>• Cadlow shoulder stabilizer</li> <li>• Sully shoulder stabilizer</li> <li>• Quadrant Shoulder Brace (DonJoy)</li> </ul>
Elbow	<ul style="list-style-type: none"> <li>• 130° (flexion/extension)</li> </ul>	<ul style="list-style-type: none"> <li>• Comfy Spring Loaded Goniometer Elbow Splint</li> <li>• IROM Elbow Brace</li> <li>• Easy On Elbow Brace</li> <li>• QualCare ROM Elbow Orthosis brace</li> </ul>

The EMU severely limits torso motion. Likewise, the use of the external frame backpack, connected to our hip joint, makes torso motion (flexion/extension, lateral motion, or twisting) nearly impossible, except from the hip joint. Thus, we chose not to add additional torso constraints.

We considered three general options for the shoulder: compression resistance, elastic resistance, and an exoskeleton (Figure 6.13). Compression resistance, as shown in Figure 6.13 by the McDavid support, provides resistance through a neoprene or neoprene-like compression garment. The advantages of this system are that it is lightweight and simple, and may easily be worn on both sides. The disadvantages are that it does not provide directed resistance, does not provide any range of motion limitations, and is entirely non-adjustable. Elastic resistance, shown in Figure 6.13 by the Cadlow Shoulder Stabilizer, acts essentially as an exercise device resisting motion through the use of elastic exercise bands. Though this system provides resistance, we are concerned about the neutral point of the joint, since even with bands attached ventrally and dorsally, the direction of resistance is necessarily in the direction of the bands, not necessarily the direction we wish to simulate. An exoskeleton-type device, as shown in Figure 6.13 by the DonJoy Quadrant Shoulder Brace, provides the most flexible option as range of motion can be limited by

the hardware, and axes are aligned with the subject's joint axes. However, resistance must be provided externally, as this only provides range of motion limitation. We would be required to add a resistive element. Both the DonJoy and Cadlow options were suggested by Mosher, Mitchell et al. (2006). The McDavid and DonJoy Quadrant Shoulder Brace were obtained for characterization in-house.



Figure 6.13 - Three families of shoulder braces. Left: McDavid Universal Shoulder Support. Center: Cadlow Shoulder Stabilizer. Right: DonJoy Quadrant Shoulder Brace

We considered two families of braces for the elbow. As with the shoulder, we could choose to utilize a neoprene compression brace. Alternately, we could choose an exoskeleton-type brace. Two such options are shown in Figure 6.14.

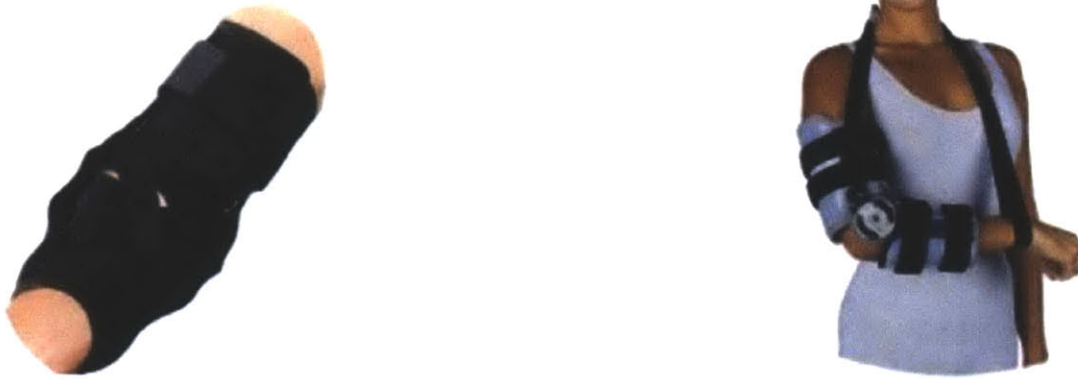


Figure 6.14 - Left: DonJoy Hinged Elbow Guard. Right: DonJoy IROM Hinged Elbow Brace

A neoprene brace with elastic supports provides resistance, but no range-of-motion limitations, and is not conducive to added external resistive elements. An exoskeleton-type brace would allow for range-of-motion limits to be added, but would require an external resistive element, as the brace itself does not provide resistance. It is also large, and would require integration with the shoulder brace. The DonJoy Hinged Elbow Guard was obtained and tested in-house.

With the exoskeleton-type braces, passive resistive elements must be used (Figure 6.15). Torsion springs are readily available and provide a known elastic resistance. Another option that provides some adjustability is to use linear extension springs attached to a central pin adjusted to provide the appropriate neutral angle.

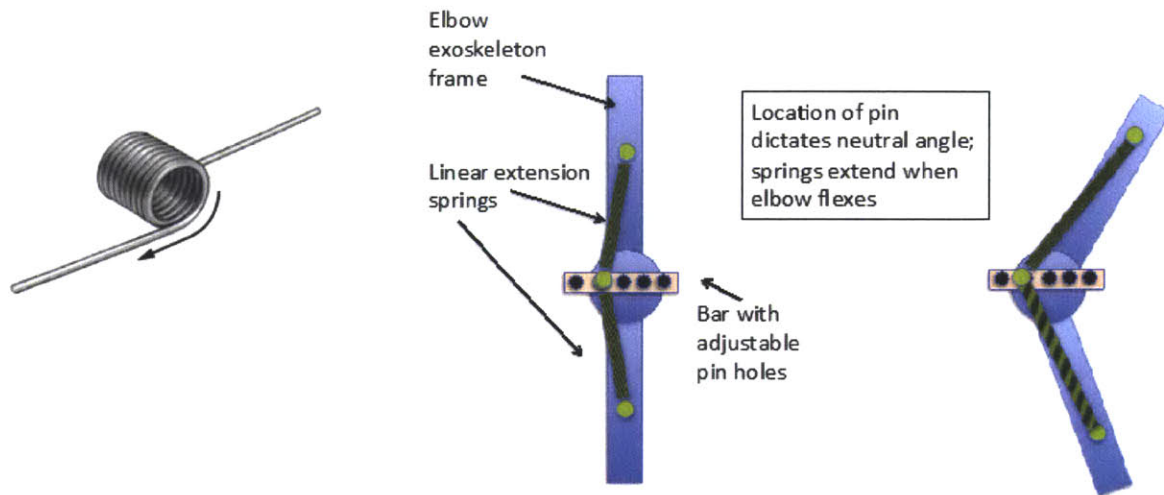


Figure 6.15 - Options for resistive elements on an exoskeleton-type brace. Left: torsion spring. Right: concept drawing using linear extension springs.

A final option, and we believe the best option, is the use of spiral torsion springs (Figure 6.15). These springs act similarly to torsion springs but are slimmer in profile and ideal for our use, because we could mount the center of the spring directly on the center of the joint, and the arm of the spring on one of the limb segments. However, these springs are quite difficult to obtain: they are generally not available off-the-shelf, and when custom-built, are sold in large quantities.



Figure 6.16 – Spiral torsion springs



Ultimately, we chose the DonJoy Quadrant Shoulder Brace to serve as both the shoulder and elbow brace. This brace can be worn (with some modification) on both sides, and is adjustable for all limb lengths. The brace does not provide any resistance.

Since spiral torsion springs were not realistic for logistical reasons (see above), standard COTS torsion springs were used for resistance in flexion and extension of the elbow and shoulder, and abduction/adduction of the shoulder.

Torsion springs were selected to provide resistance commensurate with the EVA S3 requirements. Plastic spools were machined, to which the torsion springs were mounted. The metal arms of the springs were mounted to the structure of the shoulder brace using metal brackets. A complete upper body right side is shown in Figure 6.17, and the individual joint components are shown in Figure 6.18.

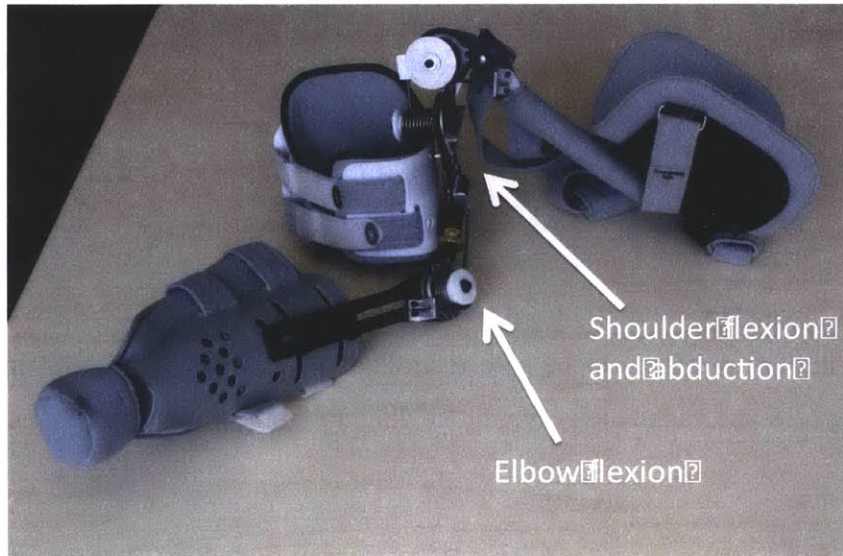


Figure 6.17 - Complete right side of the upper body. All gray padded portions are part of the COTS DonJoy shoulder brace

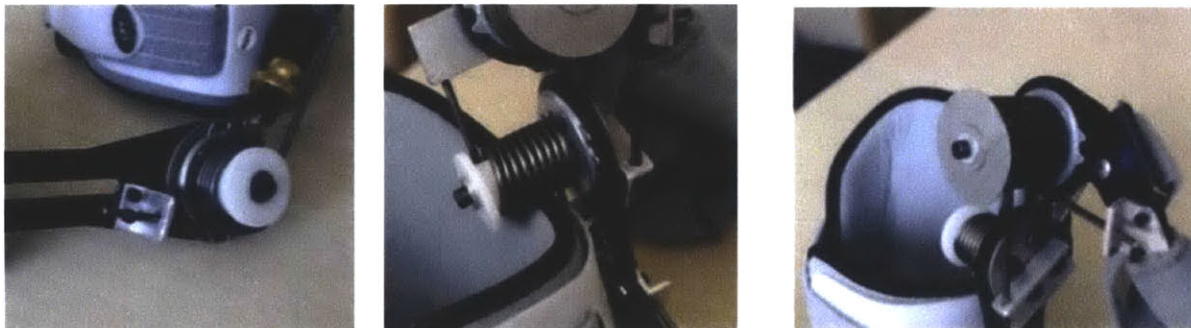


Figure 6.18 - (Left) elbow joint; (center) shoulder flexion joint; and (right) shoulder abduction joint, with shoulder flexion joint visible in the background.

#### 6.1.4 Pneumatics and Control

To support the initial phases of testing of the joints, we developed a prototype controller that could be quickly and easily implemented to support an arbitrary number of pneumatic actuators and sensors.

For the processor, we chose an Atmel STK600 development kit, and an AT32UC3C0512C 32-bit microcontroller. This particular microcontroller offers a maximum of 123 I/O pins, and supports a

clock frequency of up to 66 MHz: enough to support several pneumatic actuators and sensors right out of the box.

With this rapid-prototype setup, we tested a variety of choices for pneumatic valves, pneumatic transducers, and joint-angle sensors as well. Some of the components tested are discussed below.

We assembled a pneumatics and control system that included all the necessary tubing, piping, pneumatics and digital interfaces to be able to inflate and deflate the McKibben actuators on command. Figure 6.19 shows the high-level block diagram of the prototype system.

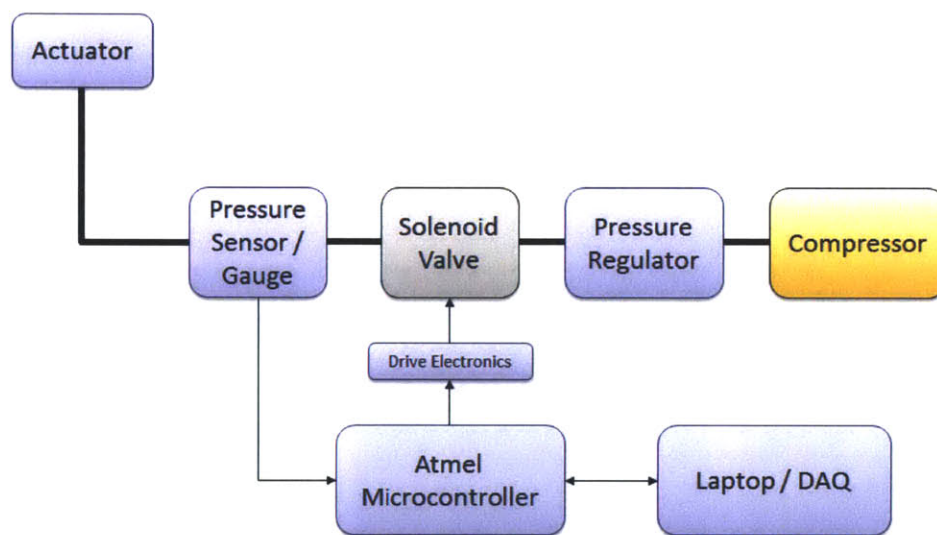


Figure 6.19 – Block diagram on pneumatic controller

Initially, the microcontroller software could interface with the pressure sensor and obtain pressure readings. We worked to characterize the pressure sensor readings and verify the accuracy of the sensor. The drive electronics for the solenoid valve were built on a prototyping bread-board and were driven by the microcontroller. The switching characteristics of the solenoid valve were also verified.

This initial prototyping was done so that, we could run compressed air through the system and obtain performance metrics of the system as a whole, including how much air flow we can run to the actuators, and how fast we can pressurize and de-pressurize the actuators. If we were

unsatisfied with the performance of a particular component, we could easily exchange it for any one of the other parts we have in-house.

Figure 6.20 is a snapshot of the prototype controller electronics, including the Atmel microcontroller development board, and the drive electronics for the solenoid valve. The valve and pressure sensor are shown disconnected (the air tubing and pneumatic connections are not shown).

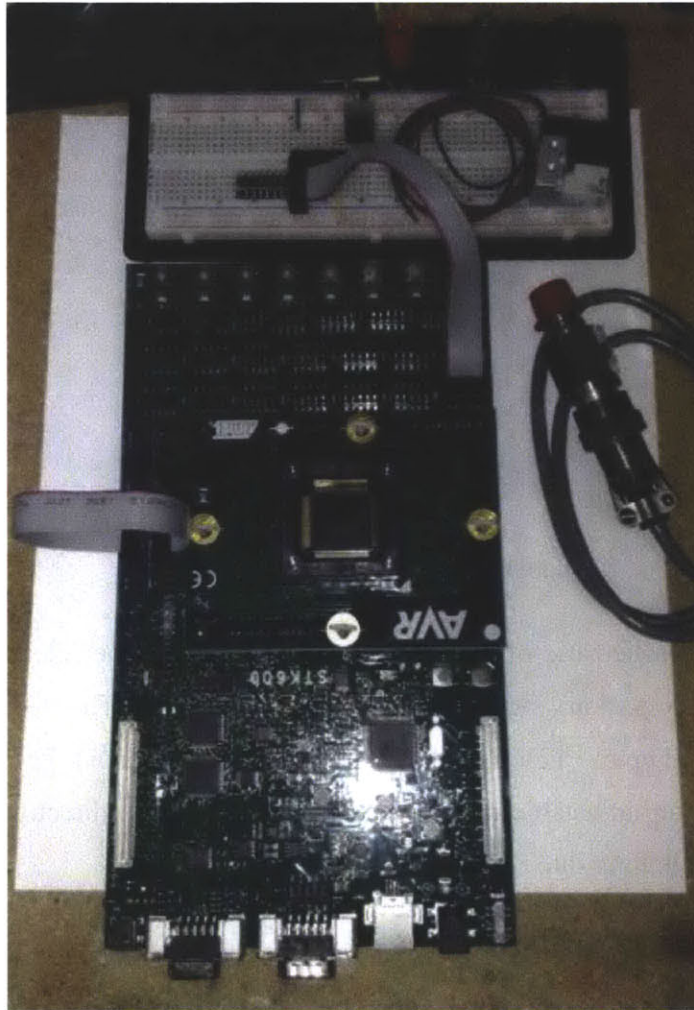


Figure 6.20 – Early Prototype Controller

Figure 6.21 shows the completed controller prototype connected to two Festo actuators (the laptop which serves as a DAQ is not shown). The system is comprised of a pressure regulator, two solenoids, two pressure transducers, solenoid driver electronics, transducer signal-conditioning



electronics, and the Atmel microcontroller development board. A 12 volt power supply (not shown) powers the electronics and pneumatic components. An external compressor (not shown) provides air to the pneumatics and actuators. The system can control the pressure of each actuator independently up to 60 psi. The solenoids are 3-way valves, which means that air can only be flowing in or out of the actuators. To hold the actuator at an intermediate pressure level, the solenoid can be switched on and off rapidly such that an average amount of air flows into the actuator over a period of time.

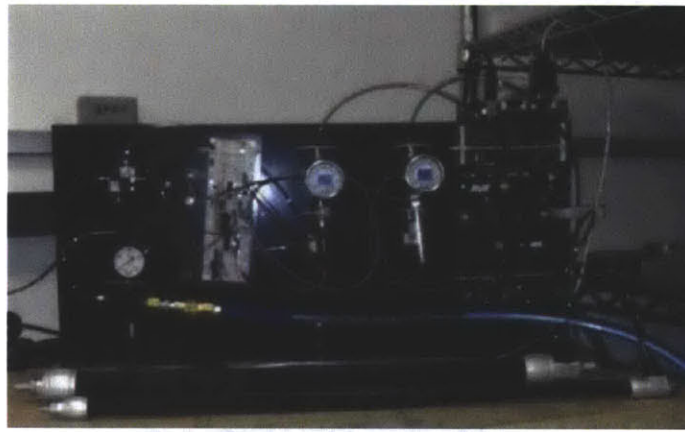


Figure 6.21 – Pneumatic control system

Figure 6.22 is a circuit schematic of the early controller system. The solenoids are driven by a PWM (pulse-width modulation) signal from the microcontroller. The +3.3V signal from the microcontroller is pulled up to +12V by a buffer IC to drive the solenoid. The PWM signal is a 20 Hz square wave with an adjustable duty cycle. The duty cycle is directly proportional to the average amount of air flowing into the actuator.

The pressure transducers are powered by a +5V excitation voltage, and produce a differential voltage proportional to the pressure in the actuator. The transducers have a very small sensitivity, approximately  $31.5 \mu\text{V}/\text{psi}$ . At a 100 psi, the sensor output is 3.15 mV. The built-in analog-to-digital converter (ADC) on the microcontroller can read voltages in the range of 0.0 to 1.0 V, producing a 12-bit digital reading. Feeding a voltage on the order of 3.15 mV directly to the microcontroller will swamp the signal with noise as a result of mismatched input/output impedances, making it impossible to obtain an accurate pressure reading. Instead the transducer's





After sampling at a frequency of 1 kHz, a digital filter was applied with a cutoff frequency of 100 Hz, which removed the unneeded high frequency oscillations. This has appeared to remove the noise from our signal.

Early testing of the knee joint indicated that there were several issues with the pneumatic setup. Specifically, air leaked at high pressures, the system was loud, and the air flow was slow enough to require unnaturally slow joint movements in order to properly simulate the joint torques. The pneumatic system initial version of the pneumatic system is shown in Figure 6.23.

The concern we felt that must be initially addressed was the speed of the system. As an initial step, the size of the pneumatic tubing was increased from 1/8" to 1/4". Pneumatic fittings for the pressure sensor, the actuators, the solenoid, and the pressure regulator were also replaced to accommodate this larger sized tubing.

Second, we considered the use of a single solenoid. The solenoid functions by alternately fully opening and shutting the input and exhaust ports. This regulates the pressure output to the actuator, depending on the command signal. However, because the two ports (exhaust and input) must alternately open, it may take several seconds for a fully depressurized actuator to fully pressurize. As an alternative, we considered the use of a single pressure regulator to replace the solenoid. While more expensive, this straightforward solution would control the pressure directly based on the input signal. As an added benefit, it does not require a feedback signal from a downstream pressure sensor – the regulator includes a pressure sensor internally. These two options are shown in Figure 6.23 and Figure 6.24.

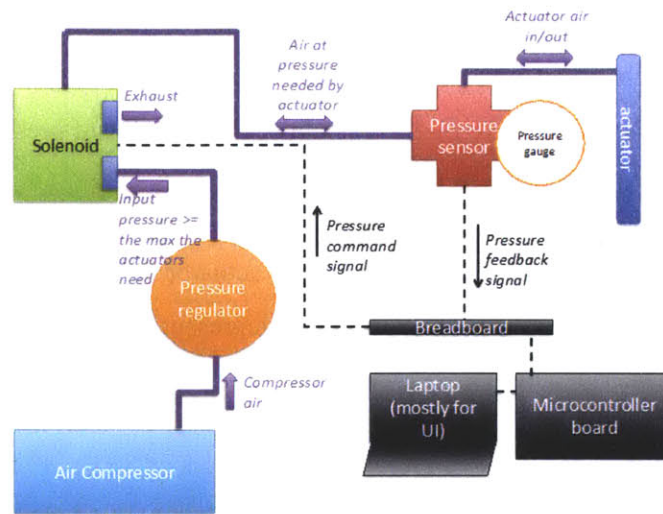


Figure 6.23 – Pneumatic system using a solenoid (system shown for one actuator)

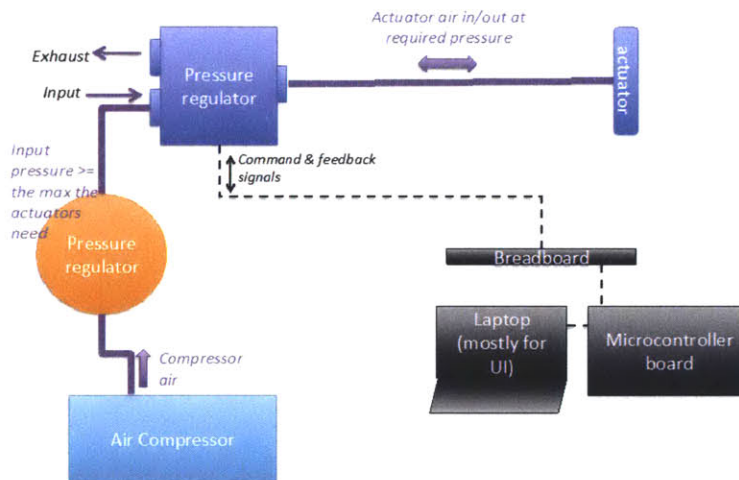


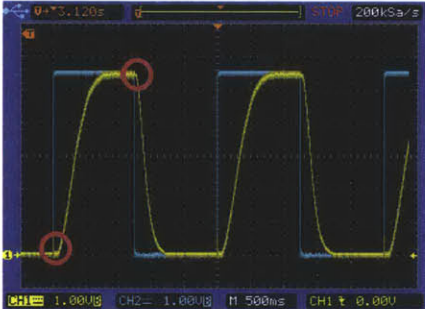
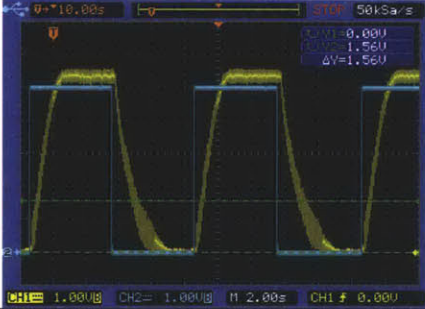
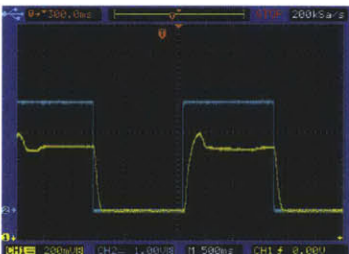
Figure 6.24 – Pneumatic system using a pressure regulator (system shown for one actuator)

Given the simplicity and expected accuracy of pressure regulators over solenoids, we spent nearly two months testing pressure regulators for use in our S3 system. One was exemplary, but impossible to implement for the fourteen actuators used in our system due to the high cost per regulator. Two other regulators, comparable in specifications, proved considerably inferior (Table 6.2).

Because we were unable to find a pressure regulator solution that would fit our needs, we reverted to using solenoids, which could meet our response time and accuracy requirements. A Festo solenoid (model MHE4-MS1H-3/2G-1/4-K) was chosen, with a Festo pressure transmitter (Type SPTW-P10R-G14-VD-M12).

The solenoid can fully pressurize and depressurize the actuator at a frequency of 1 Hz. However, since most motions do not require full pressurization/depressurization, they can operate at higher frequencies in most cases.

Table 6.2 – Pressure Regulators Tested

Brand	Cost per regulator	Performance notes	Results
Festo	\$1000	<p>Easy to control, linear 1<sup>st</sup> order response, time delay = 0.186s, cutoff frequency=1.1 Hz</p> 	Rejected due to price
MetalWorks	\$300	<p>Difficult to control; time delay = 0.191s; low cutoff frequency of 0.6 Hz.</p> 	Rejected due to inaccuracy of actuator pressure.
Parker	\$407	<p>Difficult to control; built in sensor is inaccurate so resulting pressure is inaccurate. An external pressure sensor doubles the price.</p> 	Rejected due to inaccuracy and requirement for external pressure sensor.



## Appendix B. Initial Optimization Code

### Hipflex.m

```
%Name: Hipflex - A script to determine actuator selection for hip flexion
%of the exoskeleton
%Author: Forrest Meyen
%Date: 6-19-2012

%Goal: Minimize weight of required actuators (Shorter and smaller diameter
actuators are
%preferred)

%Cost Functions:
%1. Pivot spool weigh cost function
%2. Actuator weight cost function

%Constraints:
%1. Maximum allowable actuator pressure or force for safety considerations
%2. Factors of safety for actuator performance (Force and displacement)

%Assumptions:
%1. Weight of wire is negligible
%2. Construction of spool is aluminum 0.03m thick

% Variable      Description
%===Vars to Optimize===
% r              Hip joint pivot spool radius (m) [determines torque produced
by force, and weight]
% L              Actuator length (m) [determines weight and ROM]
% d              Actuator diameter (m) [determines force and weight]
%===Specified parameters===
% st            Spool thickness (m)
% maxl          Actuator maximum length based on system constraints (m)
%===Actuator properties===
% cr            Actuator maximum proportion of actuator length contraction
(ratio)
%===Size Specific===
% Fd            Actuator maximum force for a particular diameter (N)
% minl          Actuator minimum length for a particular diameter (m)
% wto           Fixed weight of actuator at zero length (grams)
% wtl           Weight of actuator per meter (grams)
%===Constraint Equations===
% ROM           Range of motion for hip flexion and extension (deg)
% T             Maximum expected torque (N-m)
%===Constraints===
% Fst           Factor of safety for torque generation (ratio)
% Fsr           Factor of safety for ROM (ratio)
%===Objective Function===
% w_act         Weight of the actuator
% w_spl         Weight of the spool
% W             Total weight. Minimize this.

clear all
```

```

global ii ROMmin Tmin cr Fd wto wtl st

%Indicate what actuator to use (1 = 10mm, 2 = 20mm, 3 = 40 mm)
ii = input('Indicate what actuator to use (1 = 10mm, 2 = 20mm, 3 = 40 mm): ');
%(d=0.01)

%Specify desired torque and range of motion.
Fst = 1.25;
Fsr = 1.25;
Tmin = 32*Fst; % (N-m) this is used as the baseline for both actuators. The
smaller actuator requirement is actually 25(n-m)
ROMmin = 168*Fsr;

%Diameter specific variables from Festo manual
minl = [0.040,0.060,0.120]; %Actuator minimum length for a particular diameter
(m)
Fd = [630,1500,6000]; %Actuator maximum force for a particular diameter
(N)
wto = [58,169,675]; %Fixed weight of actuator at zero length (grams)FOR
COST FUNCTION
wtl = [94,178,340]; %Weight of actuator per meter (grams)FOR COST
FUNCTION

%Initialize Other Variables
st = .03; %Spool thickness (m)FOR COST FUNCTION
maxl = 1; %Actuator maximum length based on system constraints
(m)
cr = 0.25; %Actuator maximum proportion of length contraction
(ratio)

%Spool radius initialization and bounds
r0 = 0.03; %initial spool guess (m)
lbr = 0.010; %lower bound or spool size
ubr = 0.300; %upper bound for spool size

%Actuator length initialization and bounds
L0 = minl(ii)+.5; %initial guess for actuator length
lbL = minl(ii); %lower bound for actuator length
ubL = maxl; %upper bound for actuator length

options = optimset('Display','iter','Algorithm','interior-point');

%return weight and function value
[rL,Weight] =
fmincon(@objfun,[r0,L0],[],[],[],[],[lbr,lbL],[ubr,ubL],@confun,options)

T = rL(1)*Fd(ii)
ROM = (cr*rL(2)*360)/(2*pi*rL(1))
Spool_Shear_Stress = T*2/(pi*rL(1)^3) %shear stress (Pa)

Max_torque_allowed = (pi/2)*35000000*rL(1)^3

```

**Objfun.m**

```

%Objective function
%fmincon help located at:
%http://www.mathworks.com/help/toolbox/optim/ug/brn4nh7.html;jsessionid=68fa0
1db5c5091570ec6c45edb8b

%Goal: min weight (obj func)
%subject to constraints
%1. T > Tmin
%2. ROM > ROMmin
function W = objfun(rL)

global ii wto wtl st

%Cost function is weight in grams MOVED TO OBJECTIVE FUNCTION
w_act = wto(ii)+wtl(ii)*rL(2); %Weight of actuator based on the per unit
length weight. (Assumption is tha the minimum length is the minimum length of
the tube and not the fixed weight fittings.)
w_spl = pi*rL(1)^2*st*2.7/(0.01^3); %6061 aircraft grade aluminum is 2.7 g/cc
W = w_act+w_spl; %Total weight estimate excluding cables

```

### confun.m

```

%Constraint function
function [c, ceq] = confun(rL)

global ROMmin Tmin cr Fd ii

%optimization variables "x" = r, L, d

%Goal: min weight (obj func)
%subject to constraints
%write in form c(x) <= 0
%1. Tmin < T
%thus Tmin - T <= 0
%2. ROMmin < ROM
%thus ROMmin - ROM <= 0

%Torque Equation
%T = rL(1)*Fd(ii); %Simply the radius of the spool times the force generated
by the actuator
%Range of motion equation
%ROM = (cr*rL(2)*360)/(2*pi*rL(1));

maxstress = 35000000; %mpa
%Nonlinear inequality constraints
c = [Tmin - rL(1)*Fd(ii); %Tmin - T <= 0
     ROMmin - (cr*rL(2)*360)/(2*pi*rL(1)); %ROMmin - ROM <= 0
     rL(1)*Fd(ii)-(pi/2)*maxstress*rL(1)^3 ]; %Torq - MaxTorq <= 0

%Nonlinear equality constraints
ceq = [];

%constraint based on
%Tmax = (pi/2)*maxstress*rL(1)^3

```

## **Appendix C. RSST Repairs**

Considerable effort was spent repairing the Robotic Space Suit Tester for use in testing. When the project began, there was a significant hydraulic fluid leak originating at the robot's elbow (Figure 6.25). We opened the elbow components; inside the metal plate there were five separate O-rings, any of which could have been the source of the leak. We systematically replaced each O-ring, but the leak continued, thus we chose to bypass use of the arm altogether. We disconnected the main hydraulic fluid input line leading to the arm (which is then branched to the various arm locations), and connected it to the main hydraulic fluid output line (Figure 6.26). Thus, the upper body is entirely non-functional. This was considered acceptable since the passive upper body did not require RSST testing.



Figure 6.25 – The hydraulic fluid leak originates from the RSST elbow joint

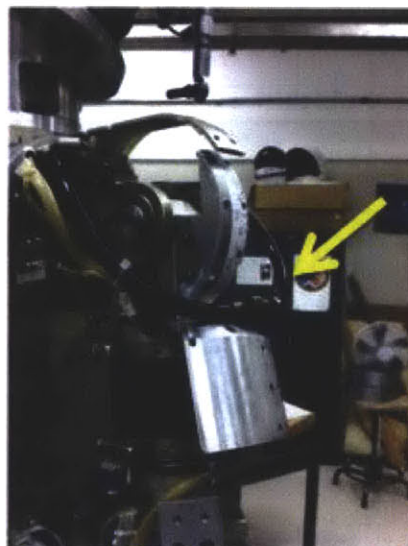


Figure 6.26 - The leak at the elbow is bypassed by connecting the hydraulic input and output lines at the shoulder.

The lower body components of the RSST required recalibration to correlate voltage to angle or torque data. Generally: protractors rigidly attached to the limb segments (hip and knee) were used



to record angle at different voltage settings. Likewise, known weights were hung from the limb segments, set to known angles, such that actual torque could be calculated and correlated to the voltage setting (Figure 6.27).



Figure 6.27 - Left: knee angle calibration (note protractor and plumb line). Right: hip flexion/extension torque calibration (note weight hanging from ankle).

In attempting to calibrate the lower body limbs, we found that three degrees of freedom (DOF) in the robot spacesuit tester leg were not functioning: ankle flexion/extension, ankle inversion/eversion, and ankle rotation. The DOFs were not working due to malfunctioning or broken servo-valves in the robot. The three servo-valves were sent to Raytheon SARCOS, the manufacturer, for testing and repair. As a result of testing and repair, all three servo-valves began functioning partially or at full capacity. Specifically, the servo-valves at the ankle rotation and ankle flexion/extension DOFs began functioning at full specification according to SARCOS. The valves were cleaned, received new magnets, and were pneumatically tested. The ankle inversion/eversion DOF was apparently disassembled improperly at some time and was physically damaged, and consequently the jet pipe tip was not repairable. We did not plan to use ankle inversion/eversion testing for this program, so this was not a problem. However, despite several iterations of repairs after reinstallation on the RSST, ankle flexion/extension continued to be non-

functional (did not respond when commanded). Thus, we were unable to use the RSST for ankle testing conventionally. Our testing method is covered in section 3.9.2.

Also during calibration, we found that the torque voltage values for hip flexion were not predictable and could not be calibrated. Actuation was functional, and the voltage values or angle were predictable and readily calibrated. Thus, we mounted an external strain gauge to the hip joint to allow us to record hip torque data. The strain gauge used was an “Omega Precision Strain Gauge”, part number SGD-3/350-DY11. This is a dual strain gauge (two parallel strain gauges, side-by-side) with 350 Ohm resistance and a gage factor of 2.14. The gauge was bonded to the RSST at a position next to the original (defective) strain gauge. Orientation of the gauge was aligned with the original gauge. A National Instruments cDAQ system was used for data collection, using a NI 9236 quarter-bridge analog input model. LabView 2010 was used to create a Virtual Instrument to measure and record the strain data.

In summary:

- The knee joint was fully functional and recorded angle and torque.
- Hip abduction/adduction was fully functional and recorded angle and torque.
- Hip flexion/extension was operational and controllable, but only recorded angle; torque was recorded using an external strain gauge.
- The ankle was not functional at all; it had to be moved manually, and angle was recorded from the S3 ankle joint, and torque was measured using a load cell.

## References

- Alpinestars. (2012). "Touring Kidney Belt." Retrieved October 7, 2012, from <http://www.alpinestars.com/shop/categories/moto/protection/touring-kidney-belt>.
- Beyl, P., M. Van Damme, R. Van Ham and D. Lefeber (2008). Design and control concepts of an exoskeleton for gait rehabilitation. Biomedical Robotics and Biomechatronics, 2008. BioRob 2008. 2nd IEEE RAS & EMBS International Conference on.
- Beyl, P., M. Van Damme, R. Van Ham, R. Versluys, B. Vanderborght and D. Lefeber (2008). An exoskeleton for gait rehabilitation: Prototype design and control principle. Robotics and Automation, 2008. ICRA 2008. IEEE International Conference on.
- BlackDiamond. (2013). "Contact Crampon." Retrieved August 9, 2013, from [http://blackdiamondequipment.com/en/climbing%2Fcrampons/contact-crampon-BD400069\\_cfg.html?dwvar\\_BD400069\\_cfg\\_color=Stainless#gclid=CNXWwKX38LgCFQee4AodzhsAEA&start=5](http://blackdiamondequipment.com/en/climbing%2Fcrampons/contact-crampon-BD400069_cfg.html?dwvar_BD400069_cfg_color=Stainless#gclid=CNXWwKX38LgCFQee4AodzhsAEA&start=5).
- Blaya, J., D. Newman and H. Herr (2002). Active Ankle Foot Orthoses (AAFO), MIT AI Lab Abstracts.
- Bowen, J. D. (1968). Evaluation of Manned Orbiting Laboratory Design Definition Pressure Garments, Aerospace Medical Research Laboratories.
- Carr, C. E. and J. McGee (2009). "The Apollo Number: Space Suits, Self-Support, and the Walk-Run Transition." PLoS ONE **4**(8): e6614.
- Carr, C. E. and D. J. Newman (2005). "When is running more efficient than walking in a space suit." SAE Transactions Journal of Aerospace **114**.
- Carr, C. E. and D. J. Newman (2007). "Space Suit Bioenergetics: Cost of Transport During Walking and Running." Aviation, Space, and Environmental Medicine **78**(12): 1093-1102.
- Carr, C. E. and D. J. Newman (2007). "Space suit bioenergetics: framework and analysis of unsuited and suited activity." Aviation, space, and environmental medicine **78**(11): 1013-1022.
- Carr, C. E. and D. J. Newman (2008). "Characterization of a lower-body exoskeleton for simulation of space-suited locomotion." Acta Astronautica **62**(4-5): 308-323.
- Carr, C. E. and D. J. Newman (2008). "Characterization of a lower-body exoskeleton for simulation of space-suited locomotion." Acta Astronautica **62**(4-5): 308-323.
- Cavanagh, P. R., J. Polliner and B. L. Davis (1989). "Design principles for a zero-gravity locomotion simulator." Journal of Biomechanics **22**(10): 998.
- Chen, J. Z. and W. H. Liao (2010). "Design, testing and control of a magnetorheological actuator for assistive knee braces." Smart Materials and Structures **19**(3): 035029.
- Clark, D., N. DeLeys and C. Matheis (1962). EXPLORATORY INVESTIGATION OF THE MAN AMPLIFIER CONCEPT. Wright-Patterson Air Force Base, Ohio, Aerospace Medical Division, Air Force Systems Command: 75.

- Company, G. E. (1971). Final Report on Hardiman I Prototype for Machine Augmentation of Human Strength and Endurance. Schenectady, New York, General Electric Company.
- CYBERDYNE. (2013). "Robot Suit HAL." Retrieved June 7th, 2013, from <http://www.cyberdyne.jp/english/robotsuithal/>.
- DonJoy. (2012). "ROM hip." Retrieved October 7, 2012, from <http://www.djoglobal.com/products/donjoy/rom-hip>.
- Duda, J. E. and S. Hart (2010). Space Suit Simulator for Partial Gravity EVA Experimentation and Training, Phase 1, Final Report.
- Duda, J. E., D. J. Newman, J. Hoffman, J. Peverill and G. P. Perusek (2011). The Use of Artificial Muscles in Space Suit Simulation for Partial Gravity Experimentation and Training.
- Ferreira, I. M. (2007). Develop, Test and Model a Space Suit Simulator. Master of Aerospace Engineering, Instituto Superior Tecnico, Universidade Tecnica de Lisboa.
- Ferris, D. P., J. M. Czerniecki and B. Hannaford (2005). "An ankle-foot orthosis powered by artificial pneumatic muscles." Journal of Applied Biomechanics **21**(2): 189.
- FESTO (2011). Fluidic Muscle DMSP/MAS. Instruction manual.
- FESTO (2011). MAS/DMSP ML. Operating instructions (Operation - Fluidic muscle).
- Frazer, A. L. (2003). Modeling Human-Spacesuit Interactions. Master of Science in Aeronautics and Astronautics, Massachusetts Institute of Technology.
- Freudenrich, C. (2011). "How Space Suits Work." Retrieved 8 January, 2013, from <http://science.howstuffworks.com/space-suit4.htm>.
- Gilkey, A. L. (2012). Space Suit Simulator for Partial Gravity Extravehicular Activity Experimentation and Training.
- Guizzo, E. (2011). "Sarcos Exoskeleton Bringing Iron Man Suit Closer To Reality." Retrieved June 7th, 2013, from <http://spectrum.ieee.org/automaton/robotics/military-robots/sarcos-exoskeleton-iron-man-suit>.
- Harris, G. L. (2001). The Origins and Technology of the Advanced Extravehicular Space Suit. San Diego, California, Univelt, Incorporated.
- Herr, H. and A. Wilkenfeld (2003). "User-adaptive control of a magnetorheological prosthetic knee." Industrial Robot: An International Journal **30**(1): 42-55.
- Hian Kai, K., J. H. Noorden, M. Missel, T. Craig, J. E. Pratt and P. D. Neuhaus (2009). Development of the IHMC Mobility Assist Exoskeleton. Robotics and Automation, 2009. ICRA '09. IEEE International Conference on.
- Hoggett, R. (2010, May 14th, 2010). "1830c – Walking by Steam – Robert Seymour (British)." Retrieved June 3rd 2013, from <http://cyberneticzoo.com/?p=2957>.
- Holschuh, B., J. Waldie, J. Hoffman and D. Newman (2009). Characterization of Structural, Volume and Pressure Components to Space Suit Joint Rigidity. International Conference On Environmental Systems. Savannah, Georgia, United States, SAE International.

- ILC Dover, I. (1994). Space Suit Evolution From Custom Tailored To Off-The-Rack.
- Jamwal, P. K., X. Shengquan and K. C. Aw (2010). Design analysis of a pneumatic muscle driven wearable parallel robot for ankle joint rehabilitation. Mechatronics and Embedded Systems and Applications (MESA), 2010 IEEE/ASME International Conference on.
- Kelty. (2013). "TREKKER 65." Retrieved July 12, 2013, from <http://www.kelty.com/p-430-trekker-65.aspx>.
- Klute, G. K., J. M. Czerniecki and B. Hannaford (1999). McKibben artificial muscles: pneumatic actuators with biomechanical intelligence. Advanced Intelligent Mechatronics, 1999. Proceedings. 1999 IEEE/ASME International Conference on, IEEE.
- Lewis, C. L. and D. P. Ferris (2011). "Invariant hip moment pattern while walking with a robotic hip exoskeleton." J Biomech **44**(5): 789-793.
- Makinson, B. (1971). Research and development prototype for machine augmentation of human strength and endurance. hardiman i project, DTIC Document.
- Mao, Y. and S. K. Agrawal (2011). A cable driven upper arm exoskeleton for upper extremity rehabilitation. Robotics and Automation (ICRA), 2011 IEEE International Conference on, IEEE.
- Martin, L. (2008). HULC Exoskeletons Augment Strength and Endurance.
- Matty, J. E. and L. Aitchison (2009). "A Method for and Issues Associated with the Determination of Space Suit Joint Requirements."
- MatWeb. (1996-2013). "Material Property Data." 2013, from <http://www.matweb.com/index.aspx>.
- Meyen, F., B. Holschuh, R. Kobrick, S. Jacobs and D. Newman (2011). Robotic Joint Torque Testing: A Critical Tool in the Development of Pressure Suit Mobility Elements. International Conference on Environmental Systems.
- Miller, J. S. (1968). THE MYOTRON -- A SERVO-CONTROLLED EXOSKELETON FOR THE MEASUREMENT OF MUSCULAR KINETICS. Buffalo, NY, Cornell Aeronautical Laboratory Inc: 55.
- Morgan, D. A. and L. B. J. S. Center (1996). Comparison of extravehicular mobility unit (EMU) suited and unsuited isolated joint strength measurements, National Aeronautics and Space Administration.
- Mosher, T. J., M. Mitchell and K. Packard (2006). "The Eva Evaluation Exoskeleton (e3): A Proposed Tool for Studying Humansystem Interaction in the Space Environment." Habitation **11**(1): 63-68.
- NASA (1995). NASA-STD-3000 Man-Systems Integration Standards NASA-STD-3000 Volume I Revision B, July 1995.
- NASA. (2013). "Active Response Gravity Offload System." Retrieved June 25, 2013, 2013, from [http://www.nasa.gov/centers/johnson/engineering/integrated\\_environments/active\\_response\\_gravity/](http://www.nasa.gov/centers/johnson/engineering/integrated_environments/active_response_gravity/).
- Newman, D. J. and H. L. Alexander (1993). "Human locomotion and workload for simulated lunar and Martian environments." Acta Astronautica **29**(8): 613-620.
- Newman, D. J., H. L. Alexander and B. W. Webbon (1994). "Energetics and mechanics for partial gravity locomotion." Aviation, space, and environmental medicine **65**(9): 815.



- Norcross, J. R., K. G. Clowers, T. Clark, L. Harvill, R. M. Morency, L. C. Stroud, L. Desantis, J. R. Vos and M. L. Gernhardt (2010). "Metabolic Costs and Biomechanics of Level Ambulation in a Planetary Suit." NASA Technical Report TP-2010-216115.
- Norton, R. L. (1999). Design of machinery: an introduction to the synthesis and analysis of mechanisms and machines, WCB McGraw-Hill.
- Perusek, G. P., J. K. DeWitt, P. R. Cavanagh, C. M. Grodzinsky and K. M. Gilkey (2007). "Zero-Gravity Locomotion Simulators: New Ground-Based Analogs for Microgravity Exercise Simulation."
- Pons, J. L. (2008). Wearable robots: biomechatronic exoskeletons. Wiley.
- Pratt, J., B. Krupp and C. Morse (2002). "Series elastic actuators for high fidelity force control." Industrial Robot: An International Journal **29**(3): 234-241.
- Pratt, J. E., B. T. Krupp, C. J. Morse and S. H. Collins (2004). The RoboKnee: an exoskeleton for enhancing strength and endurance during walking. Robotics and Automation, 2004. Proceedings. ICRA '04. 2004 IEEE International Conference on.
- REI. (2012). "Black Diamond Climbing Harness." Retrieved October 7, 2012, from <http://www.rei.com/product/819452/black-diamond-momentum-sa-climbing-harness>.
- REI. (2012). "Osprey Bioform CM A/X Hipbelt." Retrieved October 7th, 2012, from [http://www.rei.com/product/764283/osprey-bioform-cm-a/x-hipbelt-large?preferredSku=7642830033&cm\\_mmc=cse\\_froogle\\_-datafeed\\_-product\\_-7642830033&mr:trackingCode=BA894FFE-FB85-DE11-B7F3-0019B9C043EB&mr:referralID=NA](http://www.rei.com/product/764283/osprey-bioform-cm-a/x-hipbelt-large?preferredSku=7642830033&cm_mmc=cse_froogle_-datafeed_-product_-7642830033&mr:trackingCode=BA894FFE-FB85-DE11-B7F3-0019B9C043EB&mr:referralID=NA).
- SBIR.gov. (2013). "Space Suit Simulator (S3) for Partial Gravity EVA Experimentation and Training." Retrieved August 8, 2013, from <http://www.sbir.gov/sbirsearch/detail/369401>.
- Schaffner, G. (2007). Space Suit Simulator Development Project. Unpublished presentation.
- Schmidt, P. B., D. J. Newman and E. Hodgson (2001). Modeling Space Suit Mobility: Applications to Design and Operations. 31st International Conference on Environmental Systems, SAE International.
- Shields, G. (2010). "Unveiling coincides with release of Marvel Studios' Iron Man 2 on Blu-ray and DVD." Retrieved July 7th, 2013, from <http://raytheon.mediaroom.com/index.php?s=43&item=1652>.
- Skoog, A. I., I. P. Abramov, A. Y. Stoklitsky and M. N. Doodnik (2002). "The Soviet-Russian space suits a historical overview of the 1960's." Acta Astronautica **51**(1-9): 113-131.
- Stirling, L. A. (2008). Development of Astronaut Reorientation Methods: Acomputational and Experimental Study. Doctor of Philosophy, Massachusetts Institute of Technology.
- Suzuki, K., G. Mito, H. Kawamoto, Y. Hasegawa and Y. Sankai (2007). "Intention-based walking support for paraplegia patients with Robot Suit HAL." Advanced Robotics **21**(12): 1441-1469.
- Thomas, K. S. and H. J. McMann (2006). US Spacesuits, Springer.
- Zoss, A. and H. Kazerooni (2005). Architecture and Hydraulics of a Lower Extremity Exoskeleton. ASME 2005 International Mechanical Engineering Congress and Exposition (IMECE2005).

Zoss, A. B., H. Kazerooni and A. Chu (2006). "Biomechanical design of the Berkeley lower extremity exoskeleton (BLEEX)." Mechatronics, IEEE/ASME Transactions on **11**(2): 128-138.

Zoss, A. B., H. Kazerooni and A. Chu (2006). "On the mechanical design of the Berkeley lower extremity exoskeleton (BLEEX)."

